Combining Multiple Iris Matchers using Advanced Fusion Techniques to Enhance Iris Matching Performance

By

NTHATHENI NORMAN NELULFULE

A dissertation submitted in fulfillment of the requirements for the Degree

of

Magister Philosophiae (M.Phil)

in

Electrical and Electronics Engineering

Faculty of Engineering and the Built Environment

UNIVERSITY OF JOHANNESBURG

Supervised by Professor Fulufhelo Nelwamondo

Co-Supervised by Professor Tshilidzi Marwala

2014

Declaration of Authorship

I, Nthatheni Norman Nelufule hereby declare that the work contained in this dissertation titled "Combining Multiple Iris Matchers using Advanced Fusion Techniques to Enhance Iris Matching Performance", is my original work, and that any work done by others or by myself previously has been acknowledged and referenced accordingly. I confirm that this work was done wholly or mainly in candidature for a research at the University of Johannesburg, South Africa.

Signature..

Date................................

Acknowledgement

Firstly, I wish to thank God Almighty for making this golden opportunity possible, and the Council for Scientific and Industrial Research (CSIR), Modelling and Digital Science (MDS) and Information Security (IS) Competency Area together with the Department of Science and Technology (DST) RSA, for their funding opportunity and their working space. I also wish to thank my supervisors Professor Fulufhelo Vincent Nelwamondo and Professor Tshilidzi Marwala and my mentor Tendani Malumedzha (IS) for their invaluable advice and support throughout the duration of this project.

Portions of this dissertation used the publicly available iris databases; namely the Chinese Academy of Science's Institute of Automation (CASIA) and the University of Beira Interior (UBIRIS) iris image databases, and I thank them for these eye images, which proved extremely useful to this research. Without their data contribution this dissertation would have not been realized. All the MATLAB and LaTeX errors were debugged and fixed with the help of Alex Mngenge, and Yaseen Moolla; i thank them for being very supportive colleagues throughout this work. Finally I must thank my family and all my friends for their support and encouragement over all these years.

Abstract

The enormous increase in technology advancement and the need to secure information effectively has led to the development and implementation of iris image acquisition technologies for automated iris recognition systems. The iris biometric is gaining popularity and is becoming a reliable and a robust modality for future biometric security. Its wide application can be extended to biometric security areas such as national ID cards, banking systems such as ATM, e-commerce, biometric passports but not applicable in forensic investigations. Iris recognition has gained valuable attention in biometric research due to the uniqueness of its textures and its high recognition rates when employed on high biometric security areas. Identity verification for individuals becomes a challenging task when it has to be automated with a high accuracy and robustness against spoofing attacks and repudiation. Current recognition systems are highly affected by noise as a result of segmentation failure, and this noise factors increase the biometric error rates such as; the FAR and the FRR. This dissertation reports an investigation of score level fusion methods which can be used to enhance iris matching performance. The fusion methods implemented in this project includes, simple sum rule, weighted sum rule fusion, minimum score and an adaptive weighted sum rule. The proposed approach uses an adaptive fusion which maps feature quality scores with the matcher. The fused scores were generated from four various iris matchers namely; the NHD matcher, the WED matcher, the WHD matcher and the POC matcher. To ensure homogeneity of matching scores before fusion, raw scores were normalized using the tanh-estimators method, because it is efficient and robust against outliers. The results were tested against two publicly available databases; namely, CASIA and UBIRIS using two statistical and biometric system measurements namely the AUC and the EER. The results of these two measures gives the AUC = 99.36% for CASIA left images, the AUC = 99.18% for CASIA right images, the AUC = 99.59% for UBIRIS database and the Equal Error Rate (EER) of 0.041 for CASIA left images, the EER = 0.087 for CASIA right images and with the EER = 0.038 for UBIRIS images.

Table of Contents

List of Figures

List of Tables

List of Acronyms

AAD	**A**verage **A**bsolute **D**eviation
ATM	**A**utomatic **T**eller **M**achine
AUC	**A**rea **U**nder the **C**urve
CASIA	**I**nstitute of **A**utomation **C**hinese **A**cademy of **S**ciences
DCT	**D**iscrete **C**osine **T**ransform
DFT	**D**iscrete **F**ourier **T**ransform
EER	**E**qual **E**rror **R**ate
FAR	**F**alse **A**cceptance **R**ate
FMR	**F**alse **M**atch **R**ate
FN	**F**alse **N**egative
FNMR	**F**alse **N**on **M**atch **R**ate
FNR	**F**alse **N**egative **R**ate
FPR	**F**alse **P**ositive **R**ate
FRR	**F**alse **R**ejection **R**ate
GEC	**G**enetic and **E**volutionary **C**omputation
NHD	**N**ormalized **H**amming **D**istance
HPB	**H**erarchical **P**hase **B**ased
LDA	**L**inear **D**iscriminant **A**nalysis
MLDF	**M**ulti **L**obe **D**ifferential **F**ilter
NIR	**N**ear **I**nfrared
PCA	**P**rincipal **C**omponent **A**nalysis
POC	**P**hase **O**nly **C**orrelation
ROC	**R**eceiver **O**perating **C**haracteristic
SVM	**S**upport **V**ector **M**achine
TAR	**T**rue **A**accept **R**ate
TN	**T**rue **N**egative
TPR	**T**rue **P**ositive **R**ate
UBIRIS	**U**niversity of **B**eira **I**terior **Iris**
UPOL	**U**niversity of **P**alack'echo and **O**lomopuc
WED	**W**eighted **E**uclidean **D**istance
WHD	**W**eighted **H**amming **D**istance

List of Symbols

σ	Sigma	Standard deviation
μ	Mean	Average
π	Pi	Radian of an angle
$\sum$	Summation	Sum
ω	Angular frequency	Rads^{-1}
θ	Angle of orientation	Degrees
ϕ	Function of θ	Degrees
δ	Scaling parameter of a Gaussian filter	Dimensionless
ρ	Polar system coordinate	Degree^{-1}
α	Wavelet size	Dimensionless
β	Wavelet size	Dimensionless

Dedication

This dissertation is dedicated to my late father Azwidohwi Alpheus Nelufule and my entire family.

Chapter 1

Introduction

This dissertation is devoted to developing an advanced score level fusion model for multiple iris matching algorithms. In this chapter, the motivation and objectives of this work, proposed approach and focus, and the dissertation outline are presented in detail.

1.1 Background

Biometric security systems exploits physiological or biological human features which can be collected and processed by electronic means and used to identify individuals. Various biometric modalities have been explored and identified as possible measures of robustly and effectively securing information with iris particularly gaining more popularity due to its reliability as a strong future biometric security [1, 2, 3]. Amongst the widely used modalities, such as face, fingerprint, finger veins, hand geometry, retina, iris and voice, iris is growing more popular due to its distinctive unique features that are known to remain stable throughout life. These features are so distinctive such that even the monozygotic twins can be subtly identified [4, 5, 6]. Iris features are known to contain more than 400 statistical distinguishing features (unique patterns) or degrees of freedom which can be quantified and used for personal identification [7]. Approximately 260 degrees of freedom from 400 identifiable characteristics, can be computed for identification, and these includes: the collarette, which is the thickest region in the iris which has zigzag shapes separating the pupillary portion from the ciliary portion, the darkened area of an iris itself (crypts) which are defined as the series of holes or openings which are located on either side of the collarette which allows the stroma and the deeper iris tissues to be bathed in the aqueous humor, contraction of muscles within the iris (radial furrows and contraction furrows) which are defined as the series of very fine radial folds in the pupillary portion of the iris extending from the pupillary portion margin to the collarette, collagenous fibres, filaments, pigments spots, striations, serpentine vasculature, freekles and some rings. Figure 1.1 clearly shows the iris features from the eye image extracted from the University of Palack'echo and Olomouc (UPOL) [8] iris images database .

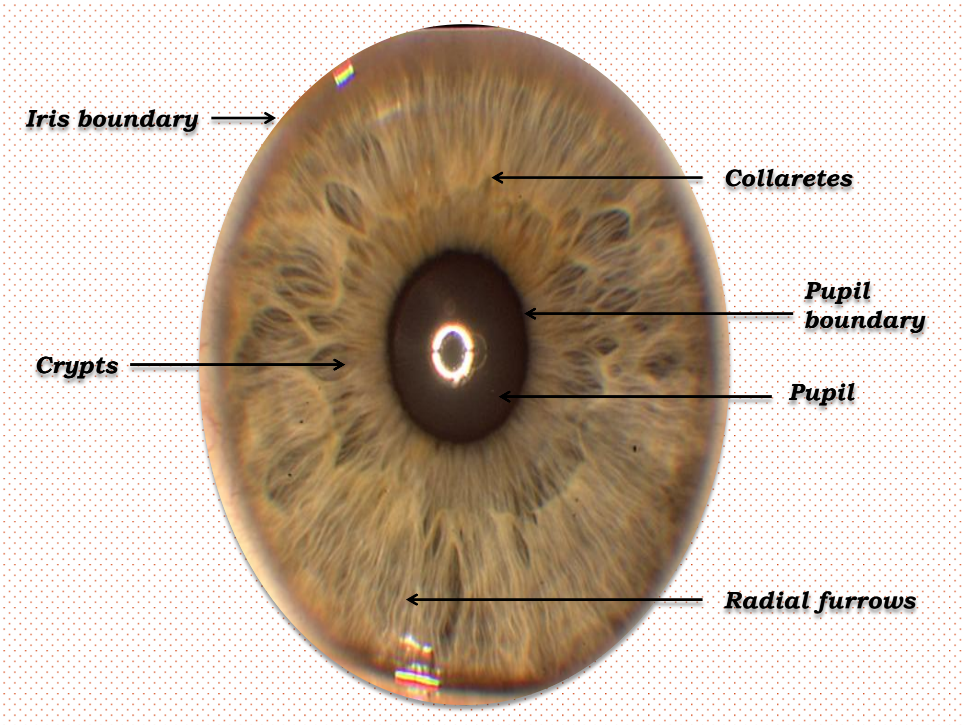

FIGURE 1.1: Structure of an iris

In [2, 9, 10, 11, 12, 13, 14] it is reported that the iris features have made it to possess six times more distinctively identifiable unique patterns than the well-known grandparent modality, fingerprint. The first fundamental scientific study on iris patterns dates back to ophthalmologist Frank Burch's discovery in 1936 [15]. In his study he discovered the potential of an iris to distinguish individuals from each other, and also to distinguish the left and right irises of the same person. The uniqueness and permanence of iris features have been well established and its potential to remain stable was confirmed by ophthalmologists Flom and Safir [15] in their clinical trials which earned them a patent in 1987. It was also mentioned in [15] that besides its stability, the iris is also easier to capture, protected within the interior eye and deformation of its unique patterns is unlikely. From these discoveries, they proposed that an iris could be used as a biometric if it can be automated. Daugman [10] introduced iris recognition as a young and active research by automating the first iris recognition system as proposed [15]. Daugman in his first automated iris recognition system discovered that its wide application can be extended to biometric security areas such as national ID cards, banking systems, e-commerce, biometric passports but with no application in surveillance and forensic investigations [16]. As computing power advances in technology, iris recognition research also picked up speed. The development and implementation of iris imaging technologies, and the need to secure information effectively using automated iris recognition systems became more apparent. More public iris image databases were developed to study and enhance iris recognition performance under various conditions. These advances in technology since the 1990's triggered increased need in non-forensic applications of robust iris biometric systems in high security areas. As mentioned in [10], a typical iris recognition consists of three modules namely; the segmentation module which involves denoising the input image and separating the iris region from other parts of the eye image, the feature extraction module which encode the iris information into a digital template and the feature matching module which classify the encoded templates as either a match or a non-match. The challenges posed by each module have been identified by various iris biometric researchers, with noise being the major problem leading to high false matches and high false rejections [17, 18, 19, 20, 21, 22, 23, 24]. Solutions have been proposed to overcome these challenges by reducing the amount of noise during segmentation module. In [25] normalized images were assessed based on the amount of occlusion by eyelashes and eyelids in order to map image quality measures to improve the recognition accuracy. Segmentation module is considered the most fundamental stage of iris recognition because information falsely encoded leads to poor recognition rate and cannot be corrected during or after feature extraction module. Iris image is highly occluded by natural noise such as eyelashes and eyelids which need to be removed or accounted for during segmentation. Various techniques and approaches have been proposed to improve segmentation phase, but segmenting every iris image in the database accurately is still an unresolved problem [26, 27, 28, 29]. In [10, 24, 30] noise masking techniques were used to reduce the effect of noise during the feature matching module. In [31], eyelashes and eyelids detection were avoided by extracting various blocks within the none occluded iris region. However, the challenge remains in making iris recognition system to be 100% accurate which has not been achieved yet as a result of occlusion by noise which results from segmentation failure. This problem is usually posed by occlusions with eyelashes and eyelids, camera reflections and pupil dilation posing serious effects in recognition performance. An intelligent adaptive algorithms for accurate segmentation is in demand and has not been established yet, and accounting for these noisy regions during the matching module is imperative. Different techniques have been proposed to alleviate this occlusion problem, especially when the acquired image is noisy. Recent research

[17, 18, 19, 20, 21, 22, 23, 24, 32, 33, 34, 35], have reported different approaches of improving recognition accuracy by managing the effect of noise. In [28], segmentation was done using Hough transform, histogram-bisection and eccentricity using regularization of iris boundaries using Fourier series and radial gradients of the iris image. In [29], a non-circular iris localization method using iris image projection function and gray level statistics was introduced to enhance the segmentation module. Bachoo and Tapamo [26] used the grey level co-occurrence matrix to segment the iris image in order to reduce the effect of noise posed by eyelashes and eyelids. Li and Ma [36] did a thorough investigation and develop an algorithm called random sample consensus for segmenting non-circular iris boundaries, based on iris image captured under non-ideal environments where the output image is highly invaded with various kinds of noise. The results of this approach were tested against noisy University of Beira Interior Iris (UBIRIS) database. De Marsico *et al.* [37] developed an integration approach which combines linear binary pattern and discriminable textons to enhance the iris matching performance. This approach was also based on eliminating the effect of noise factors within an iris image. Rathgeb *et al.* [38, 39] used adaptive bloom filters to extract an alignment-free cancelable iris template which has been tested against Institute of Automation Chinese Academy of Sciences (CASIA) iris database. However, the error rates reported in the literature still reports that they evolved from occlusions and reflection from the camera. Besides these noise reduction failure during segmentation, poor biometric performance has been also discovered to be deep rooted from feature extraction module. Various feature extraction techniques have also been proposed in order to implement feature extraction robust against noise [9, 10, 21, 22, 24, 31]. In [40], investigation was done to compare the optimal 2D Haar-Hilbert Wavelet Transform and classical Log-Gabor filter feature extractors, with their results tested on Bath iris database in order to deduce the efficient algorithm. Besides the comparison of various approaches as done in [40], other techniques were also introduced such as; block sum method [41] which extracts iris features using multi-resolution feature extraction and Haar transforms. Ghodrati *et al.*, [42] used an optimized Gabor filter parameter estimation approach implemented using Genetic algorithms in order to reduce the length of the feature vector by employing a robust feature selection strategy. Various iris matching techniques have also been proposed to reduce the effect of noise and to improve the robustness of iris feature matching. No single biometric system has proved to be robust against all capturing environments and attention has been shifted towards combining information in order to complement individual modalities. With more attention growing towards fusion; the effect of noise has not been accounted for during fusion because most fusion approaches such as reported in [5, 43, 44, 45, 46, 47, 48, 49, 50, 51, 52, 53, 54] use simple sum rule and weighted sum rule based methods which do not account for noise. Fusion of information should be able to produce robust results based on the data, information or type of fusion and the approach taken. This work investigates some feature extraction techniques, feature matching techniques and fusion methods proposed in the literature in order to establish the gaps and improve from the current state of iris recognition. An adaptive fusion method is proposed based on the quality of the features in order to cater for features extracted from the noisy region. This approach offers potential solution of solving the poor recognition rates caused by noisy regions as discussed above.

1.2 Problem Statement

State-of-the-art iris recognition systems [17, 18, 19, 20, 21, 22, 23, 24, 28, 29, 32, 33, 34, 35], experience high False Rejection Rate (FRR), False Acceptance Rate (FAR) and Equal Error Rate (EER). Since Daugman's system [13, 55] iris biometric research advanced with technology and begins to pick up speed. Research contribution evolved and new methods were proposed to challenge and improve Daugman 's algorithm [11, 17, 22, 24, 31, 33, 56]. Various feature extraction techniques and matching techniques have been proposed to improve reliability and robustness of iris recognition systems [57]. However, the target has not been successfully realized as aimed in iris recognition research. The main objective is to achieve 0% of false rejection and false acceptance in both ideal and non-ideal conditions of which in an ideal condition and in real world applications seems to be difficult to achieve and maintain due to noise. Current techniques address this problem by minimizing the false rejection and false acceptance, including the equal error rate using combination of iris matching algorithms. Individual matchers always have efficiency problems and it has been adopted and widely accepted that multiple biometrics offers added advantage and overcome most challenging problems posed by individual modalities. Fusion approaches were therefore introduced to enhance the recognition performance and accuracy of biometric systems based on their FAR and FRR. Multiple representation of features using multiple biometrics or using multiple feature extractors and matching techniques has received considerable attention and proved to be a promising alternative which is robust against spoofing and repudiation. Within the proposed fusion methods implemented within the iris recognition parlance, research has been shifted to simple sum fusion and weighted sum fusion due to their ease of implementation. Simple sum fusion averages the scores from individual matching algorithms and produce one fused score. The bias by one matching algorithm as a result of poor performance also influence the fusion score in a bad way. The weighted fusion approach on the other hand assigns weights to each matching algorithms based on the recognition accuracy of each individual matcher. If the individual algorithms have been implemented without taking noise into effect, the weighted fusion cannot be efficient. For this reason, an adaptive multi-algorithmic fusion was proposed and implemented by combining matching scores generated from four individual matching techniques to produce a robust advanced fusion technique. The proposed fusion approach solves the above mentioned challenges faced with other fusion approaches by devising the optimal fusion strategy based on the feature quality measures.

1.3 Research Objectives

The key objective in this work was to investigate the effects of varying feature quality parameters tested against two public databases and then incorporate them into the proposed adaptive weighted fusion technique of four iris matching algorithms.

1.4 Research Questions

This work investigates the effect of quality parameters measured at the feature level before feature extraction to enhance recognition performance based on fusion techniques. For this reason, this work intends to answer the following research questions:

1. Can fusion of multiple matching improves the performance of an iris recognition system?
2. Can quality parameters based on feature quality measures improves the accuracy of a fusion algorithm?

1.5 Research Hypothesis

This work aims to test the following hypothesis based on the known score level fusion approaches:

1. If fusion of simple sum and weighted sum rule improves the performance of iris recognition system, then an adaptive weighted fusion should improve the performance of the system even more.

2. If image quality parameters improves recognition performance and system accuracy then quality parameters assigned at feature level can improve performance and accuracy even more.

1.6 Research Contribution

This work contributes to the iris recognition literature by introducing a novel adaptive score level fusion technique based on weighted minimum fusion rule.

1.7 Delimitation, Limitations and Assumptions

The focus of this study will concentrate mainly on iris matching algorithms, and therefore the following assumptions are made:

1. This study is limited to CASIA and UBIRIS because images from other databases have not been accessed.

2. This study is constrained to sum rule and minimum fusion rule only.

3. The segmentation algorithms, iris feature extraction algorithms and the feature matching algorithms have been adopted from the previous research works.

4. The performance of this work is evaluated only against simple sum rule, non-adaptive weighted sum rule and minimum rule only.

1.8 Summary

This chapter gave a full description of the work done in this dissertation. The chapter started with an introduction to various automated iris recognition system. The introductory section gave basic concepts about automated iris recognition systems, current achievements and challenges currently faced by them. The ”research problem statement” section gave a full description of the problem that this work solves. Research objectives, research questions, research hypothesis and research contribution followed immediately after the research problem statement. The objectives of the research are clearly defined and they are fully described in the methodology section. Research questions that this work is trying to answer are also given followed by the claims. Research questions and claims are answered and proved in the methodology and results chapter. The research contribution section gave new knowledge contributed in the iris recognition field.

1.9 Dissertation Overview

The remainder of this dissertation is arranged as follows: Chapter 2 present a review of relevant literature about iris recognition systems as unimodal and multi-biometric. Chapter 3 covers the theory of the general works done in iris fusion and general frameworks of fusion architectures. Chapter 4 presents the research methodology and design strategy employed in this research work. Chapter 5 presents results and interpretation their interpretation. Chapter 6 presents discussion of the overall research and results obtain in chapter five. Recommendations, based on the analysis of results are also presented in this chapter. Possible future directions of research in this topic are also proposed. Finally, concluding remarks are made. The detailed steps for pre-processing, segmentation, feature extractions and feature matching have been outlined in the appendices.

Chapter 2

Related Work

This chapter reviews different techniques used to automate iris recognition system. The literature surveyed in this work exclusively contains more work on uni-modal iris recognition systems and multi-algorithmic iris recognition systems. Score level fusion techniques are discussed more than other levels of fusion, and all the gaps are outlined. The gaps filled in this work have been explicitly explained.

2.1 Related Work in Iris Recognition systems

For the past decade, iris biometric has been showing advances in automated authentication services. Since the first iris recognition system pioneered by Daugman, research has grown with immense interest in making iris recognition systems 100% accurate in both ideal and unconstrained environments. The iris recognition became an interesting research topic since the fundamental work of Daugman [10] which has attracted iris biometric researchers from all corners of the globe. Daugman who was approached by two eye scientists (Ophthalmologists) implemented and documented the first working iris recognition system detailed in [10, 13] which has been patented and deployed in many countries. In [10], monochrome CCD iris capturing camera (480×640) was used to capture the rich iris features because Near Infra-red (NIR) illumination in the range of 700nm-900nm was required to capture an iris image which will be visible also to a human vision. To locate the region of interest from the acquired eye image, the parameters for capturing the center of iris and pupil were determined by using an integrodifferential operator discussed in [10, 13] which locates and segments the pupil and the iris regions with their varying centre coordinates. Equation 2.1 is used in this technique.

$$max_{(r,x_0,y_0)} \left| G_\sigma(r) \frac{\partial}{\partial r} \oint_{r,x_0,y_0} \frac{I(x,y)}{2\pi r} \mathrm{d}s \right| . \tag{2.1}$$

here $G_\sigma(x,y)$ is the Gaussian kernel and $I(x,y)$ is the image and (x_0, y_0) and r are the center coordinates and radius of the circle respectively. In a survey carried out in

[58], it was discovered that the iris images encounter problem of size variation due to illuminations, pupil dilation and varying distances from the capturing camera. These variations need to be covered in all robust iris recognition systems, by implementing iris image normalization algorithms. Daugman used the Daugman's rubber sheet model to carter for image size variations, which assigns to each point within the iris region a pair of coordinates in polar form (r, θ) where the radial radius is in the interval $[0; 1]$ and θ is in the interval $[0; 2\pi]$. This mapping of an image $I(x, y)$ from its Cartesian coordinates (x, y) to polar coordinates (r, θ), is represented by a homogeneous rubber sheet model as shown in the following equation:

$$I\left(x(r, \theta), y(r, \theta)\right) \rightarrow I(r, \theta). \tag{2.2}$$

where $x(r, \theta)$ and $y(r, \theta)$ are the linear combination of the set of pupillary boundary point, $(x_p(\theta), y_p(\theta))$ and the iris boundary point $(x_s(\theta), y_s(\theta))$ which borders the sclera. These parameters are detected within the region of interest by computing the maximum values of the operator in equation 2.1, as:

$$x\left(r, \theta\right) = \left(1 - r\right) x_p(\theta) + r x_s(\theta). \tag{2.3}$$

$$y\left(r, \theta\right) = \left(1 - r\right) y_p(\theta) + r y_s(\theta). \tag{2.4}$$

The changes in size of the pupil which causes the iris to have an elastic deformation is corrected by the radial coordinates during normalization which ranges from 0 to 1, starting at the inner iris region to its outer region. The diagram in figure 2.1 represent the process of iris normalization to a rectangular block of equal dimensions. In figure 2.1, the segmented image is transformed into a rectangular block with the radial and angular parameters expressed in terms of breadth and length respectively. The height represents the radial direction and the length represents the orientation. To extract the features from the normalized iris region, the iris patterns were demodulated in order to get the phase information of the iris using the quadrature 2D complex even and odd symmetric Gabor wavelets as shown in figure 2.2. The use of Gabor wavelets in image processing has a long history as evidenced in [59, 60, 61, 62, 63, 64, 65, 66, 67, 68, 69, 70, 71], and their application in iris recognition is expanding, as reported recently in [72, 73, 74, 75, 76, 77, 78, 79, 80, 81, 82, 83, 84, 85, 86]. The equation for a 2D Gabor

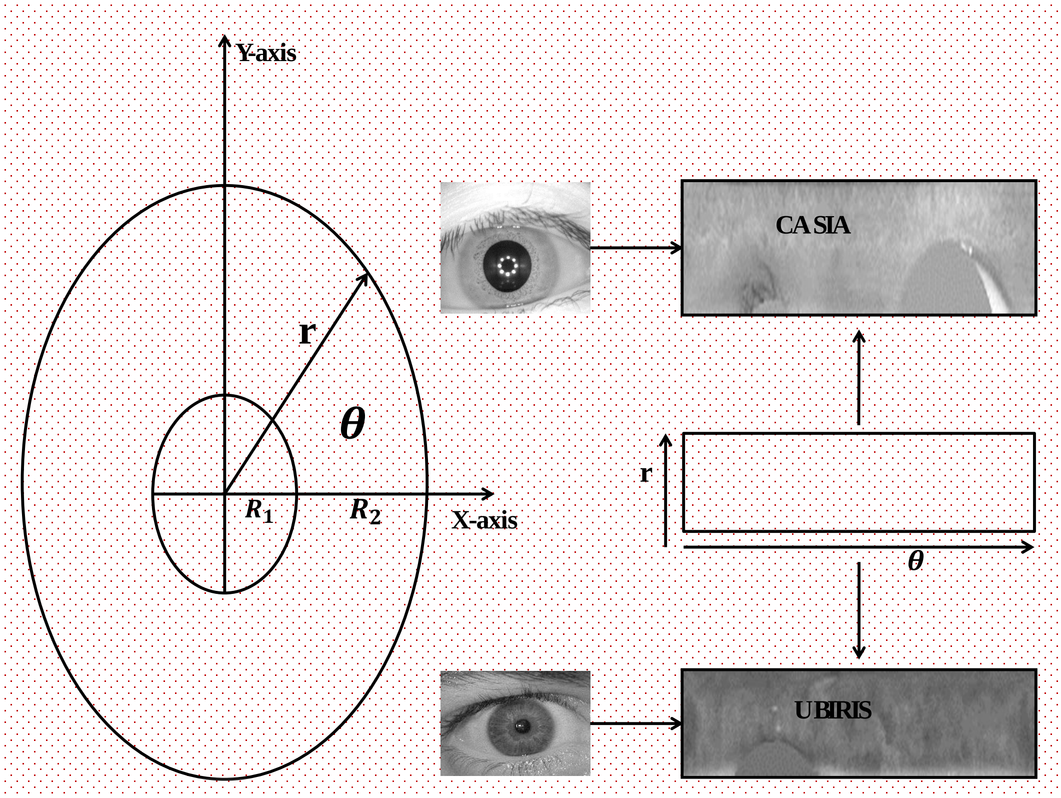

FIGURE 2.1: Daugman 's Rubber Sheet model for iris image normalization [10, 13]

filter in the image domain as discussed in [65, 70], is shown in equation 2.5 below:

$$G(x,y) = e^{-\pi\left((x-x_0)^2/\alpha^2+(y-y_0)^2/\beta^2\right)}.e^{-2\pi i(u_0(x-x_0)+v_0(y-y_0))}. \tag{2.5}$$

where the parameters, (x_0, y_0) is the pixel position of the image, α, β are the effective width and length of the filters respectively, u_0, v_0 is the modulation parameters with a spatial frequency given by $\omega_0 = \sqrt{(u_0^2 + v_0^2)}$ and their orientation is given by $\theta_0 = \arctan\left(\frac{v_0}{u_0}\right)$. In polar coordinates, equation 2.5 can be written as:

$$G(r,\theta) = e^{-i\omega(\theta-\theta_0)}e^{-(r-r_0)^2/\alpha^2}e^{-(\theta-\theta_0)^2/\beta^2}. \tag{2.6}$$

where the parameters α and β co-vary in reverse proportion with the spatial frequency ω in order to generate the self-similar multi scale 2D wavelet frequency selective quadrature filters located at θ_0 and r_0. With this information, the phase quantization identifies in which quadrant of the complex plane does the resultant phasers lie when an iris image

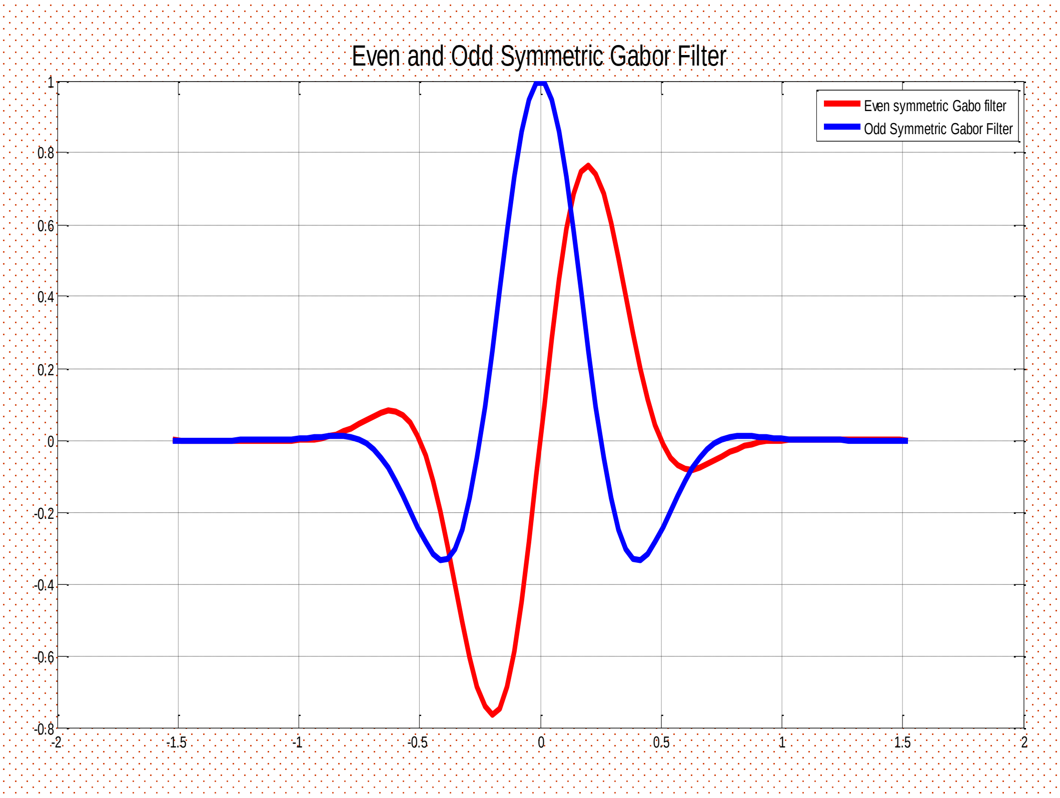

FIGURE 2.2: Even and Odd symmetric Gabor filters

is passed onto complex-valued 2D Gabor wavelets using the equation 2.7

$$h_{\{Re,Im\}} = sgn\left\{R_e, I_m\right\} \int\limits_{\rho} \int\limits_{\phi} I\left(\rho,\phi\right) e^{-iw(\theta_0-\phi)}.e^{-(r_0-\rho)^2/\alpha^2}.e^{-(\theta_0-\phi)^2/\beta^2}\rho \mathrm{d}\rho \mathrm{d}\phi. \quad (2.7)$$

where $h_{\{Re,Im\}}$, is considered the complex-valued bit whose real and imaginary values are in $\{0;1\}$ depending on the sgn, $I\left(\rho,\phi\right)$ is a dimensionless polar coordinate system which is scale and rotation invariant and which can correct the pupil dilation, α and β are the multi-scale 2D wavelets size parameters ranging from 0.15mm to 1.2mm on the iris, ω is the wavelet frequency spanning 3 octave inversely proportional to β, (r_0, θ_0) represents the polar coordinates of the each iris region computed. The idea of image processing at multi-scale level dates back to the works of Lindeberg as discussed in [87, 88, 89]. To classify the extracted phase information, Daugman used Normalized Hamming Distance (NHD) shown in equation 2.8 to perform 2.9 billion of iris comparisons.

$$HD = \frac{\|\left(CodeA \oplus CodeB\right) \cap \left(MaskA \cap MaskB\right)\|}{\|MaskA \cap maskB\|}. \quad (2.8)$$

where A and B are the two bit patterns and $A \oplus B$ is the sum of the disagreeing bit between A and B bit patterns $MaskA$ and $MaskB$ represent the mask bit vectors for the two bit patterns. Masek [30] prototyped Daugman 's automated system for research purposes. In [30], Hough transform was used to locate the region of interests instead of integrodifferential operator. The Hough transform takes the form shown in equation 2.9:

$$x_c^2 + y_c^2 - r^2 = 0. \tag{2.9}$$

where the parameters x_c, y_c and r are the center coordinates of the Hough circle. Parabolic Hough transform is also a useful tool which can approximate the eyelashes, top and bottom eyelids using parabolic arcs as represented by equation 2.10.

$$\left(-\left(x-h_j\right) sin\theta_j + \left(y-k_j\right) cos\theta_j\right)^2 = a_j \left(\left(x-h_j\right) cos\theta_j + \left(y-k_j\right) sin\theta_j\right). \tag{2.10}$$

where a_j controls the curvature of the circle, (h_j, k_j) is the point of peak of the parabolic function and θ_j is the angle of rotation with respect to the $x - axis$ axis. There are couple of disadvantages of using the Hough transform because it requires the threshold value to be assigned before edge detection which may lead to removal of useful edge points, which poses enormous challenges when it fails to detect both the pupil circle and the iris circle. To extract the rich iris features, [30] used the 1-D log-Gabor wavelet shown in equation 2.11 instead of 2D Gabor wavelet used in [10, 13]:

$$G(f) = exp\left(\frac{-\log\left(f/f_0\right)^2}{2\log\left(\sigma/f_0\right)^2}\right) \tag{2.11}$$

where f_0 and σ are defined as the central frequency and the bandwidth of the filter respectively. The extracted features were matched using the NHD matcher in equation 2.8 as used in [10, 13]. The Gabor filter, despite being a valuable texture extractor has its disadvantages as it assigns similar weights for both fragile and consistent bits which require different scale measurement. The low frequency components are under represented by this technique, and each time the even symmetric Gabor filter has a bandwidth of more than an octave it will have a DC component [90] which suppresses the significance of low frequency components in the feature vector. These drawbacks have a serious impact on the recognition of subjects posing serious threats to system performance. Various iris region extractors have been proposed to challenge the bias posed by Gabor filters [9, 17, 21, 22, 24, 91, 92]. Various techniques are still under review in pursuit of an anticipated iris recognition system especially where the features have different weights measurements as used in Weighted Euclidean Distance (WED) and Weighted Hamming Distance (WHD) which are also considered efficient. Tan [9] proposed a Multi-Channel Gabor Filtering which Zhu *et al.* [93] and Ma *et al.* [94] adopted, modify and reused in their iris recognition system. This technique uses the same iris preprocessing technique of Hough transform as used in [30] to locate the region of interest from a captured iris image. The segmented image was then normalized to compensate for the changes in image sizes caused by illumination changes, pupil dilation which may seriously affect the template matching stage. The image was then transformed into a block of fixed size of (64×512) which were then subdivided into eight sub smaller images of block size (64×64). As normalized images can be prone to noise and low contrast that may have emerged as a result of non-uniform illumination due to varying light source positions, the normalized iris image was enhanced using histograms equalization method, and high frequency noise was removed using a low pass Gaussian filter. The desired features where extracted by employing the multi channel Gabor filtering technique shown in equation 2.12.

$$G(x,y;\theta,f) = exp\left(-\frac{1}{2}\left(\frac{(xcos\theta + ysin\theta)^2}{\delta_x^2} + \frac{(ycos\theta - xsin\theta)^2}{\delta_y^2}\right)\right) cos\,(2\pi f x)\,. \quad (2.12)$$

where f is the frequency of the sinusoidal plane wave along the direction θ from the $x - axis$, δ_x and δ_y are the space constants of the Gaussian envelope along the x and y axes respectively. The frequency parameter f was chosen to be the power of 2, and the central frequencies used in [94], where $2, 4, 16, 32$ cycles per degree. For each central frequency f, filtering was done using $\theta = 0°, 45°, 90°, 135°$. With these set parameters, twenty Gabor filters were obtained, each with a different frequency and orientation, and each of the eight sub images where filtered by these twenty Gabor filters leading to 160 output images from which the iris features where extracted. In [93], the features were extracted without dividing a normalized image into blocks. To upgrade the recognition system presented in [93], Ma *et al.* [94] divided the normalized iris image into eight blocks of equal size. These eight blocks of images were processed separately for the purpose of obtaining more well distributed features. The features from [93] were expressed in terms of the mean and the standard deviation and stored in a 24×2 matrix, while in [94] the feature vector was calculated as the Average Absolute Deviation (AAD) of each output image, and obtained from equation 2.13 :

$$V = \frac{1}{N}\left(\sum_{N} |f(x,y) - m|\right). \tag{2.13}$$

where, N is the number of pixels in each image, m is the mean of each image, $f(x,y)$ is the pixel value at position (x,y). The AAD feature was reported in [94] as a statistic value similar to the variance, but results from [94] demonstrated that it performs better than variance. The AAD of each filtered image constitute the components of the desired feature vector arranged to form a 1D feature vector of length 160 for each output image. The process of extracting the features is explained in equations 2.14-2.19:

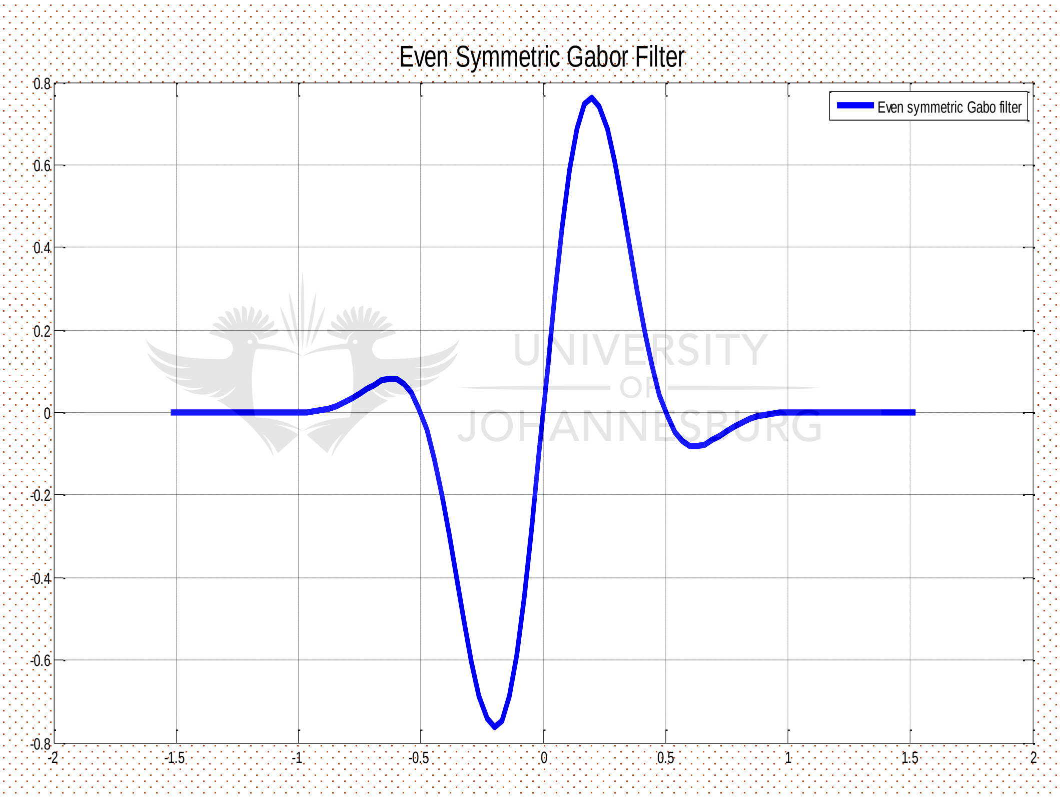

FIGURE 2.3: Even symmetric Gabor filter

$$G_E(x,y) = e^{-\left(\frac{x^2+y^2}{2\sigma^2}\right)} cos(2\pi f(\phi)). \tag{2.14}$$

and the odd symmetric Gabor filter is expereesed the form shown in equation 2.15

$$G_O(x,y) = e^{-\left(\frac{x^2+y^2}{2\sigma^2}\right)} sin(2\pi f(\phi)). \tag{2.15}$$

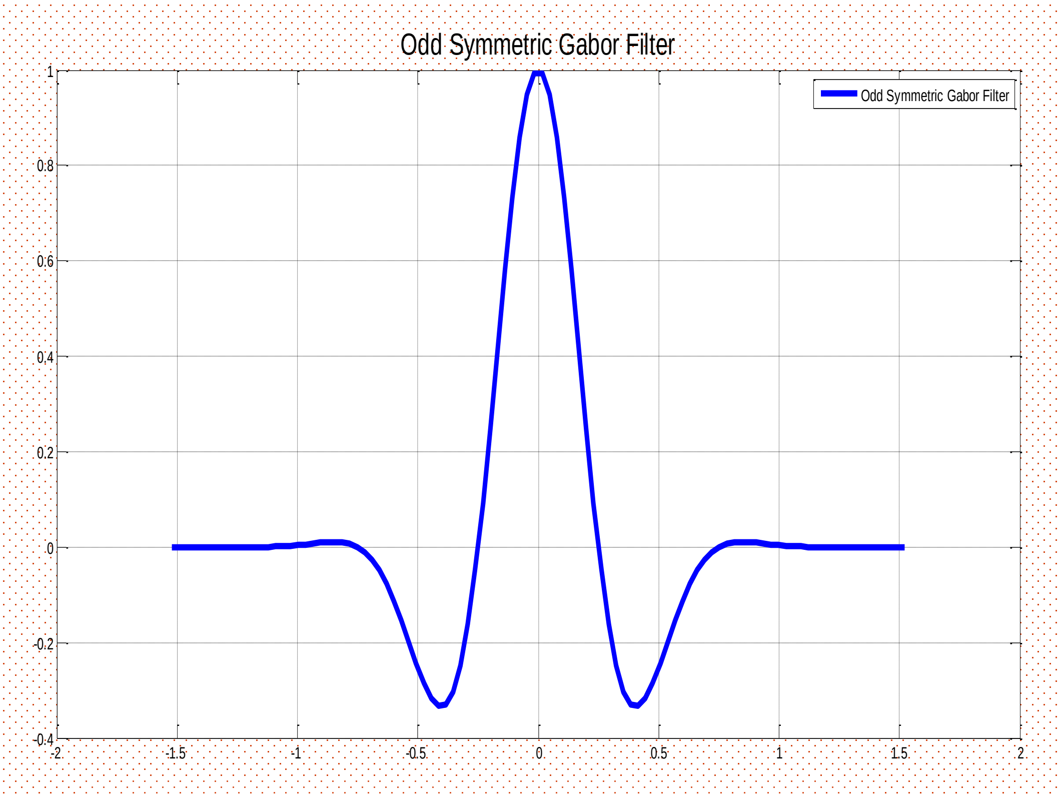

FIGURE 2.4: Odd symmetric Gabor filter

where the function ϕ in equations 2.14 and 2.15 is represented as a function of θ in equation 2.16,

$$\phi = xcos\theta + ysin\theta. \tag{2.16}$$

The output of the image was obtained by convolving an input image with a filter, as shown in the following equation:

$$P_E(x, y) = G_E(x, y) * I(x, y). \tag{2.17}$$

where P_E in equation 2.17 represent the output images of the even Gabor filter

$$P_O(x, y) = G_O(x, y) * I(x, y). \tag{2.18}$$

where P_O in equation 2.18 is the output image of the odd symmetric Gabor filters. The extracted features are expressed in terms of the mean and standard deviation, using the following equation;

$$Q(x, y) = \sqrt{P_E^2(x, y) + P_O^2(x, y)}. \tag{2.19}$$

The features obtained in equation 2.19 are matched using WED, shown in equation 2.20, which measures how similar the collection of values are, between two given vectors. This method computes WED between the corresponding extracted feature vectors, and is very useful when the templates are represented in terms of integers or floating point values. The variables for the weighting coefficients, number of sub images and the total number of features extracted from each image are defined as parameters of WED formula defined in equation 2.20, as used by [9] and [93].

$$WED(K) = \sum_{i=1}^{N} \frac{\left(f_i - f_i^{(k)}\right)^2}{\left(\delta_i^{(k)}\right)^2}. \tag{2.20}$$

where f_i represents the i^{th} feature of the unknown iris, $f_i^{(k)}$ is the i^{th} feature of the iris k considered as mean of iris k, and $\delta_i^{(k)}$ is the standard deviation of the iris k. When matching the features, the unknown iris is considered a known iris k, if the WED is a minimum at iris k. However, with these same conditions, Ma *et al.*, [94] used a different version of the weighted euclidean distance, in iris recognition, based on the same feature extraction techniques as used by both [9] and [93]. The formula used by [94] is given in equation 2.21

$$WED(K) = \sqrt{\sum_{i=1}^{B} A_i \sum_{j=1}^{N} \left(f_{(i,j)}^{k} - f_{(i,j)}\right)^2}. \tag{2.21}$$

where the parameters B is the number of sub-images, A_i is the i^{th} weighting coefficient, N is the total number of features extracted from the image ,f_i is the i^{th} feature of the unknown iris, f_i^k is the i^{th} feature of the k^{th} iris template as used in equation 2.21. The WED compares the features of an unknown iris with the enrolled irises in the database to get a match. When matching the input feature vectors with the class templates, the minimum of the five scores is taken as the final matching distance score, and this minimum is considered the threshold. The WED approach is very useful when the template is composed of integers [93]. Mitra *et al.*, [95], reported an interesting result from different of Gaussian employed on correlating illegally packed vehicles in local patches. Difference of Gaussian has so many fundamental applications in image processing, some of them have been reported in [96]. Sun *et al.*, [19, 21] and Dong *et al.*, [24] proposed a Multi-Lobe Differential filter (MLDF) which is a type of a Gaussian filter with multiple lobes, giving it an advantage over Gaussian filters because it can capture and encode iris regions ranging from small to large regions. This technique was proposed in an attempt to model the iris features in an ordinal scales. They measured the region of iris as being either dark or light, thereby coding a digital iris template from the iris regions. The MLDF shares the same properties as the difference off-set Gaussian, and they all evolved from difference of Gaussian. The difference of Gaussian takes the following form;

$$DoG(x, y) = G(x, y, \sigma_1) - G(x, y, \sigma_2). \tag{2.22}$$

The difference of Gaussian as defined by equation 2.22, has been receiving attention as a useful tool in image processing research since the works in [97, 98, 99, 100]. The equation of MLDF as shown in equation 2.23, has its basis grounded on [21, 95, 96, 101, 102, 103];

$$MLDF = C_p \sum_{i=1}^{N_p} \frac{1}{\sqrt{2\pi\delta_{pi}}} e^{\frac{-(X-\mu_{pi})^2}{2\delta_{pi}^2}} - C_N \sum_{j=1}^{Nn} \frac{1}{\sqrt{2\pi\delta_{nj}}} e^{\frac{-(X-\mu_{nj})^2}{2\delta_{nj}^2}}. \tag{2.23}$$

where the parameters μ denotes the mean of the 2D Gaussian filter, δ denotes the scaling factor of the 2D Gaussian filter, N_p is the total number of positive lobes detected, N_n is the total number of negative lobes detected. C_p and C_n are the coefficients which ensure that the total sum of the MLDF is zero, i.e, $C_pN_p = C_nN_n$, as used in equation 2.23. The features extracted using this technique were digitized based on the ordinal representation of the iris regions. Despite the ease of computation of ordinal measure, the parameters involved in MLDF needs major attention when selecting the intra-regions and inter-regions. The main parameters include the shape of the region, the spatial location of the region, the spatial configuration of the region, their inter-region distances; details of these parameters are discussed later in this section. The type of the desired features in all the chosen regions, should be taken into consideration, such as the average pixels intensity in each region, the wavelet coefficient of the region and so forth. Figure 2.5 which depicts the odd and the even Gabor filters and their associated ordinal measures before features are extracted. Figure 2.5, (i) shows the odd Gabor filter and its ordinal measures designated by positive lobes (+) and negative lobes (-) and (ii) depicts the even Gabor filters with its ordinal measures. The positive and negative lobes are also called the excitatory and inhibitory lobes respectively. Figure $B.1$, in appendix B represents the process of comparing the regions and how the regions can be encoded into an iris digital signature. To extract the iris ordinal features, the input image has to be passed

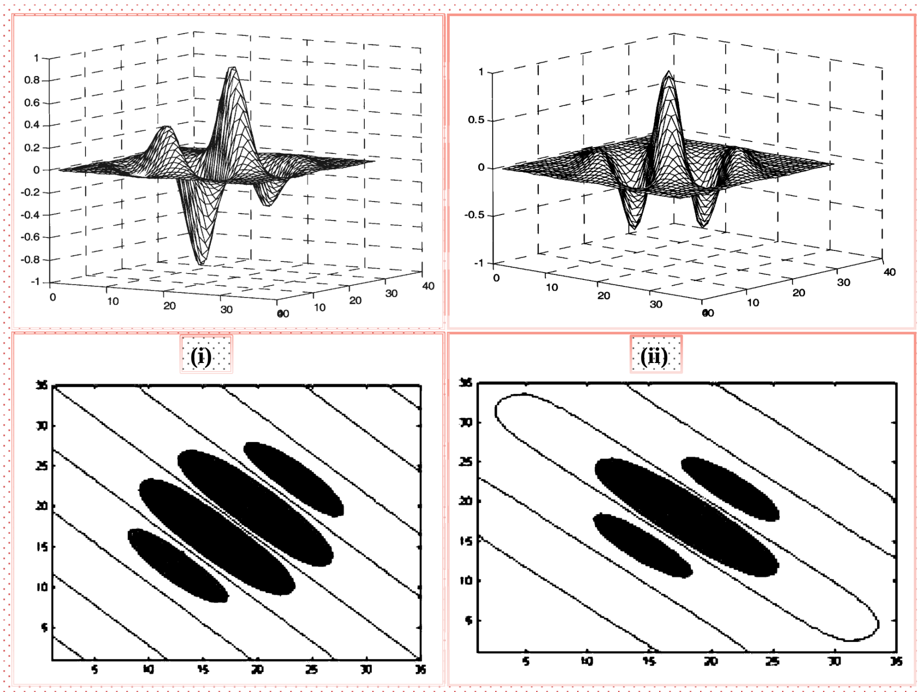

FIGURE 2.5: The Even and Odd Gabor filters with their ordinal measures [21]

into an ordinal filters. There are prime parameters that needs to be considered; namely (i) the scaling parameter ($\sigma = \pi/2$) which controls the shape or the scale of the lobe. Sigma (σ) was taken as a standard deviation because the lobes were selected as Gaussian filers, (ii) the parameter $d = 4, 8, 12, 16$ separates the measures the distance between the centres of the excitatory and inhibitory lobes and (iii) the orientation of the filters which is determined by measuring the angle $\theta \in [0; 2\pi]$ between the horizontal axis and the lines which cuts the excitatory and inhibitory lobes, as mentioned above. The features extracted using this approach were classified using the WHD which is an improved NHD. The improvement from the hamming distance was done by introducing the weight map W_A in the iris matching function of the registered iris class A, which is denoted by an n-dimensional vector,

$$W_A = \{w_1, w_2, ..., w_n\}. \tag{2.24}$$

shown in the formula below:

$$D_A = \frac{\|(codeA \oplus codeB) \times W_A\|}{\|W_A\|}. \tag{2.25}$$

The weight map is generated using the following formula:

$$P = \frac{1}{k \times k} \sum_{a=1}^{k} \sum_{b=1}^{k} code_a \odot code_b. \tag{2.26}$$

and the parameter,

$$P = p_1, ..., p_2. \tag{2.27}$$

where P is a vector with the same length as the iris codes. Durai and Karnan [31] argued, that feature-based iris recognition matching performance is highly influenced by various parameters in the feature extraction process. To overcome this challenging concern, they proposed a Hierarchical Phase Based (HPB) matching technique adopted from phase based matching technique introduced in [92]. The technique here is to bypass some of the phases in template matching algorithm such as image normalization, specular reflection, eye lashes detection and removal or masking. This algorithm only masks the bottom eyelid as the top eyelid and eye lashes are avoided from the feature extraction. To accomplish this task a given image say $f(n_1, n_2)$ is divided into five blocks sub-images of equal dimensions. The details of implementation of this process is shown in appendix D, figure D.1. The feature vectors are created independently for query images in each block and then compared with the stored database. Based on the proximity of the features vectors and the templates, each subsystem computes its individual matching score. These individual matching scores are finally combined into a total score which is passed to the decision making module, [31]. Matching the features from each blocks demands the computation of Phase Only Correlation (POC), and then sum the POC value for each block to contribute into a single match score value, as shown in the following equations:

$$F(K_1, K_2) = \sum_{-M_1}^{M_1} \sum_{M_2}^{M_2} f(n_1, n_2) W_{N_1}^{k_1 n_1} W_{N_2}^{k_2 n_2}. \tag{2.28}$$

where the variables $F(K_1, K_2)$ represents the 2D Discrete Fourier Transform (DFT) of image $f(n_1, n_2)$, as used in equation 2.28.

$$G(K_1, K_2) = \sum_{-M_1}^{M_1} \sum_{-M_2}^{M_2} g(n_1, n_2) W_{N_1}^{k_1 n_1} W_{N_2}^{k_2 n_2}. \tag{2.29}$$

where the variables $G(K_1, K_2)$ represents the 2D DFT of image $g(n_1, n_2)$, as used in equation 2.29. simplifying equation 2.28, we get the following equation:

$$F\left(K_1, K_2\right) = A_F\left(k_1, k_2\right) \mathrm{e}^{j\theta f\left(k_1, k_2\right)}. \tag{2.30}$$

where A_F is the amplitude phase component as used in equation 2.30. Equation 2.29 can also be simplified and produce the following equation:

$$G\left(K_1, K_2\right) = A_G\left(k_1, k_2\right) \mathrm{e}^{j\theta f\left(k_1, k_2\right)}. \tag{2.31}$$

The cross spectrum of the two 2D DFT images $F\left(k_1, k_2\right)$ and $G\left(k_1, k_2\right)$ is given by $R_{FG}\left(k_1, k_2\right)$, and is given by the following equation:

$$R_{FG}\left(k_1, k_2\right) = \frac{F\left(k_1, k_2\right)\overline{G\left(k_1, k_2\right)}}{\left|F\left(k_1, k_2\right)\overline{G\left(k_1, k_2\right)}\right|}. \tag{2.32}$$

which can be simplified to give the following equation:

$$R_{FG}\left(k_1, k_2\right) = \mathrm{e}^{j\theta\left(k_1, k_2\right)}. \tag{2.33}$$

where $k_1 = -M_1, ..., M_1$ and $k_2 = -M_2, ..., M_2$, $\overline{G\left(k_1, k_2\right)}$ is the complex conjugate of $G\left(k_1, k_2\right)$ and $\theta(k_1, k_2)$ is the phase difference between the two images $F\left(k_1, k_2\right)$ and $G\left(k_1, k_2\right)$. The location of the peak can be estimated by finding the changes in the maximum value in (x, y) domain as shown in the equation below:

$$(\Delta x, \Delta y) = \arg\max_{(x,y)}\{R_{FG}\}. \tag{2.34}$$

Chaskar and Sutaone [104] presented a novel technique for fast iris recognition using the match color to detect the rich iris features and generate a stable key from the iris image. In this approach, color comparison was used to detect color variations within an image, and use this information to check if the same color pattern variations is available between the probe image and the reference image. A fuzzy membership weighting function is applied to the color spectrum between the probe image and the reference image before the matching process. The matching was computed using the Manhattan distance measure to generate the similarity scores ranging from 0 to 1000. Khaladkar and Ganorkar [56] presented another iris recognition system using features extracted from the Haar wavelet transform. In [56], the segmentation and normalization of the segmented iris image followed the Daugman process, using the intergrodifferntial operator showed in equation 2.1 and the rubber sheet model for normalization. The matching was done using the same normalized hamming distance, even though the procedure of getting the features differed between the Gabor filters and Haar Wavelets. The results reports an improved recognition accuracy of 99.94%, FAR of 0.005 and FRR of 0.01. In [105, 106], noisy iris images were used to assess improvement in recognition accuracy. A classification approach was implemented which measures the difference between the distribution of eyelashes between the right and left eye images. Classification was also done based on the color of iris region which bests discriminate between the intra class and inter class variations. The comparison between the iris templates were measured in terms of the Euclidean distance, NHD and χ_{square} distances with the color space models and produce a discriminative index of 1.6398. The effect of noise and failure of feature extraction techniques is evidenced in [33, 35, 36, 37, 41, 107, 108, 109], where the recognition failure of 21.2% was detected based on images collected over a monthly intervals. Sibai *et al*, in [110] used an artificial feed forward network to estimate the parameters for iris image preprocessing to avoid noisy regions to reduce recognition accuracy. The recognition accuracy was measured using BrainMaker simulations and report an achievement of 93.33% regardless of similarity metric used. Durai and Karnan [31], used the HPB matching technique which uses the approach adopted from phase based matching algorithms. However, even though their matching technique seemed robust, their method for extracting features is not and cannot be automated. Dong *et al.* [24], used the personalized weight map approach which uses features extracted using ordinal measures extracted using the MLDF. In [111], two methods were used to detect the region of interests namely; the Canny edge and the circular-Mellin algorithms. The features were extracted using three feature extractors namely: Haar wavelet, Embedded-tree zero wavelets and fuzzy neural networks. Classification was done using the normalized hamming distance. A recognition of 99.25% was reported by this method. Although many techniques have been proposed, identity verification of individuals remains a challenging task when it has to be automated with a high accuracy and robustness against spoofing attacks and repudiation. To overcome this challenge, robust iris feature extractors and iris matchers should be implemented. However, within the current iris recognition systems, iris feature matching has not been exhaustively explored and it remains a very important module which can reduce the false accept rates FAR and the false rejection rates FRR. Ng *et al.,* [23] introduced a Rapid Haar Wavelet decomposition for extracting the rich iris feature. The features were classified using the hamming distance matcher and achieved recognition accuracy of 98.45% tested on CASIA-IrisV3-Interval. Abhyankar and Schuckers [112, 113] used a biorthogonal wavelet which encode the iris information by lifting technique. The encoded information was classified using the NHD matcher. The performance of the system was tested against CASIA dataset and produced a FRR of 0% and FAR of 0.03% at a threshold value of 0.4. Ross [114] stressed the ongoing research in iris recognition and mentioned the need to increase the accuracy and robustness of iris recognition systems even on unfavorable imaging environment. It is also stressed in that research that iris biometric should be extended to template protection. In [115, 116] a secure iris biometric system is introduced using the local intensity variations and visual cryptography respectively, within the iris region. In [117], fusion of information extracted from visible light source and NIR was introduced, based on a newly established iris images. The proposed study challenges the current iris matching algorithms by developing a novel approach to improve iris matching performance by combining selected current iris matchers to produce a robust iris matching technique.

2.2 Related Work in Iris Fusion

Score level fusion is considered a very promising approach having greatest potential of improving biometric system recognition accuracy, system performance and system robustness against spoofing attacks and repudiation. The problem of feature matching has long been studied, and has led to the introduction of some techniques that enhance the matching decisions. Various fusion techniques have been introduced with different fusion levels. However, the process involved in implementation and data collection of some levels of fusion can be a challenging task, and this makes a score level fusion the best choice because of its use of computation and data collection. Matching scores, have valuable information which describes the performance of both feature extractors and the feature matchers. Fusion techniques can be implemented at various levels for various reasons and giving different levels of recognition accuracy and performance. Amongst the fusion techniques with different levels of fusion as discussed in [43, 45, 49, 53, 54, 118, 119, 120, 121, 122, 123, 124, 125], score level fusion is the most widely used. This is due to its ease of acquiring data from individual matching algorithms both from mono-modal and multi-modal point of view. Score level fusion has appeared in literature on different view points. A detailed review of iris recognition systems and various fusion strategies at different fusion level has been presented in [43, 122]. Challenges may arise in implementing weighted sum fusion in order to optimize the weights. A Genetic Evolutionary Computation (GEC) based score level fusion was introduced in [126] to optimize the weights in score level fusion. As mentioned in [47], fusion of information creates robustness against spoofing attacks and improves recognition performance. A comprehensive evaluation of score level fusion, assessing the normalization techniques and the score level based fusion techniques is found in [127]. Fusion for single biometric such as iris was introduced in [128, 129, 130, Gawande et al.]. Wang *et al.,* [131] did an interesting research when he integrated the information from left and right eye irises collected from the phase information and the Discrete Cosine Transform (DCT) using multi-level fusion, which includes multi-algorithmic and multi instance fusion. The multi-algorithmic fusion combines the matching scores generated from the improved phase information and tDCT. The multi instance data was collected from the left and right irises taken from each subject. The results of this experiment was tested against the noisy UBIRIS image database and demonstrated improved recognition performance and accuracy over a single database. Zhanga *et al.,* [44] combined the iris global and local features extracted using the 2D log Gabor filters. The resulting features were classified using the WED and the NHD. Woodard *et al.,* [132], combined the periocular and the iris patterns at a matching score level using a simple sum fusion rule. The templates for iris and periocular regions were extracted separately using different feature extraction techniques. Fusion of scale invariant transform and speed up robust features has been discussed in [52]. The results of this fusion demonstrated that a recognition accuracy of 88.70% from CASIA and 98.02% from BATH databases have been achieved. Tan *et al.*, [133] introduced a multi-modal iris image fusion strategy based on four matching techniques based on ordinal measures matching, color histogram matchings, texton representation and matching the semantic information from the image. Colores-Vargas *et al.,* [134] implemented an iris fusion technique based on video images using Principal Component Analysis (PCA) to enhance the iris recognition accuracy under unconstrained environment. They reported 83% of success on their overall experiments. Desoky *et al.,* [135] combined the iris information at the base templates at the feature level fusion using a plain majority rule voting system. Each base template assigns an input feature vector to various classes which are fused to produce one feature vector of fused template. In [48], various factors influencing image noise were estimated individually based on different forms of occlusions. The estimated factors were then fused using the Dempster-Shafer theory of evidence. In [136], fusion was done by combining the rotation invariant and rotation compensation iris code based scheme. The motive was to reduce the computational speed and complexity, which has been reduced by 20%. In [50], an incremental fusion strategy was implemented in order to reduce the computational time. The results reports reduction of about 5%. Soltana *et al.,* [120] used an adaptive feature and score level fusion techniques to select and fuse the most relevant features and optimize the fused score using genetic algorithms. To measure the recognition accuracy and performance, a Linear Discriminant Analysis (LDA) was used to reduce the dimensionality for each feature type. Radu *et al.*, [137] implemented a score level fusion for combination of images from various scanners and various color intensities based on unconstrained environments. The images captured were from iris digital cameras and mobile phones. The development of this method was based on remedying the matching of noisy iris images.

2.3 Summary

This chapter gave a full review of current automated iris recognition systems, including their fusion approaches. It was discovered that the discussed approaches face many challenges posed by noise and they fail to account for noise regions during matching module. It was also discovered that there is no single biometric system introduced so far which can produce excellent performance and achieve a 100% recognition accuracy alone in all the imaging conditions. Migration to multi-algorithmic techniques have been clearly introduced bridging the gap between individual systems and fusion techniques. The challenges faced by each method reviewed were identified as failure to map the noise regions during fusion using feature quality components, which leaves a gap to be filled. For this reason an adaptive weighted fusion was introduced in this work to bridge the gap. Accounting for noise using feature quality metrics can reduce the effect of noise which results from segmentation failure. The details of fusion architecture and their categories are discussed in the next chapter.

Chapter 3

Theoretical Considerations

This chapter explores widely used fusion approaches and their architectures. The fusion approach introduced in this work was not discussed but its counter parts namely simple sum, best linear and minimum fusion are heavily discussed.

3.1 Fusion Architectures

Multiple integration of information has been receiving enormous attention due to its potential to produce large amounts of non-integrated results. It improves biometric recognition performance and offers potential to reduce the failure to enroll rates and failure to acquire rates. This is accomplished by the weights assigned to different modalities with varying levels of recognition performance. Modalities which produces low errors are assigned more weights to compensate for other modalities with potential of producing high errors. Fusion algorithms enables individual modalities to support each other which leads to improved recognition performance.

3.2 Categories of Fusion

Fusion can be categorized in three different architectures; namely (i) Serial Fusion: where features are extracted and matched sequentially, (ii) Parallel Fusion: where the features from individual modalities are extracted and matched simultaneously and (iii) Hierarchical Fusion: where serial and parallel fusion techniques are combined together to produce a more robust fusion results. Hierarchical fusion approach is more flexible and secure but computationally expensive due to the hardware and processing power needed. More information about these fusion categories have been detailed in [53, 122, 123, 125]. From each architecture mentioned above, fusion of information occurs in one of the following five categories. The choice of category depends on the availability of information to be fused and the application which the system is aimed to be used in. Table 3.1 and the following item explain these categories:

TABLE 3.1: Table of categories of fusion [122]

Fusion Category	Modality	Algorithms	Biometric trait	Sensors
Multi-Sensor	One	One	One	Two or more
Multi-Algorithmic	One	Two or more	One	One
Multi-Instance	One	One	Two or more	One
Multi-Sample	One	One	Two or more	One
Multi-Modal	Two or more	Two or more	Two or more	Two or more

(a) **Multi-Sensor :** A single biometric trait is acquired using various sensors giving varying levels of input.

(b) **Multi-Algorithmic :** Single biometric trait is acquired using same sensor but features are extracted using different features extraction techniques. Extracted features are matched using different feature matching techniques, leading to non-homogeneous scores generated from each matching technique.

(c) **Multi-Instance :** Multiple instances are captured from the same subject using same sensor and fused together. For iris biometric, instances includes left and right eye of the same person.

(d) **Multi-Sample :** Multiple samples of the same biometric modality are acquired using the same sensor but with varying illumination changes and capturing angles.

(e) **Multi-Modal :** Multiple modalities are captured using different sensors. These modalities includes, face and iris, face and fingerprint or iris and fingerprint.

3.3 Levels of Fusion

Fusion of evidence can be done at various levels depending on the purpose and application of the proposed system. The development of an architectural fusion structure depends on the type and level of fusion. The architectural design of a multi-biometric system gives the fusion approach to be implemented. The choice of architecture highly affects system accuracy and recognition performance [122, 131, 134, 137, 138, Gawande et al.]. The choice of a fusion architecture also relies on the type of available data to be fused. Various levels of fusion are discussed below.

3.3.1 Sensor Level Fusion

Integration of information can be done at the sensor level by combining raw data from different sensors. This fusion level can be accomplished if the same sensor can produce multiple reads of the same biometric modality from the same sensor or from different sensors. Information at this level is rich in content with highest level of noise which increase complexities. Complexities also arise when the raw data is not compatible to each other. Raw data from multiple sensors with varying degrees of sample quality may also impact compatibility. It is imperative to study the raw data and sensors thoroughly before fusion in this level.

3.3.2 Feature Level Fusion

Features are extracted from different sensors and then fused together using multi-sensor fusion category. Each sensor computes its own feature vector which will be encoded or represented in a different approach as compared to other features from other sensors or scanners. The combination of these feature vectors from various sources will lead to a high dimensional single feature vector which will demand feature reduction which will extract the optimal and robust features from the super set of features before further processing of the feature. This level of fusion is only achieved by incorporating features from multiple sensors reading a single biometric modality or multiple representation of the same biometric modality. Information is less rich in content but noise has been minimized during pre-processing and image normalization. Challenges faced with this level of fusion includes: (i) Normalization of compatible features can be computationally expensive, in order to bring all the features to a common scale and location, (ii) Adding features may fail to improve accuracy and recognition performance as a result of curse in dimensionality, a robust feature selection algorithm may be required in order to fuse only the best distinctive features. This level of fusion becomes impractical in many applications making integration at this level less useful.

3.3.3 Matching Score Level Fusion

The most widely used level of fusion is the score level fusion because of its ease in integrating raw scores representing individual modalities. Matching score fusion incorporates matching scores generated from different matchers, usually with different feature extractors. The obtained scores from each matchers represent the similarity or difference between the templates being matched. There are several approaches used to fuse the matching scores. The main idea of this type of fusion is to minimize the FAR at a given FRR [45, 51, 54, 118, 124]. A new score will be used for comparison with a new threshold. Integration of scores can be done in three main ways:

- **Classification Based Approach:** In classification approach, a feature vector is created from individual matching scores. The matching scores are then classified in terms of "accept as genuine" or "reject as impostors" classes using machine learning techniques such as Support Vector Machines (SVM). Serious challenges exist in the classification approach which includes; (i) unbalanced training data sets between the genuine and impostor distribution, (ii) varying costs of misclassification between accepting an impostor and rejecting a genuine user, which also depends on the type of application and (iii) the choice of classification technique to be used also creates problems.

- **Density Based Approach:** Density based approach depends on the likelihood ratio test which demands explicit of both the genuine and impostor score distributions. If the densities can be accurately estimated, density based approach can achieve optimal performance at any FAR. However, modelling of scores distribution can be computationally expensive.

- **Combination or Transformation Based Approach:** In a combination approach, the individual scores generated from individual matchers are integrated to generate one single score vector for use in the final decision. The combination approach is the most widely used and improved performance of this approach has been reported by various researchers. Combination approach appears in different forms which includes simple sum, min and max score, weighted scores and user weighting. In this fusion approach, scores need to be transformed into a homogeneous scale using normalization techniques. The choice of normalization depends on the available scores data. An adaptive approach also falls within the combination approach but it has not been well established within the iris domain. Examples of combination approach are discussed below:

3.3.3.1 Simple Sum Rule

The scores are combined together and averaged with the idea of producing robust decision.The simple sum rule takes the following expression:

$$SS = \sum_{1=1}^{N} S_i + \sum_{j=1}^{N} S_j. \tag{3.1}$$

3.3.3.2 Weighted Sum Rule

The weighted sum rule is also called the best linear fusion technique, and has been designed in such a way that, it uses weights to compensate the inefficiencies in the individual algorithms. The matchers that performs badly are assigned low weights and the matchers that performs better gets bigger weights. The weighted sum fusion takes the following form:

$$WS = W_i \sum_{i=1}^{N} S_i + W_j \sum_{j=1}^{N} S_j. \tag{3.2}$$

3.3.3.3 Minimum Score

This fusion rule takes the minimum value of the scores amongst the fused matching scores. The formula for this fusion method is as follows:

$$MinS = min\Big(S_i, S_i\Big) \tag{3.3}$$

3.3.3.4 Maximum Score

This fusion takes the maximum of the given scores to be fused. The formula used for this fusion is as follows:

$$MaxS = max\Big(S_i, S_i\Big) \tag{3.4}$$

3.3.3.5 Adaptive Sum Rule

An adaptive fusion technique depends on the quality of the image or the quality parameters of the extracted features. In this work the quality parameters are base on the extracted features. This type of fusion has not been used on iris recognition systems before. It includes quality parameters heavily weighted to compensate for the noisy iris data against the noiseless iris features during iris matching. The weights incorporated here are different from the weights assigned to the matchers because adaptive weights weighs the features in terms of the amount of noise detected.

3.3.4 Rank Level Fusion

Rank level fusion is mostly useful in identification rather than verification mode. The resulting matching score from each system is considered as ranking of reference data. The objective in the rank level fusion is to integrate the ranks from the biometric systems to establish a consensus rank for each identity. The outputs of these ranks from multiple biometric modalities are compared for identification without using the matching scores.

3.3.5 Decision Level Fusion

This type of fusion incorporates decisions (accept genuine or reject impostor) from various systems which mostly uses different sensors. The final decision is done mainly by implementing a majority voting systems which determines the majority of votes which selects decisions, either accept genuine or reject impostor. At the decision level fusion, authentication results are produced from each biometric system. Combination techniques like majority rule voting are applied to integrate the decisions from various authentication results. Integration occurs at the accept as genuine or reject as impostors decision levels. Integration at this level has been used by various researchers and is reported as being too simple due to limited information during fusion.

3.4 Summary

This chapter discussed the categories and fusion architectures implemented in iris recognition. Score level fusion was discussed more than the other levels of fusion because it is the choice of fusion in this work due to its ease of data acquisition in terms of matching scores and its performance reliability. An increase in interest of score level fusion research is evidenced by the cited literature in this chapter. For this reason, this work has also adopted the score level fusion because it gives more information about the level of discrimination between the genuine users and the impostor users. The score from different matching algorithms provides detailed information about the performance and accuracy of the matching algorithm. The information about the genuine and impostor users can also be easily established.

CHAPTER 4

Methodology

This chapter presents the research design of the proposed approach taken to solve the problem mentioned in chapter 1. The research instruments and techniques implemented are presented in detail.

4.1 Introduction

A quantitative research based on four iris matching algorithms was adopted to measure the acquired features extracted from each algorithm. The algorithms selected are NHD, WED, WHD and POC. The matching scores generated from each matching algorithm were analyzed and classified as either genuine and impostor based on the produced score. The procedure for assessing the quality scores and matching scores has been clearly attributed. The results reported in chapter 5 in terms of table and ROC curves were generated using MATLAB.

4.2 Research Design

This research was designed to be implemented from the iris matching level in order to get the matching scores. However, the need to conduct the research from the pre-processing stage was considered crucial in order to implement the existing segmentation algorithms, feature extraction and the matching algorithms all together. The main idea was to implement four iris feature extraction techniques in each of the two iris databases chosen, namely the CASIA [cas] and the UBIRIS [139] image databases. Each technique has its associated matcher believed to perform better using the features extracted using the desired feature extractor. From this phase, each matcher has to generate its own matching scores, and then the scores where normalized using the tanh estimators normalization technique, because it is robust and efficient against outliers. The algorithms selected in this work uses different approaches of minimizing the effect of noise within the image before and after segmentation. Normalized images where used to compute the global quality score from each image before feature extraction. The fusion experiment was done using various methods of score level fusion; namely the (i) sum rule which includes the simple sum and the weighted sum rule (also known as best linear fusion), (ii) minimum score level fusion and an adaptive fusion which is also a form of sum rule based score level fusion. From the four matching algorithms mentioned above, deeper probing was done when pairs of matchers were investigated so that an informed decision can be made based on the performance of fused matchers. The fusion of all the four algorithms were lastly implemented and investigated over the fusion approaches outlined above. Details of the results has been reported and documented on the experimental results and discussions in chapter 5.

4.3 Research Instruments

This work used two publicly available iris image databases as shown in table 4.1. The images were selected based on the instances of each images as detailed in the next section. For each image in each database five instances were desired in order to set the threshold for each matching algorithm based on the amount of information from both genuine users and impostor users. Images which failed to segment properly were discarded in order to avoid recognition failure as a result of segmentation failure.

4.4 Data

The data used in this work include two publicly iris databases, namely CASIA and UBIRIS. The data has various images, but for this work, images have been selected based on the availability of five instances from each image so that informed decision can be made when setting a threshold value. After segmentation images which were accurately segmented were selected, and images which failed segmentation were removed from test data. Remaining test images were 275 images selected from the CASIA left eye images and 815 images from the CASIA right eye images, see table 4.1. Each image is an 8 bit grey-level JPEG format of size 320×280. These images were captured in two sessions with extremely clear and rich texture details. For UBIRIS, 1200 images where selected from the right eye images. These images were captured in a constraint environment to cater for noise and huge variation in illumination, defocus and pupil dilation. Each image was captured at a resolution of 300 dpi, with pixel sizes of 2560×1704, in a JPEG format.

TABLE 4.1: Table of iris images used

Name of Database	**Number of Left Images**	**Number of Right Images**
CASIA	275	815
UBIRIS	000	1200

4.5 Proposed Method

The proposed method combines four iris matching algorithms, namely: NHD, WED, POC and WHD as shown in figure 4.1, which demonstrates the processes from the segmentation phase. The segmented image was then passed into the feature extractor and the extracted features were matched using a iris matcher related to the feature extractor. The scores were normalized using tanh estimator normalization technique. Fusion was implemented after numerous experiments on the performance of the four iris matchers with various parameters were conducted. The fusion approach exhibited in figure 4.1-, can be summarized by means of a proposed algorithm explained in algorithm 3. Only the major steps in the following algorithm has been included, some of the less important stages have been left out. To conduct the fusion experiment, data from the scores files where loaded. There were two iris databases with different capacity for each features extractor used.

4.6 Iris Image Pre-Processing and Iris Segmentation

Image pre-processing includes locating the region of interest and isolating this region from the rest of the eye image. Locating the region of interest and identifying the noisy regions are the most crucial step within the iris recognition, and it is called iris image segmentation. In this work, segmentation of iris images was done using the method proposed in [10, 13]. The procedure followed in pre-processing and segmenting an iris image has been detailed in appendix A.

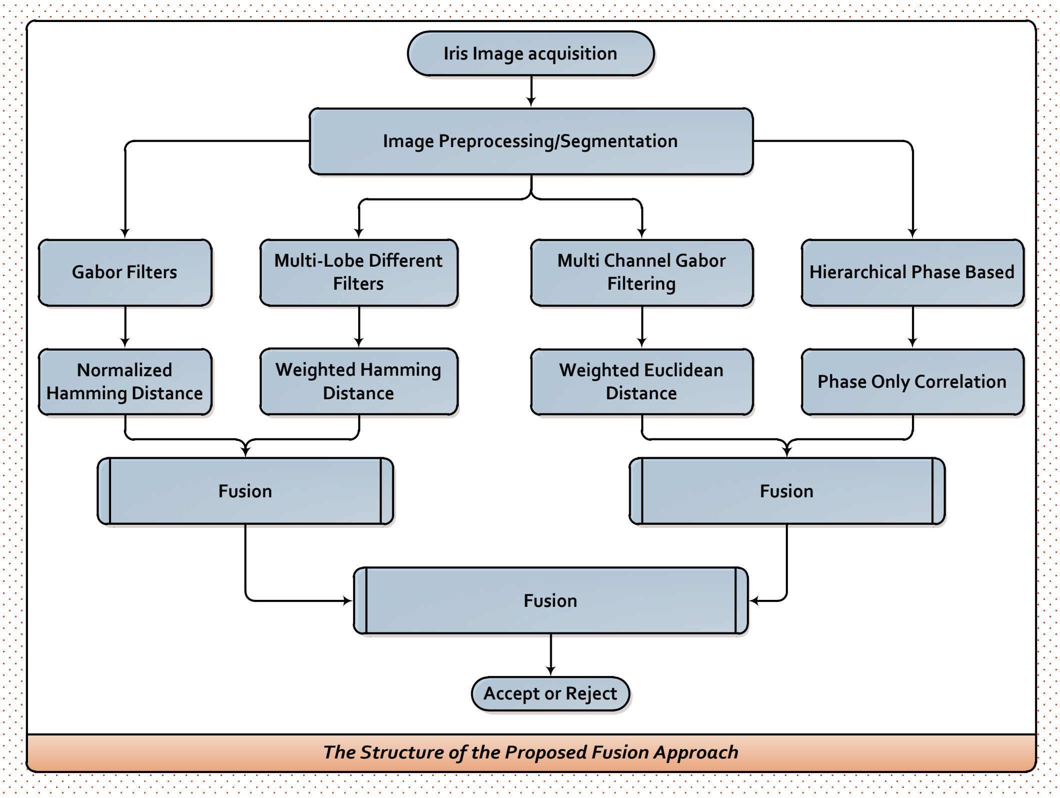

FIGURE 4.1: The Structure of the proposed fusion approach.

4.7 Iris Feature Extraction

Four iris features extraction were considered in this work which includes, phases of 2D complex Gabor filters [10, 13], Multi-Channel Gabor filtering [9, 93, 94], MLDF [19, 21, 24] and HPB [31]. The selected feature extractors have been explained in detail in the reviewed literature in chapter 2, for the purpose of their implementation. The choice of algorithms depends on the type of features extraction and type of features extracted in order to complement each algorithm. All implementations were done using MATLAB, and using built-in functions where appropriate. The phase information features were extracted using the 2D complex Gabor filters shown in equation 2.7. To extract these features, the following conditions as shown in algorithm 1 where implemented:

The parameter h represent the one bit either 0 or 1 which results from a sign of both the real and the imaginary parts of the phase quadrature image projection which is produced from a convolution between a normalized iris image and 2D complex Gabor filter. The encoded template is stored in a database and ready for comparison. The second set of

features were extracted using the Multi-Channel Gabor filters. The procedure has been

Algorithm 1: An algorithm to encode iris information using 2D Complex Gabor filter

Algorithm: Extracting the phase information using 2D complex Gabor filter
input : A normalized iris image $I(\rho, \phi)$
output: An iris template
—Get the normalized iris image and convolve it with the feature extractor—
if $R_e \int_\rho \int_\phi e^{-iw(\theta_0 - \phi)}.e^{-(r_0-\rho)^2/\alpha^2}.e^{-(\theta_0-\phi)^2/\beta^2} I(\rho, \phi)\, \rho \mathrm{d}\rho \mathrm{d}\phi \geq o$ **then**
  $h_{Re} \leftarrow 1$
else
$h_{Re} \leftarrow 0$
if $I_m \int_\rho \int_\phi e^{-iw(\theta_0 - \phi)}.e^{-(r_0-\rho)^2/\alpha^2}.e^{-(\theta_0-\phi)^2/\beta^2} I(\rho, \phi)\, \rho \mathrm{d}\rho \mathrm{d}\phi \geq o$ **then**
  $h_{Im} \leftarrow 1$
else
$h_{Im} \leftarrow 0$
return *Template*

explained in detail in appendix B. The procedure for extracting the features using the MLDF and HPB has been explained in appendix C and appendix D, respectively.

4.8 Iris Feature Matching

The extracted features were matched using different feature matching algorithms due to the type of features extracted. Different matching algorithms were used to match templates generated from different feature extractors. For the phase information, the templates were matched using NHD shown in equation 2.8. This matching algorithm weighs all the bits equally and uses masked bits to reduce the effect of noise during matching. The templates generated using Multi-Channel Gabor filters were stored in a 24×2 matrix. The matching algorithm efficient for this type of data was the WED shown in equation 2.20. The details has been explained in chapter 2 and appendix B. The templates generated using MLDF takes the same form as the templates created using phase information. To improve the matching performance an advanced version of NHD called WHD as shown in equation 2.25 was used to match the templates. The 2.25, assigns different weights to different bits giving improved matching results. To match the block based generated templates extracted using HPB, POC was used and this process proceeds as a tree traversal starting the matching at the root node until to the leaves. The matching process used the phase only correlation method to assess phase values from each individual block. The procedure for the matching process is shown in algorithm 2:

Algorithm 2: Algorithm for Matching the blocks of sub-images

```
Input: A root Image S_i
Output: Matching Score
for ∀ L ∈ Leaf do
    if f(L) ← i then
        marknodeSelect(L)
        return marknodeSelect(L) for matching score calculation
        if Score ← Genuine then
            return GenuineScore
            back to leaf

else
    topDownEvaluates
return Match Score
```

4.9 Scores Normalization

Since the matching scores produces non-homogeneous scale, it was necessary to transform the matching scores into a homogeneous scale using score normalization techniques. The choice of normalization was based on robustness and efficiency of normalization technique. There are challenges involved in score level fusion, due to the metrics used to measure the templates similarities. Scores output in different scales, and these poses serious challenges over the system performance and robustness of the system based on the recognition accuracy. To solve this problem, all the scores needs to be converted to homogeneous scale. Various techniques such as detailed in Ribaric *et al.*, [140] and He *et al.*, [127] can be implemented to normalize the scores. These normalization techniques suffers from some lack of robustness against outliers. The normalization technique adopted in this report is the tanh estimators which is a hyperbolic tangent. The *tanh* estimators is robust against outliers and is highly efficient. The formula for hyperbolic tangent is as follows:

$$S_{Normalized} = \frac{1}{2}\left\{ \tanh\left(0.01\left(\frac{S_i - \overline{S}}{\sigma}\right)\right)\right\} \tag{4.1}$$

This normalization depends on Hampel parameters [141], which is a challenging task to estimate those parameters. Below is an influence function which estimates Hampel parameters:

$$H(Y) = \begin{cases} y, & o \leq |y| < a \\ a * sign(y), & a \leq |y| < b \\ a * sign(y) * \left(\frac{c-|y|}{c-b}\right) & b \leq |y| < c \\ 0 & |y| \geq c \end{cases} \tag{4.2}$$

These three parameters were chosen based on the tuple $(\alpha = 80, \beta = 90, \gamma = 95)$ that produced high recognition performance in terms of Area Under Curve (AUC) and EER. From this tuple, the parameters (a, b, c) where chosen in such a way that $\alpha\%$ of all the genuine scores should at least fall within the range of $(m - a), (m + a), \beta\%$ of the all the genuine scores should at least lie within the range of $(m - b), (m + b)$ and $\gamma\%$ of all the genuine scores should at least fall within the range of $(m - c), (m + c)$, where the parameters (a, b, c) are as they appear in equation 4.2 for estimating the parameters of the influence functions.

4.10 Score Level Fusion Implementation

As discussed in chapter 2, this dissertation presents different approaches of sum rule based fusion. The approach introduced here uses feature quality measures to map the quality value with each matching algorithm during the fusion process. In every biometric system, noise is the major source of poor recognition performance and poor recognition accuracy. Various methods handle noise regions differently, but as discussed in chapter 2, within an iris region, not every noise can be catered for during masking especially the eyelashes. Removing eyelashes using thresholding techniques cannot eliminate or detect every eyelash in different eye images. The reason being that, the eyelashes vary in pixel intensities due to the imaging conditions, leaving the light eyelashes not detected and not masked during noise masking. To cater for these challenges during matching, an adaptive fusion which assigns quality value for each algorithm is introduced using relative entropy which measure the amount of none-corrupted features available in each normalized iris image. The approach adopted here for mapping iris feature quality using relative entropy was proposed in [142]. The issue of measuring iris feature quality has attracted many iris biometric researchers, and various methods have been proposed such as reported in [143]. The relative entropy or the Kullback-Leibler divergence between two probability density function can be approximated using equation 4.3 below:

$$D\,(z \parallel w) = \int_X z(x) \log_2 \frac{z(x)}{w(x)} \tag{4.3}$$

where the functions $z(x)$ and $w(x)$ represents the probability mass functions for intra-class distribution and inter-class distribution respectively, over the iris feature dimension X. From each feature dimension within the normalized iris image, the mean intensity for each distribution $z(x)$ and $w(x)$ of an image can be measured using equations 4.4 and 4.5 below:

$$E_z\,(X) = \frac{1}{N_z} \sum_{i=1}^{N_z} X_i \tag{4.4}$$

$$E_w\,(X) = \frac{1}{N_w} \sum_{i=1}^{N_w} X_i \tag{4.5}$$

The co-variances for the two distributions can be computed using equations 4.6 and 4.7 below:

$$\sum_z = E_z\Big((X - E_z)^t \,(X - E_w) \Big) \tag{4.6}$$

$$\sum_w = E_w\Big((X - E_w)^t \,(X - E_z) \Big) \tag{4.7}$$

The two equations for $z(x)$ and $w(x)$ can be rewritten in terms of equations 4.8 and 4.9 as below:

$$z\,(x) = \frac{1}{\sqrt{|2\pi \sum_z|}} exp\Big(-\frac{1}{2}\,(X - E_z)^t \sum_z^{-1} (X - E_z) \Big) \tag{4.8}$$

$$w\,(x) = \frac{1}{\sqrt{|2\pi \sum_w|}} exp\Big(-\frac{1}{2}\,(X - E_w)^t \sum_w^{-1} (X - E_w) \Big) \tag{4.9}$$

From equations 4.8 and 4.9, the relative entropy measure can now be computed using equation 4.10 below:

$$D\,(z \parallel w) = \int z(x) \Big(\log_2 z(x) - \log_2 w(x) \Big) dx \tag{4.10}$$

After computing the quality score based on the relative entropy of the features, the fusion approach was implemented as shown in figure 4.2. The procedure to implement this flow diagram shown in figure 4.2 has been detailed in algorithm 3. To ease the process, the weighting parameters were determined after the EER, because the weights were calculated from the EER, using equation 4.11:

$$w^m = \frac{E^{e^m}}{e^m} \tag{4.11}$$

where $E = \frac{1}{\sum \frac{1}{e^m}}$. The parameters used in the equation are defined as, w is the estimated weight, m is an individual matcher and the EER produced using that matcher is defined as e.

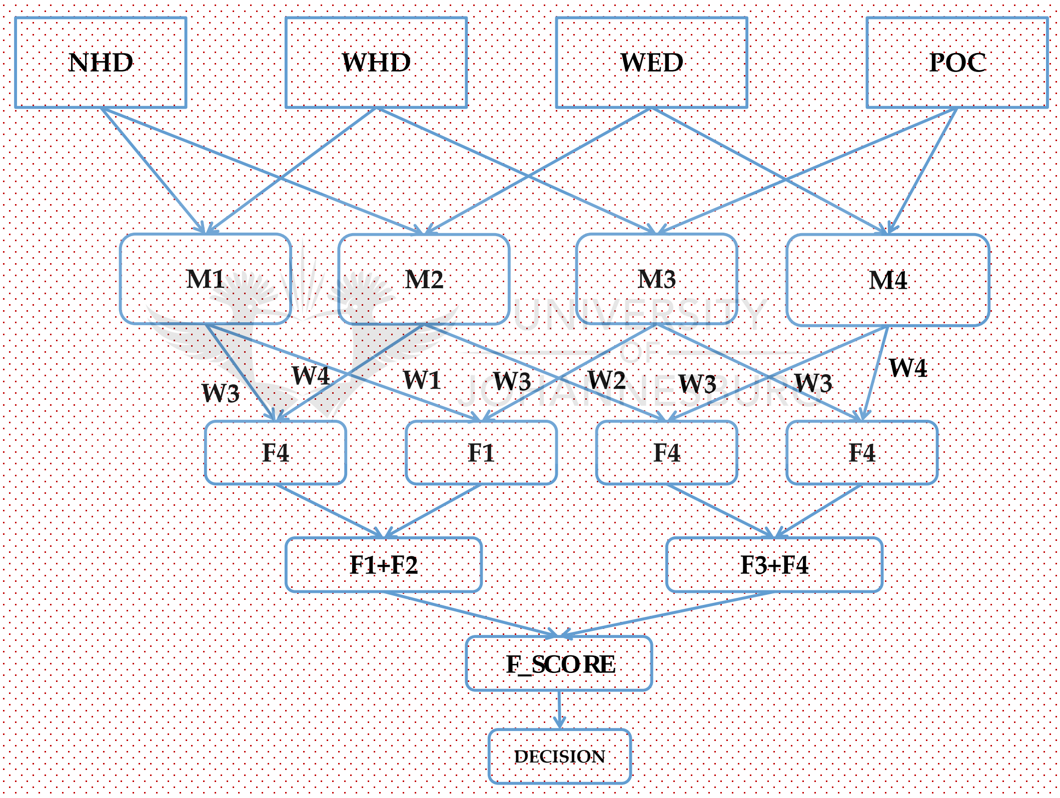

FIGURE 4.2: Structure of the proposed fusion method

Algorithm 3: Proposed algorithm

Algorithm: Adaptive Fusion Approach
input : A matrix of scores from individual matching algorithms (A(i, j))
output: A vector of fused scores
—Get the quality score for each normalized image and set the quality value for each matcher based on its recognition performance—;
—Set a threshold value, T_Q—
if $Q \geq T_Q$ **then**
    1. $M_1 \leftarrow$ min(NHD,WHD)
    2. $M_2 \leftarrow$ min(WED,POC)
else
3. $M_3 \leftarrow$ min(NHD,WED)
4. $M_4 \leftarrow$ min(WHD,POC)
5. Save $M_{(i,j)}$
—Combine the minimum scores using the EER fro each matching algorithm use—;
if $EER_{NHD} \geq EER_{WED}$ *&* $EER_{WHD} \geq EER_{POC}$ **then**
    6. $F_1 \leftarrow w_1 \times M_1 + w_2 \times M_3$
    7. $F_2 \leftarrow w_2 \times M_2 + w_3 \times M_4$
else
8. $F_3 \leftarrow w_3 \times M_3 + w_4 \times M_4$
9. $F_4 \leftarrow w_3 \times M_1 + w_4 \times M_2$
10. $F_s \leftarrow \min\Big((F_1 + F_2), (F_3 + F_4)\Big)$;
return F_s

4.11 Summary

In this section, the proposed approach has been presented in detail from each feature extraction to matching module, error rates were computed together with the quality score for each normalized image. Information from quality score and noise control in each image were analyzed in order to quantify the quality scores and the weights depending on how each algorithm employs the noise masking techniques to minimize noise. The results for the proposed fusion have been presented in terms of tables and ROC curves in chapter 5. The choice of using the minimum rule for adaptive weighted fusion was deduced from the performance of minimum fusion rule prior feature qualities parameters. It was discovered that weighted minimum rule performs better than weighted sum rule if error rates and feature quality score are mapped with the fusion parameters as seen in table of results in terms of AUC and EER in chapter 5.

Chapter 5

Experimental Results and Discussion

This chapter reports the details of results from the experiment conducted in this work. The results are presented in terms of tables and ROC curves. All the tables and figures are discussed and analyzed in the discussions and informed conclusion is drawn from the discussed results.

5.1 Introduction

The score based fusion has been proposed and implemented in this work. The results have been analyzed based on the performance of various fusion techniques implemented and tested on different iris image databases. Results have been classified based on different metrics designed only for the purpose of this work. The experiment was tested against two iris databases as mentioned in chapter 4. The CASIA has two separate image databases for left and right eyes, which reports different performance, with left eyes having high recognition performance than right eye images. The fusion approaches implemented here includes (i) the simple sum rule which takes the average of the four matching scores, (ii) the minimum rule, which takes the minimum of the four matching scores, (iii) the weighted sum fusion which incorporates the weights generated from the EER from each matching algorithm. Different weights have been tested and the best combination with low EER and AUC were used and (iv) Adaptive fusion which has been proposed in this work, which uses both the quality scores generated from each feature vector and the value of EER generated by each matching algorithm.

5.2 Iris Feature Quality

From the results of the experiment it was discovered that the quality of the extracted features play an important role in the matching decision, especially when an adaptive fusion has to be implemented. This work has demonstrated that the adaptive fusion technique is robust over various changes in illumination, pupil dilation and noise in captured images, because these anomalies can be cleaned using the generated and assigned weights, which compensate for the loss from noise and illuminations changes. This is however only possible if the quality of the features can be measured so that the amount of noise that cannot be masked can be assigned low weights during fusion process. The error rates reported from each individual matcher also plays an important role in assigning the weights for each matcher during fusion.

5.3 Performance Comparison

The performance and accuracy of a biometric system can be measured using the AUC and the system errors, such as EER. In this work, the AUC and the EER were used to measure the system performance and accuracy. The proposed fusion uses weighted sum of results from minimum fusion approach. The results from minimum approach were fused using weights assigned based on the recognition accuracy from each individual matcher. Below are the results which demonstrate the performance of each algorithm in terms of their error rates. In sections, the following measures were used to draw the depicted Receiver Operating Characteristic (ROC):

- True Positive (TP): The measure of the total number of genuine subjects who were correctly classified as genuine subjects. This measure leads to a True Positive Rate (TPR) which is computed using equation 5.1 below :

$$TPR = \frac{TP}{P} \tag{5.1}$$

  where the numerator in the fraction represents the number of TP and the denominator, P, represents the total number of genuine users in the specified biometric system.

- False Negative (FN): The measure of the total number of genuine subjects who were classified as impostor subjects. This measure leads to the False Negative Rates (FPR) which is computed using equation 5.2 below :

$$TPR = \frac{FN}{P} \tag{5.2}$$

where the numerator in the fraction which represents the number of genuine users classified as impostors and the denominator, P, is the total number of all the genuine users in the biometric system.

- True Negative (TN): The measure of total number of impostor users who were correctly classified in the system as impostor users. This measure leads to True Negative Rates (TNR) which can be computed using equation 5.3 below :

$$TPR = \frac{TN}{N} \tag{5.3}$$

where the numerator in the fraction represents the total number of subjects who were correctly classified as impostors and where the denominator represents the total number of impostor users in a biometric system.

- False Positive (FP): The measure of total number of impostor users who where incorrectly classified as genuine users. This measure leads to a False Positive Rates (FPR), which can be computed using equation 5.4 below:

$$TPR = \frac{FP}{N} \tag{5.4}$$

where the numerator in the fraction representing the total number of impostor users who were incorrectly classified as genuine users, where the denominator represents the total number of impostor users in the system.

- Equal Error Rate (EER): This is the measure of a point where the False None Match Rate (FNMR) is equal to the False Match Rate (FMR) in the ROC curve. Every biometric system assigns a threshold prior to matching, which will determine its FAR and FRR. The systems performance increases when the EER becomes zero or grows very close to zero. Excellent performance and accuracy occurs when EER is 0.

- Area under the ROC Curve (AUC): This is the measure which shows the performance and accuracy of a biometric system. These measure can be explained in terms of the table 5.1 below:

TABLE 5.1: Table of performance measures

Area under ROC Curve	**Performance**
90.0 – 1.0	Excellent Performance
80.0 – 90.0	Good Performance
70.0 – 80.0	Fair Performance
60.0 – 70.0	Poor Performance

The AUC was computed from Gini coefficient relations, which can be written mathematically as:

$$G = 2 * AUC - 1 \tag{5.5}$$

where G is the Gini coefficient given by:

$$G = 1 - \sum_{k=1}^{n} \Big(V_k - V_{k-1}\Big)\Big(U_k + U_{k-1}\Big) \tag{5.6}$$

Table 5.2 shows the performance comparison of traditional techniques and the proposed approach used in this work. As shown in the table below, the multi-channel Gabor filtering is the least performing algorithm with FRR of 0.0086% at a specified FAR of 0%. The MLDF gives significant results with low FRR of 0.0063% at a specified FAR of 0%. The HPB performed better than Phase information with FRR of 0.0065% as compared to FRR of 0.0082% produced by phase information at a specified FAR of 0%.

TABLE 5.2: Table of error rates for individual matchers

Algorithm	**FAR(%)**	**FRR (%)**
Phases of 2D Gabor Filters	0.00	0.0082
Multi Channel Gabor Filtering	0.00	0.0086
Hierarchical Phase Based	0.00	0.0065
Multi Lobe Differential Filter	0.00	0.0063

5.4 Fusion Experimental Results

Results presented here were tested against two iris databases namely: CASIA and UBIRIS, with CASIA having the left and right eye images tested separately. The images from each database where chosen based on the number of instances desired for each image. Five instances for each image where chosen from each database, so that a sensible threshold value can be easily determined when more instances are used for each subject. Images with less than five instances were left out before segmentation. Images which were not segmented accurately were discarded to avoid recognition failure. This will ensure that the results are not affected by segmentation failure because all the iris images will undergo accurate segmentation. The results for each matching algorithm implemented were analysed before fusion and various thresholds were investigated for each matching technique implemented as shown in table 5.2. During fusion, various weights for each matcher and EER, were investigated and the best combination which produces best results in terms of low error rates was chosen. Various approaches of score level fusion namely: simple sum, weighted sum and minimum fusion were also implemented and comparison was done against the proposed approach. The proposed method outperforms all sum rule based and minimum rule fusion techniques when tested against all the data sets as shown in all the tables and ROC curves. The performance of the proposed approach was based on two measures namely; the AUC and the EER. For each ROC curve databases were compared, and table of results appears after each ROC curve. The score before and after normalization are depicted in figures before their associated ROC curves and table of results, figure 5.1, shows the relationship between the scores frmr CASIA left eye images before and after normalization, figure 5.3, depicts the relationship for CAISA right eye images and figure 5.5 depicts the relationship for scores from UBIRIS images. The distribution of scores in all these three figures demonstrates the range of scores which also predict their performance as shown by their respective ROC curves for each database. The experimental results tested against the CASIA left eye images using the ROC curves are presented in figure 5.2. From the figure it shows that the CASIA left eye images performs better than the CASIA right images depicted in figure 5.4. However the images used in this work have been extracted from various subjects, due to the condition of five instances desired for each image. The weights incorporated in the adaptive fusion process were $(0.4, 0.6)$ or $(0.6, 0.4)$ as rounded to the nearest integer; which produced the best results in terms of low EER and high AUC. For the weighted sum the best results were achieved with weight of $(0.7, 0.3)$ and $(0.3, 0.7)$ when fusing the four scores from four iris matching algorithms. The distribution of scores of normalized scores and ROC curve in figure 5.1 and 5.2, below demonstrates the fusion performance from four fusion techniques implemented using the CASIA left images database.

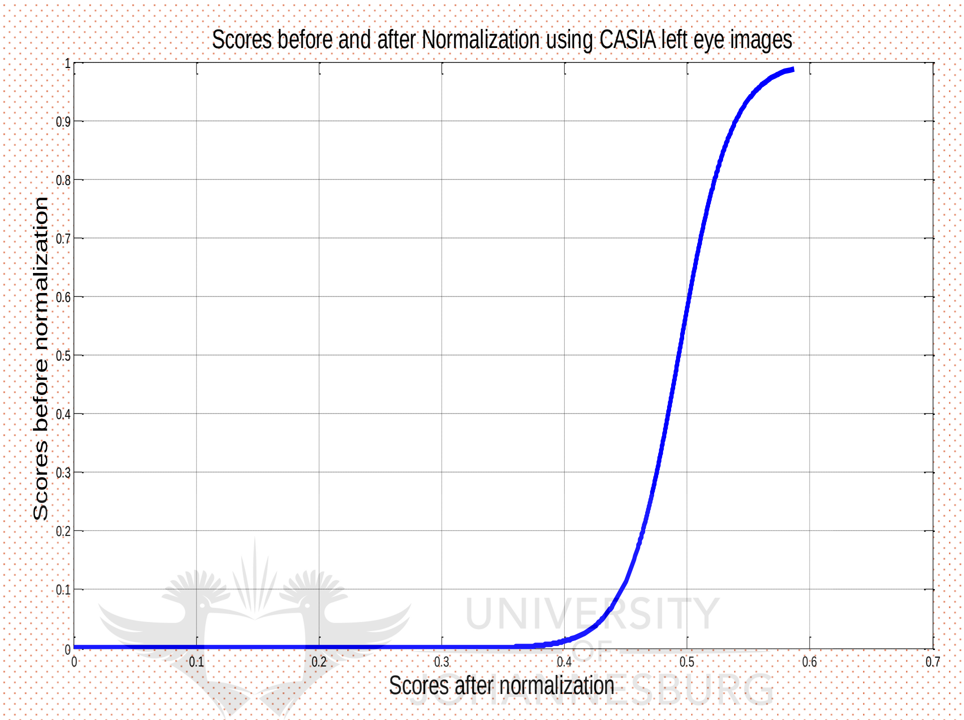

FIGURE 5.1: Scores before and after normalization using CASIA left images

The performance of the proposed approach was analyzed based on the error rates and the AUC as depicted in table 5.3: The variations in performance between the three databases demonstrates the significance of the statistical measures used to assess the system performance in this work.

TABLE 5.3: Table of simulation results using CASIA left images

Fusion Approach	**AUC %**	**EER %**
Simple Sum Rule	98.32	0.092
Minimum Score Rule	98.61	0.074
Weighted Sum Rule	98.93	0.066
Adaptive Sum Rule	99.36	0.041

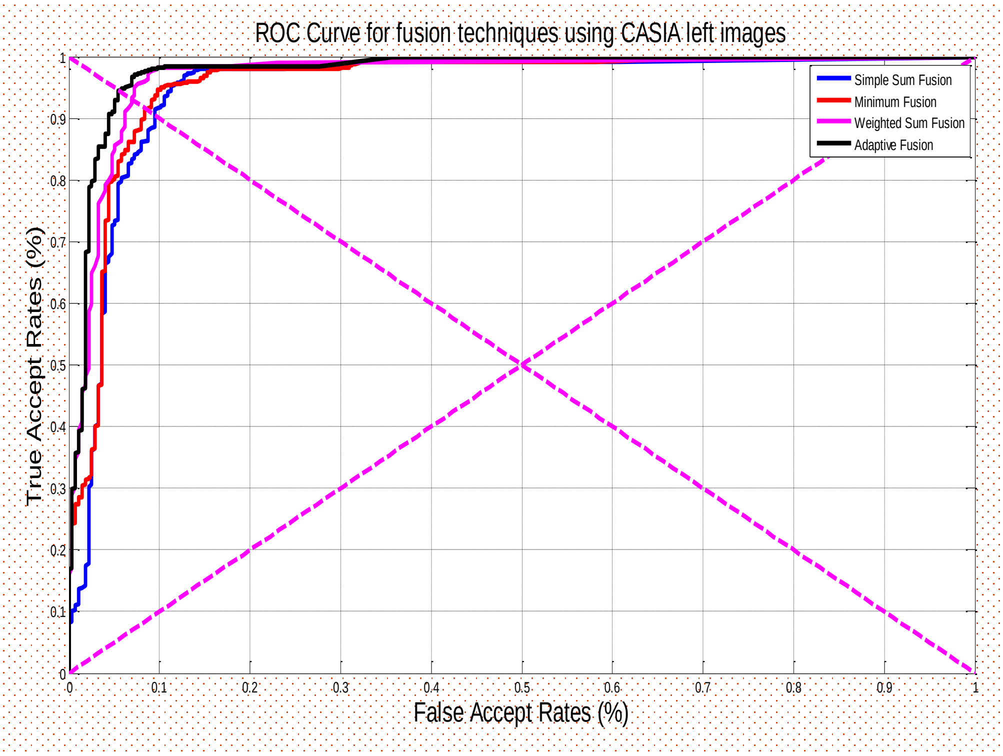

Figure 5.2: ROC Curve for proposed fusion using CASIA left images

The same comparisons were done on all the databases, for both the ROC and tables of results. From the fusion experiment it can be clearly seen that weighting of quality parameters can improve the recognition performance even on images which are highly occluded. This is evidenced in all the results presented in all the ROC curves and the tables. The UBIRIS databases outperformed the CASIA. However, this was the case even before fusion was implemented, but incorporating quality weights improved the performance of single biometric system. The comparison of the scores before and after normalization and the ROC curve for the the CASIAR are presented in figures 5.3 and figure 5.4.

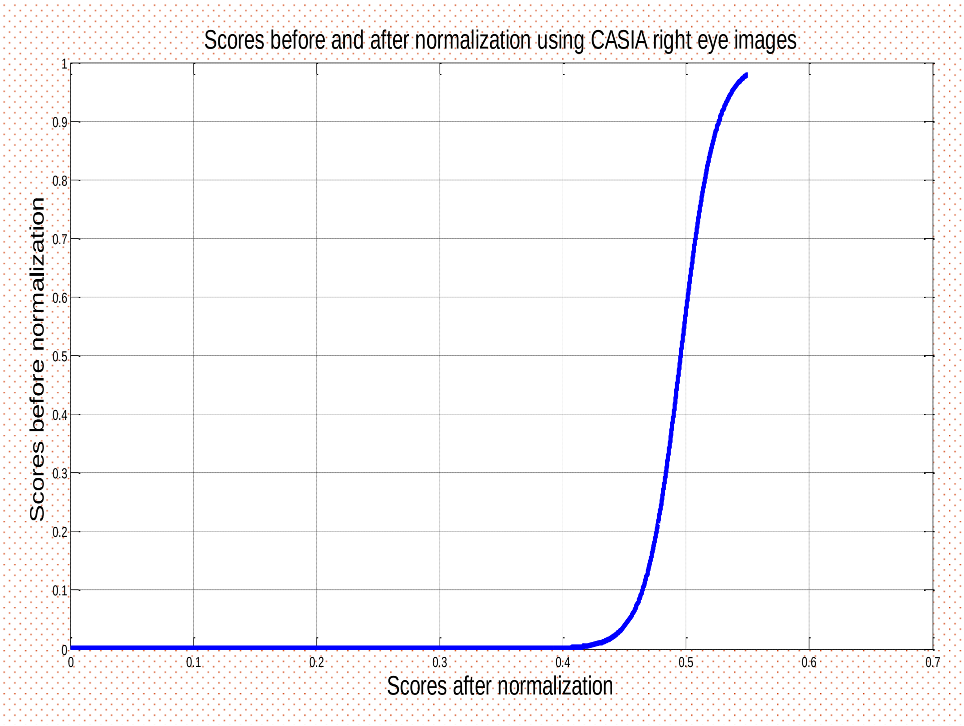

FIGURE 5.3: Scores before and after normalization using CASIA right images

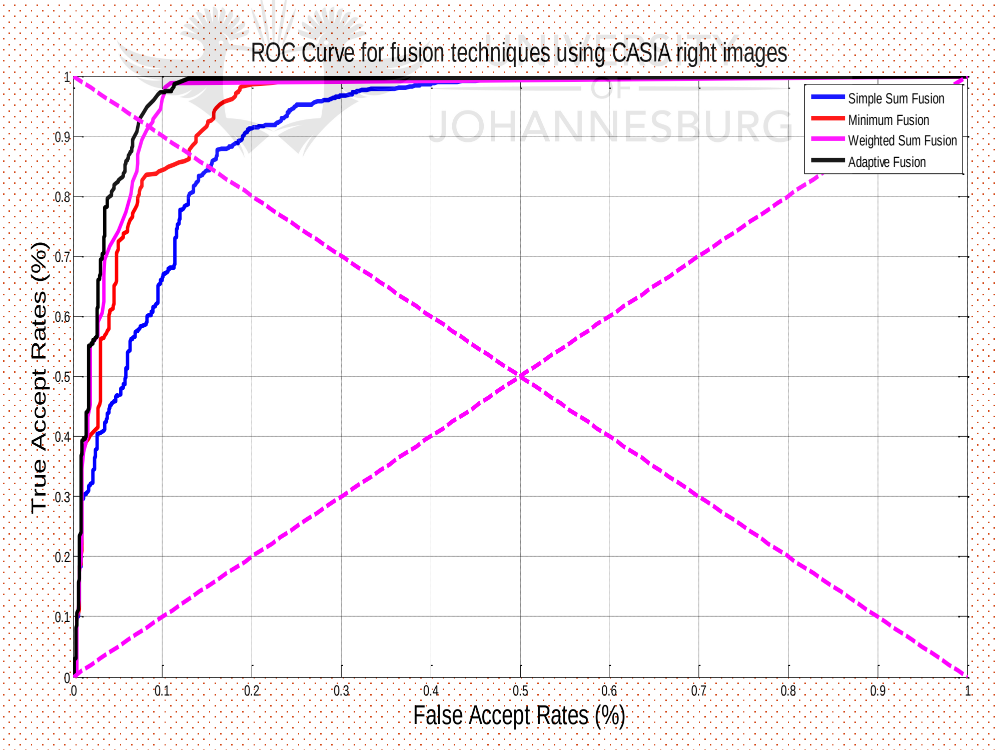

FIGURE 5.4: ROC Curve for proposed fusion using CASIA right images

The table of performance measures is presented in table 5.4 based on the performance measures discussed above:

TABLE 5.4: Table of simulation results using CASIA right images

Fusion Approach	AUC %	EER %
Simple Sum Rule	97.97	0.17
Minimum Score Rule	98.43	0.12
Weighted Sum Rule	98.81	0.096
Adaptive Sum Rule	99.18	0.087

In figure 5.5, the comparison of scores before and after normalization is presented. From the figure it can be clearly seen that the UBIRIS scores has a high discrimination as compared to the CASIA databases.

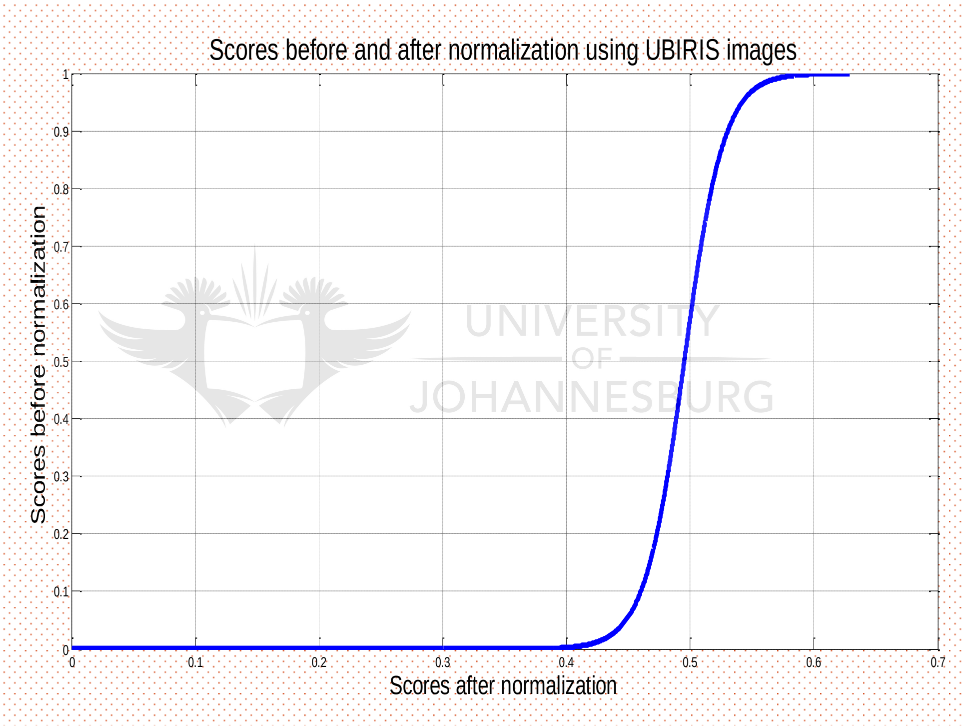

FIGURE 5.5: Scores before and after normalization using UBIRIS images

Figure 5.6 shows the ROC curve for test images from the UBIRIS database. The results of this experiment showed that even the noisy iris images can offer an improvement if quality parameters are not influenced by noise. This is evidenced by the performance of the UBIRIS data as depicted in figure 5.6. The error rates and the AUC measuring the accuracy and recognition performance are given in table 5.5.

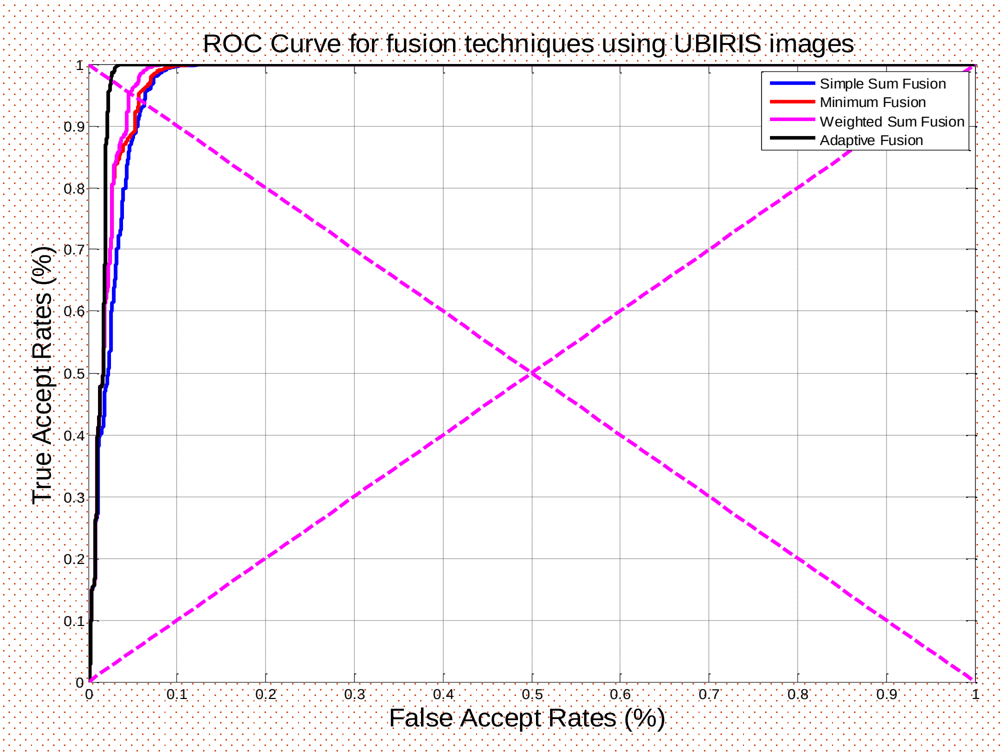

FIGURE 5.6: ROC Curve for proposed fusion using UBIRIS images

In table 5.5, analysis are presented showing the significance of the biometric measures used in this work. From the table the proposed fusion method possesses the highest AUC which implies highest accuracy and the EER is the lowest, which means improved recognition performance.

TABLE 5.5: Table of simulation results using UBIRIS images

Fusion Approach	**AUC %**	**EER %**
Simple Sum Rule	98.19	0.063
Minimum Score Rule	98.26	0.069
Weighted Sum Rule	98.53	0.074
Adaptive Sum Rule	99.59	0.038

5.5 Summary

From this experiment, it was discovered that the simple sum rule based fusion is the least performing when tested against all the databases used in this work. This is because the simple sum rule averages the scores from individual matchers without incorporating the weights from either EER or the quality map. The minimum rule based on the other hand outperforms the simple sum rule, this is because most of the genuine subjects in all the five instances for each subject posses low scores in NHD,WHD and WED, but for the POC scores for genuine has high correlation than the impostors scores. There is also some variation between the minimum scores of genuine and minimum scores of the impostors leading to better performance if measured against simple sum rule. The results from weighted sum implies that incorporating the EER during fusion offers improved recognition rate, because the EER defines the accuracy of the system in terms of these error rates. Mapping the EER with the feature quality parameters, improves the fusion approach even more, as shown in all the ROC curves for all the databases. It is also convenient to use the weights generated from the EER of each matcher to avoid bias of results by using a specified user weightings which did not originate from the system error rates. Fusion of scores using adaptive fusion based rule proved to be an advanced fusion techniques which incorporates weights from feature quality based on noise that cannot be removed during segmentation and masking. As seen in tables **??**, the adaptive fusion gives improved results as compared to other fusion methods and state-of-the-art iris recognition systems. This improvement demonstrates excellent results when feature quality parameters are accounted for during matching. It is highly encouraged to map the noise parameters during matching or fusion in order to account for the noise which remains during segmentation. In table 5.3, the proposed method achieved a recognition accuracy of 99.36% with an EER of 0.041% as compared to the weighted sum with 98.93 recognition accuracy and an EER of 0.066%. Table 5.4 demonstrates that the proposed methods achieved a recognition accuracy of 99.18 with an EER of 0.087% as compared to the weighted fusion with recognition accuracy of 98.81 and an EER of 0.096%. Table 5.5 shows that the proposed methods works best even against a very noisy iris image database by achieving a recognition accuracy of 99.59 and an EER of 0.038%.

CHAPTER 6

Conclusion and Future Work

This chapter reports the conclusion drawn from the entire work discussed in the previous chapters. Future work related to the continuation of this work is also proposed at the end of this chapter.

6.1 Conclusion

A novel approach to iris fusion has been presented in this work. During this experiment, various score level fusion techniques were investigated; which includes simple sum fusion, minimum rule fusion, weighted sum fusion and an adaptive rule based fusion. It was discovered from the experiments, that the simple sum fusion was the least performing fusion technique. The minimum fusion outperformed the simple sum fusion. The weighted sum, performed better than the minimum rule fusion. It was assumed that this happened because of the weights assigned to each matching algorithm to compensate for the least performing in terms of accuracy. The idea of developing an adaptive fusion using weighted sum of minimum scores evolve from this results. The evidence from two publicly iris database demonstrates that an improved performance is gained when weighted sum of the minimum scores gets weights assigned from both the feature quality scores and the error rates values. A shown in chapter 5, the proposed method showed significant results with high recognition accuracy and very low EER against two different iris databases. This improvement demonstrates that an adaptive fusion method reduces the effect of noise during matching process and improves recognition rates. The following hypothesis as claimed in chapter 1 has been proven:

1. Combination of multiple matching techniques improves performance, as demonstrated by the results achieved using the proposed adaptive fusion method

2. Score level fusion produces more robust results than the other levels of fusion. Even though the other methods of fusion where not implemented, this work demonstrated the potential of score level fusion and its ease of computation and resource expenses.

3. It was also showed that if weighted sum rule based fusion can produce better accuracy, adaptive rule based fusion can produce excellent results which outperforms weighted sum rule which only use error rates to compute the weights. This is evident in all the tables of results and figures showed in chapter 5. The results achieved using the proposed method offers improved recognition accuracy with significant power as discussed in chapter 5.

6.2 Future Work

From the conducted experiments, it was identified that segmentation algorithms are not robust enough to segment accurately all the images in a database without tuning the parameters. As a future work, it is intended to develop a learning based parameter estimation for iris segmentation. Dividing an image into blocks , and assign a weight which measures the block quality to be incorporated in an adaptive fusion that uses image and feature quality is also intended to be implemented, instead of using the entire normalized image to measure the feature quality.

References

[1] R.E. Garfield. Biometrics technology. Technical report, Defense Technical Information Center (DTIC) Document, 2012.

[2] R.P. Wildes. Iris recognition: an emerging biometric technology. *Proceedings of the IEEE*, 85(9):1348–1363, 1997.

[3] R.M. Hamza. Iris recognition and method, July 13 2010. US Patent 7,756,301.

[4] J. Daugman and C. Downing. Epigenetic randomness, complexity and singularity of human iris patterns. *Proceedings of the Royal Society of London Series B: Biological Sciences*, 268(1477):1737–1740, 2001.

[5] Z. Suna, A.A. Paulinob, J. Fengb, Z. Chaia, T. Tana, and A.K. Jainb. A study of multibiometric traits of identical twins. *Proceedings of the SPIE, Biometric Technology for Human Identification VII*, 7667:76670T–12, 2010.

[6] K. Hollingsworth, K.W. Bowyer, S. Lagree, S.P. Fenker, and P.J. Flynn. Genetically identical irises have texture similarity that is not detected by iris biometrics. *Computer Vision and Image Understanding*, 115(11):1493 – 1502, 2011. ISSN 1077-3142. doi: http://dx.doi.org/10.1016/j.cviu.2011.06.010.

[7] J. Daugman and G.O. Williams. A proposed standard for biometric decidability. In *Proceedings of CardTech/SecureTech Conference*, pages 223–234, 1996.

[8] M. Dobes and L. Machala. Upol iris image database. 2004. URL http://phoenix.inf.upol.cz/iris/.

[9] T.N. Tan. Texture feature extraction via visual cortical channel modelling. In *11th IAPR International Conference on Pattern Recognition. Vol. III. Conference C: Image, Speech and Signal Analysis, Proceedings*, pages 607–610. IEEE, 1992.

[10] J. Daugman. High confidence visual recognition of persons by a test of statistical independence. *IEEE Transactions on Pattern Analysis and Machine Intelligence*, 15(11):1148–1161, 1993.

[11] R.P. Wildes, J.C. Asmuth, G.L. Green, S.C. Hsu, R.J. Kolczynski, J.R. Matey, and S.E. McBride. A system for automated iris recognition. In *Proceedings of*

the Second IEEE Workshop on Applications of Computer Vision, 1994., pages 121–128. IEEE, 1994.

[12] J. Daugman. The importance of being random: statistical principles of iris recognition. *Pattern recognition*, 36(2):279–291, 2003.

[13] J. Daugman. How iris recognition works. *IEEE Transactions on Circuits and Systems for Video Technology*, 14(1):21–30, 2004.

[14] J. Daugman. Probing the uniqueness and randomness of iriscodes: Results from 200 billion iris pair comparisons. *Proceedings of the IEEE*, 94(11):1927–1935, 2006.

[15] L. Flom and A. Safir. Iris recognition system, February 3 1987. US Patent 4,641,349.

[16] M. Negin, T.A. Chmielewski, M. Salganicoff, U.M. von Seelen, P.L. Venetainer, and G.G. Zhang. An iris biometric system for public and personal use. *Computer*, 33(2):70–75, 2000.

[17] L. Ma, T. Tan, Y. Wang, and D. Zhang. Efficient iris recognition by characterizing key local variations. *IEEE Transactions on Image Processing*, 13(6):739–750, 2004.

[18] R. Zhu, J. Yang, and R. Wu. Iris recognition based on local feature point matching. In *ISCIT'06. International Symposium on Communications and Information Technologies, 2006.*, pages 451–454. IEEE, 2006.

[19] Z. He, Z. Sun, T. Tan, X. Qiu, C. Zhong, and W. Dong. Boosting ordinal features for accurate and fast iris recognition. In *CVPR 2008. IEEE Conference on Computer Vision and Pattern Recognition*, pages 1–8, 2008.

[20] C. Belcher and Y. Du. Region-based sift approach to iris recognition. *Optics and Lasers in Engineering*, 47(1):139–147, 2009.

[21] Z. Sun and T. Tan. Ordinal measures for iris recognition. *IEEE Transactions on Pattern Analysis and Machine Intelligence*, 31(12):2211–2226, 2009.

[22] B.J. Kang, K.R. Park, J. Yoo, and K. Moon. Fuzzy difference-of-gaussian–based iris recognition method for noisy iris images. *Optical Engineering*, 49(6):067001–067001, 2010.

[23] T.W. Ng, T.L. Tay, and S.W. Khor. Iris recognition using rapid haar wavelet decomposition. In *2010 2nd International Conference on Signal Processing Systems (ICSPS)*, volume 1, pages V1–820. IEEE, 2010.

[24] W. Dong, Z. Sun, and T. Tan. Iris matching based on personalized weight map. *IEEE Transactions on Pattern Analysis and Machine Intelligence*, 33(9):1744–1757, 2011.

[25] S. Cremer, B. Dorizzi, S. Garcia-Salicetti, and N. Lemperiere. How a local quality measure can help improving iris recognition. In *Biometrics Special Interest Group (BIOSIG), 2012 BIOSIG - Proceedings of the International Conference of the*, pages 1–6, 2012.

[26] A.K Bachoo and J. Tapamo. Texture detection for segmentation of iris images. In *Proceedings of the 2005 annual research conference of the South African institute of computer scientists and information technologists on IT research in developing countries*, pages 236–243. South African Institute for Computer Scientists and Information Technologists, 2005.

[27] J.R. Matey, R. Broussard, and L. Kennell. Iris image segmentation and sub-optimal images. *Image and Vision Computing*, 28(2):215 – 222, 2010. doi: http://dx.doi.org/10.1016/j.imavis.2009.05.006.

[28] F. Jan, I. Usman, and S. Agha. Reliable iris localization using hough transform, histogram-bisection, and eccentricity. *Signal Processing*, 93(1):230 – 241, 2013. ISSN 0165-1684. doi: http://dx.doi.org/10.1016/j.sigpro.2012.07.033.

[29] F. Jan, I. Usman, and S. Agha. A non-circular iris localization algorithm using image projection function and gray level statistics. *Optik - International Journal for Light and Electron Optics*, 124(18):3187 – 3193, 2013. ISSN 0030-4026. doi: http://dx.doi.org/10.1016/j.ijleo.2012.09.018.

[30] L. Masek. *Recognition of human iris patterns for biometric identification*. PhD thesis, University of Western Australia, 2003. URL http://http://www.csse.uwa.edu.au/~pk/studentprojects/libor/sourcecode.html.

[31] C.A.D. Durai and M. Karnan. Iris recognition using modified hierarchical phase-based matching (hpm) technique. *International Journal of Computer Sciences Issues*, page 43, 2010.

[32] C. Rathgeb, A. Uhl, and P. Wild. On combining selective best bits of iris-codes. In *Biometrics and ID Management*, pages 227–237. Springer, 2011.

[33] Y.X. Liu, L.L. Wang, H.B. Zhou, and X.Y. Zhang. A iris fast recognition algorithm based on dsp. *Applied Mechanics and Materials*, 303:1067–1071, 2013.

[34] K. Nguyen, C. Fookes, S. Sridharan, and S. Denman. Feature-domain super-resolution for iris recognition. *Computer Vision and Image Understanding*, 117 (10):1526 – 1535, 2013. ISSN 1077-3142. doi: http://dx.doi.org/10.1016/j.cviu.2013.06.010.

[35] A.F.M. Raffei, H. Asmuni, R. Hassan, and R.M. Othman. Feature extraction for different distances of visible reflection iris using multiscale sparse representation of local radon transform. *Pattern Recognition*, 46(10):2622 – 2633, 2013. ISSN 0031-3203. doi: http://dx.doi.org/10.1016/j.patcog.2013.03.009.

[36] P. Li and H. Ma. Iris recognition in non-ideal imaging conditions. *Pattern Recognition Letters*, 33(8):1012 – 1018, 2012. ISSN 0167-8655. doi: http://dx.doi.org/10.1016/j.patrec.2011.06.017.

[37] M. De Marsico, M. Nappi, and D. Riccio. Noisy iris recognition integrated scheme. *Pattern Recognition Letters*, 33(8):1006 – 1011, 2012. ISSN 0167-8655. doi: http://dx.doi.org/10.1016/j.patrec.2011.09.010.

[38] C. Rathgeb, F. Breitinger, and C. Busch. Alignment-free cancelable iris biometric templates based on adaptive bloom filters. In *Biometrics (ICB), 2013 International Conference on*, pages 1–8, 2013. doi: 10.1109/ICB.2013.6612976.

[39] C. Rathgeb, F. Breitinger, C. Busch, and H. Baier. On the application of bloom filters to iris biometrics. 2013.

[40] N. Popescu-Bodorin and V.E. Balas. Comparing haar-hilbert and log-gabor based iris encoders on bath iris image database. In *2010 4th International Workshop on Soft Computing Applications (SOFA)*, pages 191–196, 2010. doi: 10.1109/SOFA.2010.5565599.

[41] U. Gawande, M. Zaveri, and A.l Kapur. A novel multialgoritmic approach for improving accuracy of iris recognition using haar, multiresolution and new block

sum method. In *Proceedings of the International Conference & Workshop on Emerging Trends in Technology*, pages 576–582. ACM, 2011.

[42] H. Ghodrati, M.J. Dehghani, and H. Danyali. Two approaches based on genetic algorithm to generate short iris codes. *International Journal of Intelligent Systems and Applications (IJISA)*, 4(8):62, 2012.

[43] A. Ross and A. Jain. Information fusion in biometrics. *Pattern Recognition Letters*, 24(13):2115 – 2125, 2003. ISSN 0167-8655. doi: http://dx.doi.org/10.1016/S0167-8655(03)00079-5.

[44] P. Zhang, D. Li, and Q. Wang. A novel iris recognition method based on feature fusion. In *Proceedings of 2004 International Conference on Machine Learning and Cybernetics*, volume 6, pages 3661–3665. IEEE, 2004.

[45] K. Nandakumar, Y. Chen, A.K. Jain, and S.C. Dass. Quality-based score level fusion in multibiometric systems. In *ICPR 2006. 18th International Conference on Pattern Recognition*, volume 4, pages 473–476. IEEE, 2006.

[46] M. Vatsa, R. Singh, and A. Noore. Improving iris recognition performance using segmentation, quality enhancement, match score fusion, and indexing. *IEEE Transactions on Systems, Man, and Cybernetics, Part B: Cybernetics,2008.*, 38 (4):1021–1035, 2008.

[47] P.A. Johnson, B. Tan, and S. Schuckers. Multimodal fusion vulnerability to non-zero effort (spoof) imposters. In *2010 IEEE International Workshop on Information Forensics and Security (Workshop on Information Forensics and Security)*, pages 1–5, 2010. doi: 10.1109/WIFS.2010.5711469.

[48] N.D. Kalka, Jinyu Z., N.A. Schmid, and B. Cukic. Estimating and fusing quality factors for iris biometric images. *Systems, Man and Cybernetics, Part A: Systems and Humans, IEEE Transactions on*, 40(3):509–524, 2010. ISSN 1083-4427.

[49] Y. Xu and D. Zhang. Represent and fuse bimodal biometric images at the feature level: complex-matrix-based fusion scheme. *Optical Engineering*, 49(3):037002–037002, 2010.

[50] C. Rathgeb, A. Uhl, and P. Wild. Incremental iris recognition: A single-algorithm serial fusion strategy to optimize time complexity. In *Biometrics: Theory Applications and Systems (BTAS), 2010 Fourth IEEE International Conference on*, pages 1–6. IEEE, 2010.

[51] M. Vatsa, R. Singh, A. Noore, and A. Ross. On the dynamic selection of biometric fusion algorithms. *IEEE Transactions on Information Forensics and Security*, 5 (3):470–479, 2010.

[52] S. Bakshi, S. Das, H. Mehrotra, and P.K. Sa. Score level fusion of sift and surf for iris. In *2012 International Conference on Devices, Circuits and Systems (ICDCS)*, pages 527–531, 2012.

[53] P.D. Garje and S.S. Agrawal. Multibiometric identification system based on score level fusion. *IOSR Journal of Electronics and Communication Engineering (IOSRJECE)*, 2:07–11, 2012. ISSN 2278-2834. URL http:\www.iosrjournals.org.

[54] Q. Tao and R. N. J. Veldhuis. Robust biometric score fusion by naive likelihood ratio via receiver operating characteristics. *IEEE Transactions on Information Forensics and Security*, 8(2):305–313, 2013. ISSN 1556-6013.

[55] J. Daugman. Demodulation by complex-valued wavelets for stochastic pattern recognition. *International Journal of Wavelets, Multiresolution and Information Processing*, 1(01):1–17, 2003.

[56] M.M. Khaladkar and S.R. Ganorkar. A novel approach for iris recognition. *International Journal of Advanced Research in Computer Engineering & Technology (IJARCET)*, 1(4):pp–366, 2012.

[57] A. Ross and M.S. Sunder. Block based texture analysis for iris classification and matching. In *2010 IEEE Computer Society Conference on Computer Vision and Pattern Recognition Workshops (CVPRW)*, pages 30–37. IEEE, 2010.

[58] K.W. Bowyer, K.P. Hollingsworth, and P.J. Flynn. A survey of iris biometrics research: 2008–2010. In *Handbook of iris recognition*, pages 15–54. Springer, 2013.

[59] M.R. Turner. Texture discrimination by gabor functions. *Biological Cybernetics*, 55(2-3):71–82, 1986.

[60] I. Fogel and D. Sagi. Gabor filters as texture discriminator. *Biological cybernetics*, 61(2):103–113, 1989.

[61] A.K. Jain and F. Farrokhnia. Unsupervised texture segmentation using gabor filters. *Pattern recognition*, 24(12):1167–1186, 1991.

[62] R. Mehrotra, K.R. Namuduri, and N. Ranganathan. Gabor filter-based edge detection. *Pattern Recognition*, 25(12):1479–1494, 1992.

[63] A. Teuner, O. Pichler, and B.J. Hosticka. Unsupervised texture segmentation of images using tuned matched gabor filters. *Image Processing, IEEE Transactions on*, 4(6):863–870, 1995.

[64] D. Dunn and W.E. Higgins. Optimal gabor filters for texture segmentation. *Image Processing, IEEE Transactions on*, 4(7):947–964, 1995.

[65] T.S. Lee. Image representation using 2d gabor wavelets. *IEEE Transactions on Pattern Analysis and Machine Intelligence,*, 18(10):959–971, 1996.

[66] B.S. Manjunath and W. Ma. Texture features for browsing and retrieval of image data. *Pattern Analysis and Machine Intelligence, IEEE Transactions on*, 18(8): 837–842, 1996.

[67] A.K. Jain, N.K. Ratha, and S. Lakshmanan. Object detection using gabor filters. *Pattern Recognition*, 30(2):295–309, 1997.

[68] D.A. Clausi and M.E.M.E. Jernigan. Designing gabor filters for optimal texture separability. *Pattern Recognition*, 33(11):1835–1849, 2000.

[69] S.E. Grigorescu, N. Petkov, and P. Kruizinga. Comparison of texture features based on gabor filters. *Image Processing, IEEE Transactions on*, 11(10):1160–1167, 2002.

[70] V.S. Naga Prasad and J. Domke. Gabor filter visualization. Technical report, University of Maryland, 2005.

[71] T. Andrysiak and M. Choraś. Image retrieval based on hierarchical gabor filters. *International Journal of Applied Mathematics and Computer Science*, 15:471–480, 2005.

[72] A. Seif, R. Zewail, M. Saeb, and N. Hamdy. Iris identification based on log gabor filtering. In *Circuits and Systems, 2003 IEEE 46th Midwest Symposium on*, volume 1, pages 333–336. IEEE, 2003.

[73] J. Kim, S. Cho, J. Choi, and R.J. Marks Ii. Iris recognition using wavelet features. *Journal of VLSI signal processing systems for signal, image and video technology*, 38(2):147–156, 2004.

[74] X. Yuan and P. Shi. Iris feature extraction using 2d phase congruency. In *Information Technology and Applications, 2005. ICITA 2005. Third International Conference on*, volume 2, pages 437–441. IEEE, 2005.

[75] H. Meng and C. Xu. Iris recognition algorithms based on gabor wavelet transforms. In *Mechatronics and Automation, Proceedings of the 2006 IEEE International Conference on*, pages 1785–1789. IEEE, 2006.

[76] C. Chou, S. Shih, and D. Chen. Design of gabor filter banks for iris recognition. In *Intelligent Information Hiding and Multimedia Signal Processing, 2006. IIH-MSP'06. International Conference on*, pages 403–406. IEEE, 2006.

[77] P. Yao, J. Li, X. Ye, Z. Zhuang, and B. Li. Iris recognition algorithm using modified log-gabor filters. In *ICPR 2006. 18th International Conference on Pattern Recognition, 2006.*, volume 4, pages 461–464. IEEE, 2006.

[78] Y. Du. Using 2d log-gabor spatial filters for iris recognition. In *Defense and Security Symposium*, pages 62020F–62020F. International Society for Optics and Photonics, 2006.

[79] Y. Wei-qi, L. Wang-lan, and K.E. Li. Parameter selection of gabor filter used in iris recognition [j]. *Opto-Electronic Engineering*, 8:017, 2008.

[80] F. Wang and J. Han. Iris recognition based on 2d log-gabor filtering. *Journal of System Simulation*, 20(6):1808–11, 2008.

[81] Z. Zhou, H. Wu, and Q. Lv. A new iris recognition method based on gabor wavelet neural network. In *Intelligent Information Hiding and Multimedia Signal Processing, 2008. IIHMSP'08 International Conference on*, pages 1101–1104. IEEE, 2008.

[82] Ryszard S.C. Iris-based person identification using gabor wavelets and moments. *International Conference on Biometrics and Kansei Engineering, 2009*, 0:55–59, 2009.

[83] H. Zheng and F. Su. An improved iris recognition system based on gabor filters. In *Network Infrastructure and Digital Content, 2009. IC-NIDC 2009. IEEE International Conference on*, pages 823–827. IEEE, 2009.

[84] C. Tsai, J. Taur, and C. Tao. Iris recognition using gabor filters optimized by the particle swarm algorithm. *Journal of Electronic Imaging*, 18(2):023009–023009, 2009.

[85] Z. Lin and B. Lu. Iris recognition method based on the optimized gabor filters. In *Image and Signal Processing (CISP), 2010 3rd International Congress on*, volume 4, pages 1868–1872. IEEE, 2010.

[86] K. Gulmire and S. Ganorkar. Iris recognition using gabor wavelet. *International Journal of Engineering*, 1(5), 2012.

[87] T. Lindeberg. Scale-space for discrete signals. *Pattern Analysis and Machine Intelligence, IEEE Transactions on*, 12(3):234–254, 1990.

[88] T. Lindeberg. *Discrete Scale-space Theory and Scale-space Primal Sketch*. PhD thesis, Royal Institute of Technology, 1991.

[89] T. Lindeberg. *Scale-space theory in computer vision*. Springer, 1993.

[90] A. Kumar and A. Passi. Comparison and combination of iris matchers for reliable personal authentication. *Pattern Recognition*, 43(3):1016 – 1026, 2010. ISSN 0031-3203. doi: http://dx.doi.org/10.1016/j.patcog.2009.08.016.

[91] K. Miyazawa, K. Ito, T. Aoki, K. Kobayashi, and H. Nakajima. An efficient iris recognition algorithm using phase-based image matching. In *ICIP 2005. IEEE International Conference on Image Processing*, volume 2, pages II–49. IEEE, 2005.

[92] K. Miyazawa, K. Ito, T. Aoki, K. Kobayashi, and H. Nakajima. An effective approach for iris recognition using phase-based image matching. *IEEE Transactions on Pattern Analysis and Machine Intelligence*, 30(10):1741–1756, 2008.

[93] Y. Zhu, T. Tan, and Y. Wang. Biometric personal identification based on iris patterns. In *Proceedings. 15th International Conference on Pattern Recognition*, volume 2, pages 801–804. IEEE, 2000.

[94] L. Ma, Y. Wang, and T. Tan. Iris recognition based on multichannel gabor filtering. In *Proceedings of the Fifth Asian Conference on Computer Vision*, volume 1, pages 279–283, 2002.

[95] B. Mitra, W. Hassan, N. Bangalore, P. Birch, R. Young, and C. Chatwin. Tracking illegally parked vehicles using correlation of multi-scale difference of gaussian filtered patches. In *SPIE Defense, Security, and Sensing*, pages 805503–805503. International Society for Optics and Photonics, 2011.

[96] H. Winnemöller, J.E. Kyprianidis, and S.C. Olsen. Xdog: an extended difference-of-gaussians compendium including advanced image stylization. *Computers & Graphics*, 36(6):740–753, 2012.

[97] T. Poon and K.C. Ho. Real-time optical image processing using difference-of-gaussians wavelets. *Optical Engineering*, 33(7):2296–2302, 1994.

[98] S. Muraki. Multiscale volume representation by a dog wavelet. *Visualization and Computer Graphics, IEEE Transactions on*, 1(2):109–116, 1995.

[99] D.G. Lowe. Object recognition from local scale-invariant features. In *Computer vision, 1999. The proceedings of the seventh IEEE international conference on*, volume 2, pages 1150–1157. Ieee, 1999.

[100] G.T. Einevoll and H.E. Plesser. Response of the difference-of-gaussians model to circular drifting-grating patches. *Visual neuroscience*, 22(04):437–446, 2005.

[101] T. Tan and Z. Sun. Ordinal representations for biometrics recognition. In *Proceedings of the Fifteenth European Conference on Signal Processing, Poznan, Poland*, pages 35–39, 2007.

[102] Z. He, Z. Sun, T. Tan, X. Qiu, C. Zhong, and W. Dong. Boosting ordinal features for accurate and fast iris recognition. In *Computer Vision and Pattern Recognition, 2008. CVPR 2008. IEEE Conference on*, pages 1–8. IEEE, 2008.

[103] S. A Ajagamelle, M. Pedersen, and G. Simone. Analysis of the difference of gaussians model in image difference metrics. In *Conference on Colour in Graphics,*

Imaging, and Vision, volume 2010, pages 489–496. Society for Imaging Science and Technology, 2010.

[104] U.M. Chaskar and M.S. Sutaone. A novel approach for iris recognition. In *2nd International Conference on Computer Technology and Development (ICCTD)*, pages 495–500. IEEE, 2010.

[105] S. Dey and D. Samanta. Fast and accurate personal identification based on iris biometric. *International Journal of Biometrics*, 2(3):250–281, 2010.

[106] K.Y. Shin, G.P. Nam, D.S. Jeong, D.H. Cho, B.J. Kang, K.R. Park, and J. Kim. New iris recognition method for noisy iris images. *Pattern Recognition Letters*, 33(8):991 – 999, 2012. ISSN 0167-8655. doi: http://dx.doi.org/10.1016/j.patrec.2011.08.016.

[107] N. Feddaoui, H. Mahersia, and K. Hamrouni. Improving iris recognition performance using quality measures. *Advanced Biometric technologies*, pages 242–264, 2010.

[108] M.Y. Shams, M.Z. Rashad, O. Nomir, and R.M. El-Awady. Iris recognition based on lbp and combined lvq classifier. *arXiv preprint arXiv:1111.1562*, 2011.

[109] D.M. Rankin, B.W. Scotney, P.J. Morrow, and B.K. Pierscionek. Iris recognition failure over time: The effects of texture. *Pattern Recognition*, 45(1):145 – 150, 2012. ISSN 0031-3203.

[110] N.S. Fadi, I.H. Hafsa, M.N. Raja, D. Salima, and S. Shaikha. Iris recognition using artificial neural networks. *Expert Systems with Applications*, 38(5):5940 – 5946, 2011. ISSN 0957-4174.

[111] T. Karthikeyan. Efficient biometric iris recognition system using fuzzy neural network. *International Journal of Advanced Networking and Applications*, 1(06): 371–376, 2010.

[112] A. Abhyankar and S. Schuckers. Novel biorthogonal wavelet based iris recognition for robust biometric system. *International Journal of Computer Theory and Engineering*, 2(2):1793–8201, 2010.

[113] R. Szewczyk, K. Grabowski, M. Napieralska, W. Sankowski, M. Zubert, and A. Napieralski. A reliable iris recognition algorithm based on reverse biorthogonal wavelet transform. *Pattern Recognition Letters*, 33(8):1019–1026, 2012.

[114] A. Ross. Iris recognition: The path forward. *Computer*, 43(2):30–35, 2010. ISSN 0018-9162. doi: 10.1109/MC.2010.44.

[115] S.S. Chowhan and G.N. Shinde. Iris biometrics recognition application in security management. In *CISP'08. Congress on Image and Signal Processing*, volume 1, pages 661–665. IEEE, 2008.

[116] P.S. Revenkar and A.G Anjum. Secure iris authentication using visual cryptography. *arXiv preprint arXiv:1004.1748*, 2010.

[117] M.S. Hosseini, B.N. Araabi, and H. Soltanian-Zadeh. Pigment melanin: Pattern for iris recognition. *Instrumentation and Measurement, IEEE Transactions on*, 59 (4):792–804, 2010. ISSN 0018-9456.

[118] K. Nandakumar, Y. Chen, S.C. Dass, and A.K Jain. Likelihood ratio-based biometric score fusion. *IEEE Transactions on Pattern Analysis and Machine Intelligence,*, 30(2):342–347, 2008.

[119] K. Toh, J. Kim, and S. Lee. Biometric scores fusion based on total error rate minimization. *Pattern Recognition*, 41(3):1066 – 1082, 2008. ISSN 0031-3203. doi: http://dx.doi.org/10.1016/j.patcog.2007.07.020.

[120] W. Ben Soltana, M. Ardabilian, L. Chen, and C. Ben Amar. Adaptive feature and score level fusion strategy using genetic algorithms. In *2010 20th International Conference on Pattern Recognition (ICPR)*, pages 4316–4319. IEEE, 2010.

[121] S. Kanade, D. Petrovska-Delacrétaz, and B. Dorizzi. Obtaining cryptographic keys using feature level fusion of iris and face biometrics for secure user authentication. In *2010 IEEE Computer Society Conference on Computer Vision and Pattern Recognition Workshops (CVPRW)*, pages 138–145. IEEE, 2010.

[122] P. Radu, K. Sirlantzis, G. Howells, F. Deravi, and S. Hoque. A review of information fusion techniques employed in iris recognition systems. *International Journal of Advanced Intelligence Paradigms*, 4(3):211–240, 2012.

[123] M. Gudavalli, A.V. Babu, S.V. Raju, and D.S. Kumar. Multimodal biometrics–sources, architecture and fusion techniques: An overview. In *2012 International Symposium on Biometrics and Security Technologies (ISBAST),*, pages 27–34. IEEE, 2012.

[124] H. AlMahafzah and M.Z. AlRwashdeh. A survey of multibiometric systems. *arXiv preprint arXiv:1210.0829*, 2012.

[125] D. Kaur and G. Kaur. Level of fusion in multimodal biometrics: a review. *International Journal of Advanced Research in Computer Science and Software Engineering*, 3(2), 2013. ISSN : 2277 128X.

[126] A. Alford, C. Hansen, G. Dozier, K. Bryant, J. Kelly, T. Abegaz, K. Ricanek, and D.L. Woodard. Gec-based multi-biometric fusion. In *2011 IEEE Congress on Evolutionary Computation (CEC)*, pages 2071–2074. IEEE, 2011.

[127] M. He, S. Horng, P. Fan, R. Run, R. Chen, J. Lai, M.K. Khan, and K.O. Sentosa. Performance evaluation of score level fusion in multimodal biometric systems. *Pattern Recognition*, 43(5):1789–1800, 2010.

[128] F. Wang, X. Yao, and J. Han. Minimax probability machine multialgorithmic fusion for iris recognition. *Information Technology Journal*, 6(7):1043–1049, 2007.

[129] F. Wang, J. Han, and X. Yao. Iris recognition based on multialgorithmic fusion. *WSEAS Transactions on Information Science and Applications*, 4(12):1415–1421, 2007.

[Gawande et al.] U. Gawande, M. Z., and A. Kapur. Improving iris recognition accuracy by score based fusion method. *International Journal of Advancements in Technology, Vol 1, No 1.* doi: arXivpreprintarXiv:1007.0412.

[130] G. Santos and E. Hoyle. A fusion approach to unconstrained iris recognition. *Pattern Recognition Letters*, 33(8):984 – 990, 2012. ISSN 0167-8655. doi: http://dx.doi.org/10.1016/j.patrec.2011.08.017.

[131] F. Wang and X. Zhang. An efficient method to improve iris recognition performance based on multi-level fusion. In *2012 International Workshop on Image Processing and Optical Engineering*, pages 833511–833511. International Society for Optics and Photonics, 2012.

[132] D.L. Woodard, S. Pundlik, P. Miller, R. Jillela, and A. Ross. On the fusion of periocular and iris biometrics in non-ideal imagery. In *2010 20th International Conference on Pattern Recognition (ICPR)*, pages 201–204, 2010. doi: 10.1109/ICPR.2010.58.

[133] T. Tan, X. Zhang, Z. Sun, and H. Zhang. Noisy iris image matching by using multiple cues. *Pattern Recognition Letters*, 33(8):970–977, 2012.

[134] J.M. Colores-Vargas, M. García-Vázquez, A. Ramírez-Acosta, H. Pérez-Meana, and M. Nakano-Miyatake. Video images fusion to improve iris recognition accuracy in unconstrained environments. In *Pattern Recognition*, pages 114–125. Springer, 2013.

[135] I.D. Aly, A.A. Hesham, and B.A. Nahla. Enhancing iris recognition system performance using templates fusion. *Ain Shams Engineering Journal*, 3(2):133 – 140, 2012. ISSN 2090-4479.

[136] M. Konrad, H. Stögner, A. Uhl, and P. Wild. Computationally efficient serial combination of rotation-invariant and rotation compensating iris recognition algorithms. In *International Conference on Computer Vision Theory and Applications(1)*, pages 85–90, 2010.

[137] P. Radu, K. Sirlantzis, W.G.J. Howells, F. Deravi, and S. Hoque. Information fusion for unconstrained iris recognition. *International Journal of Hybrid Information Technology*, 4(4):1–12, 2011.

[138] U. Gawande, M. Zaveri, and A.l Kapur. Multi-algorithmic approaches to iris recognition. *Biometric Technology Today*, 2011(4):8–10, 2011.

[cas] Institute of automation, chinese academy of sciences (casia) iris database. URL http://www.cbsr.ia.ac.cn/english/IrisDatabase.asp.

[139] H. Proença and L.A. Alexandre. Ubiris: A noisy iris image database. In *Proceedings of ICIAP 2005 - International Conference on Image Analysis and Processing*, volume 1, pages 970–977, 2005. ISBN 3.

[140] S. Ribaric and I. Fratric. A matching-score normalization technique for multimodal biometric systems. *Biometrics on the Internet*, page 55, 2005.

[141] F.R. Hampel, E.M. Ronchetti, P.J. Rousseeuw, and W.A. Stahel. *Robust statistics: the approach based on influence functions*, volume 114. Wiley. com, 2011.

[142] R. Youmaran and A. Adler. Measuring biometric sample quality in terms of biometric feature information in iris images. *Journal of Electrical and Computer Engineering*, 2012:22, 2012.

[143] R.M. da Costa and A. Gonzaga. Dynamic features for iris recognition. *IEEE Transactions on Systems, Man, and Cybernetics, Part B: Cybernetics,*, 42(4):1072–1082, 2012.

Appendix A

Iris Recognition based on Phase Information

The details of iris recognition based on phase information extracted using 2D complex Gabor wavelets are presented. Each and every typical iris recognition systems has (i) Preprocessing stage which includes segmentation (ii) feature extraction module which extracts iris information and compute a template for matching and (iii) template matching module which produces a matching score which determines whether the user is genuine or impostor. Each and every stage has been explained in detail below as implemented in this work.

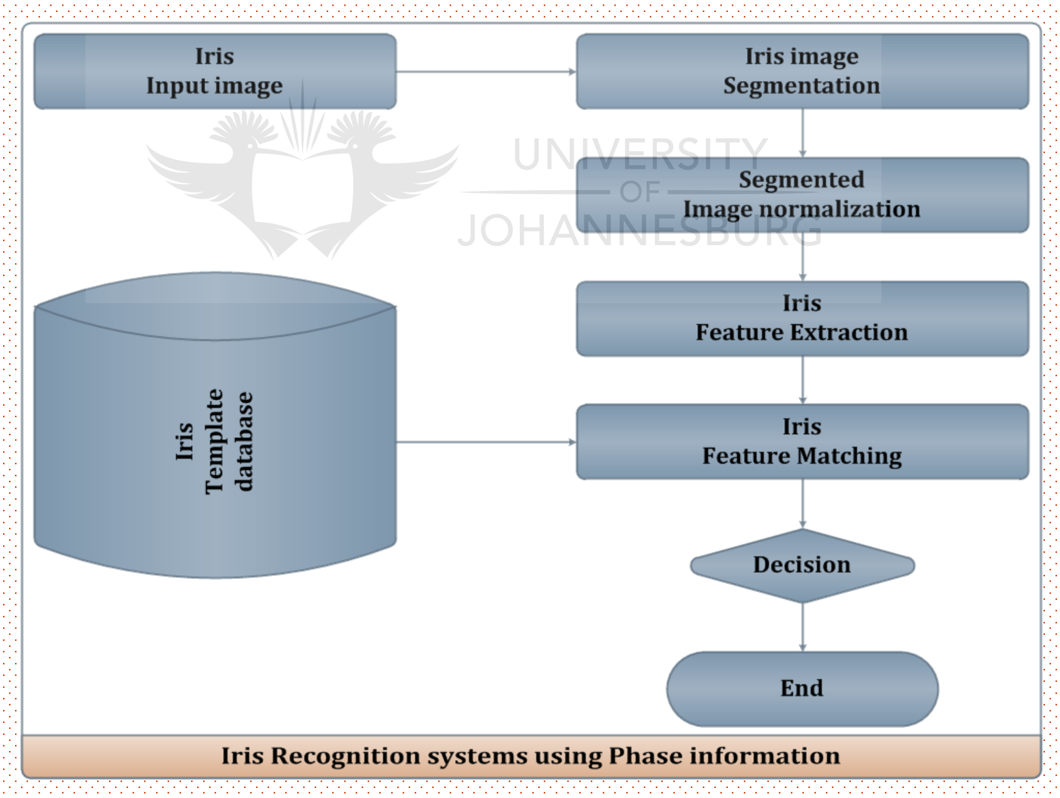

Figure A.1: Phae Informantion Flowchart [10, 55]

A.1 Iris image pre-processing

The most common way of pre-processing the image is to convert the image into gray scale level. The images in CASIA and UBIRIS are all in gray scale level. There is no need to convert the input images into gray level: Pre-processing an input image involves reducing the amount of noise in image using filtering techniques. The choice of filter used in this work was a Gaussian filter with a kernel size of 5×5 and with a $\sigma = 1.4$. The following steps were followed during pre-processing:

Step 1 : The first step is to denoise an input image using image filtering techniques. A 5×5, Gaussian filter was used to denoise the image with a standard deviation of $\sigma = 1.4$. The filter has the form shown below:

$$M = \frac{1}{159} \times \begin{bmatrix} 2 & 4 & 5 & 4 & 2 \\ 4 & 9 & 12 & 9 & 4 \\ 5 & 12 & 15 & 12 & 5 \\ 4 & 9 & 12 & 9 & 4 \\ 2 & 4 & 5 & 4 & 2 \end{bmatrix} \tag{A.1}$$

Step 2 : The second step is to compute the magnitude of the gradient and the angle of the gradient. To compute the gradient of the input image, the derivatives of the image along the x and y directions should be computed as $D_x(x, y)$ and $D_y(x, y)$ respectively. To accomplish this task a 3×3 kernel is used to compute the gradients along x and y directions. The gradient along the x direction is computed using the kernel shown in equation A.2:

$$K_{GX} = \begin{bmatrix} -1 & 0 & +1 \\ -2 & 0 & +2 \\ -1 & 0 & +1 \end{bmatrix} \tag{A.2}$$

The gradient along the y direction is computed using the kernel in equation A.2:

$$K_{GY} = \begin{bmatrix} +1 & +2 & +1 \\ 0 & 0 & 0 \\ -1 & -2 & -1 \end{bmatrix} \tag{A.3}$$

The gradient D, can be computed using equation:

$$D = \sqrt{D_x^2(x,y) + D_y^2(x,y)} \tag{A.4}$$

and the angle of the gradient can be computed using the following equation:

$$\theta = \arctan\left(\frac{D_x(x,y)}{D_y(x,y)}\right) \tag{A.5}$$

Step 3 : The next step is to convert blurred edges which are detected from the gradient magnitudes into sharp edges by preserving local maxima and ignoring the rest of the gradient image. To achieve that, for each pixel in the gradient image, the angle of the gradient θ, should be rounded to the nearest $45°$. The current edge strength is then compared with the neighboring pixels along the positive and negative directions. For every large value of the edge strength in each pixel and gradient direction, preserve the value of the edge strength and suppress the value of the edge strength if otherwise (i.e. if the value of the edge strength is less).

Step 4 : The last step is to eliminate all the edges that may have resulted due to noise, which are considered invalid edges. Hysteresis thresholding technique is used to remove all the edges resulting from the noise that remains during noise reduction. To accomplish this, hysteresis thresholding demands that two threshold values should be predefined as low threshold, T_L and high threshold, T_H. The pixels whose gradient magnitude G_M falls below the threshold value, T_L are not considered as edges and should be removed, that is when $T_L > G_M$. Some edges may fall within the range of $T_L \leq G_M < T_H$, which are only preserved if they are continuous edges, and if not they are also removed. The edges with gradient magnitude falling above the threshold value T_H, the edge is preserved as true edge.

The results of these pre-processing stage as discussed above are depicted in figure A.2 below with CASIA image in the first column and UBIRIS in the second column. Note that the value of sigma which produced this edges were set to ($\sigma = 1.4$). Most of the valuable edges can be preserved in this value, and most of the image features can be lost even when the value of sigma is increased as explained in figure A.3.

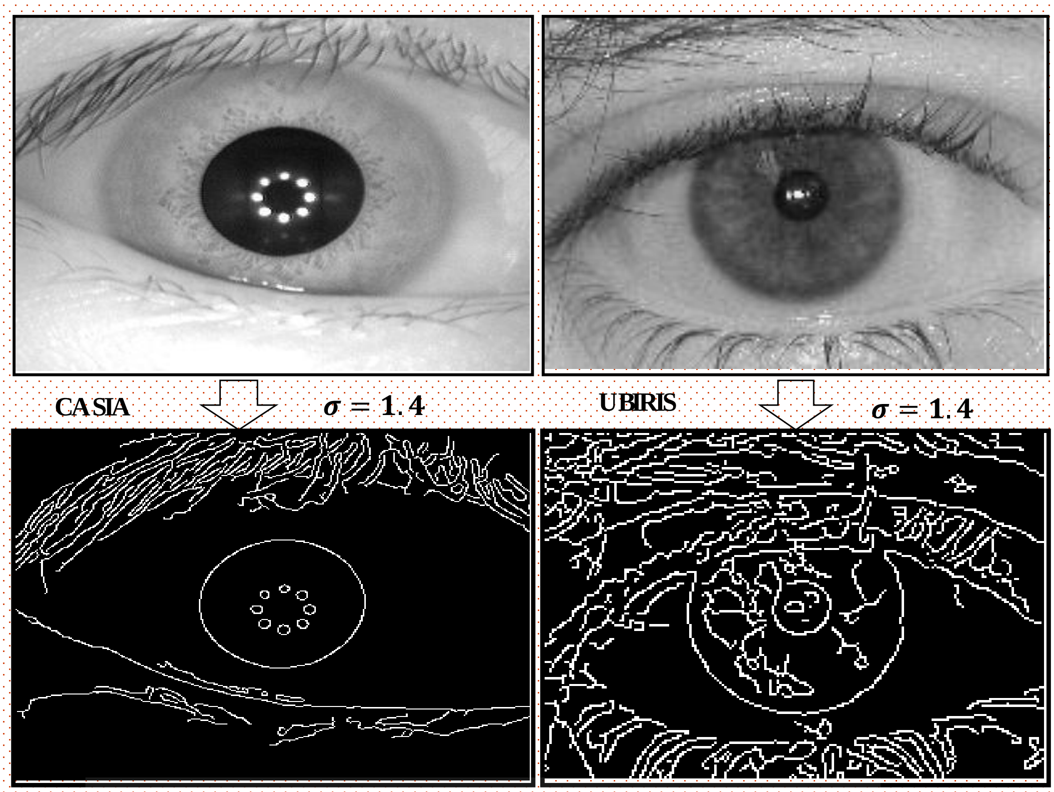

FIGURE A.2: Results of canny edge detection for CASIA and UBIRIS images

Increasing the value of sigma σ reduces the number of edges with lower magnitude values even though they are true edges. It is important to preserve all the edges needed because suppressing some of the edges may lead to valuable features being ignored. The effect of increasing sigma σ is shown in figure A.3. In this figure, first column shows the effect of increasing sigma to ($\sigma = 6, 12$) using CASIA image and second column depict the same effect using UBIRIS image. Preserving all the essential information is of primary importance because the number of stable features needed for template formation depends on the segmented regions and for iris, not every information can be computed to contribute into template formation, as discussed in chapter 2.

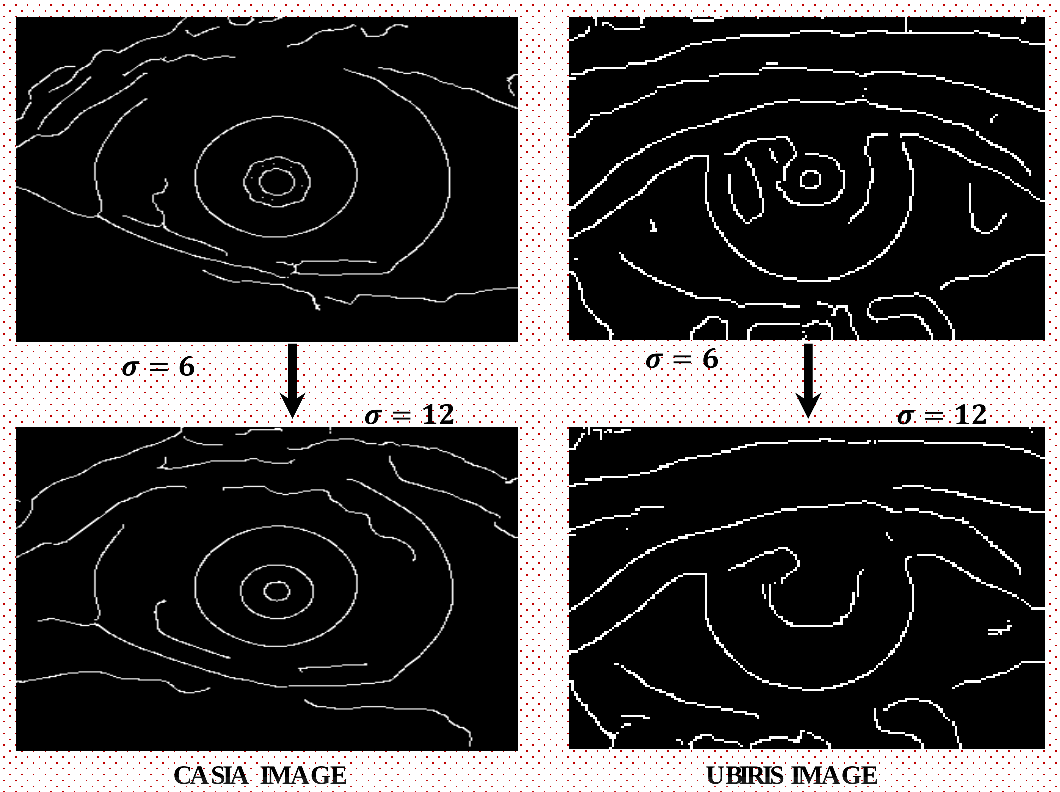

FIGURE A.3: Effect of increasing value of σ during canny edge detection for CASIA and UBIRIS images

A.2 Iris image segmentation

Segmentation is the process of isolating the non iris region from the iris region. To segment the images in this work, procedure taken from Daugman in [10, 13] were followed. Since the mentioned databases contains images of different sizes and different capturing devices and environmental conditions, segmentation parameters has been tuned per database. The process of iris image segmentation is illustrated in figure A.4, and details of steps has been explained.

A.2.1 Locating the iris and pupil region

The integrodifferential operator as shown in equation 2.1, was used to search for the center coordinates of the iris and the pupil circles. The operator searches for parameters of the iris circle (x_0, y_0, r_0) and then uses the same parameters to search for the pupil boundary. The circle is found by searching for a point where the gradient of the edge image is maximum, which indicates an edge. It is difficult to segment the entire

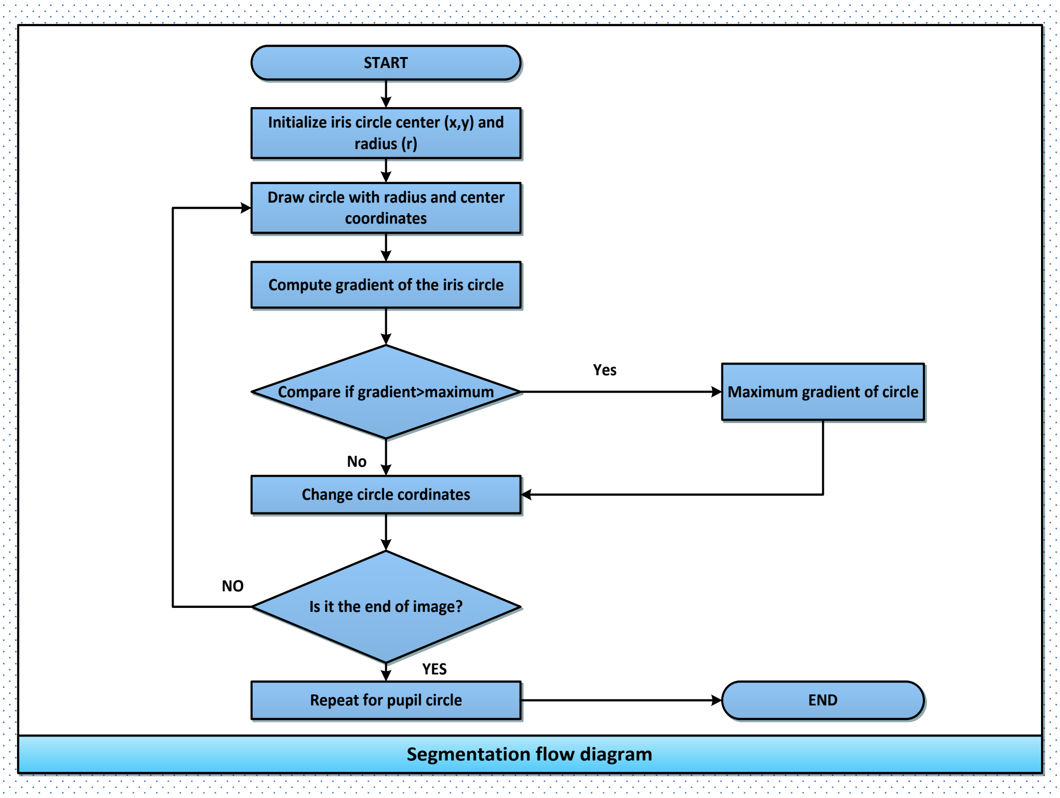

Figure A.4: Flow diagram of iris image segmentation

database due to segmentation parameters that are set like the scaling parameter σ. The segmentation parameters which segmented greater number of images accurately for the two iris image databases are tabled in table A.1 below:

Table A.1: Table of segmentation parameters

Range of pupil and iris radius	**CASIA**	**UBIRIS**
Lower Pupil Radius	27	5
Upper Pupil Radius	76	11
Lower Iris Radius	80	39
Upper Iris Radius	150	49

The success of the segmentation algorithm implemented in this work using these parameters are depicted in figure *A*.5. Images which failed the implemented segmentation algorithm as a result of illumination have been discarded from the analysis of this experiment.

The segmentation illustrated in figure *A*.5, illustrates how the region of interest is located

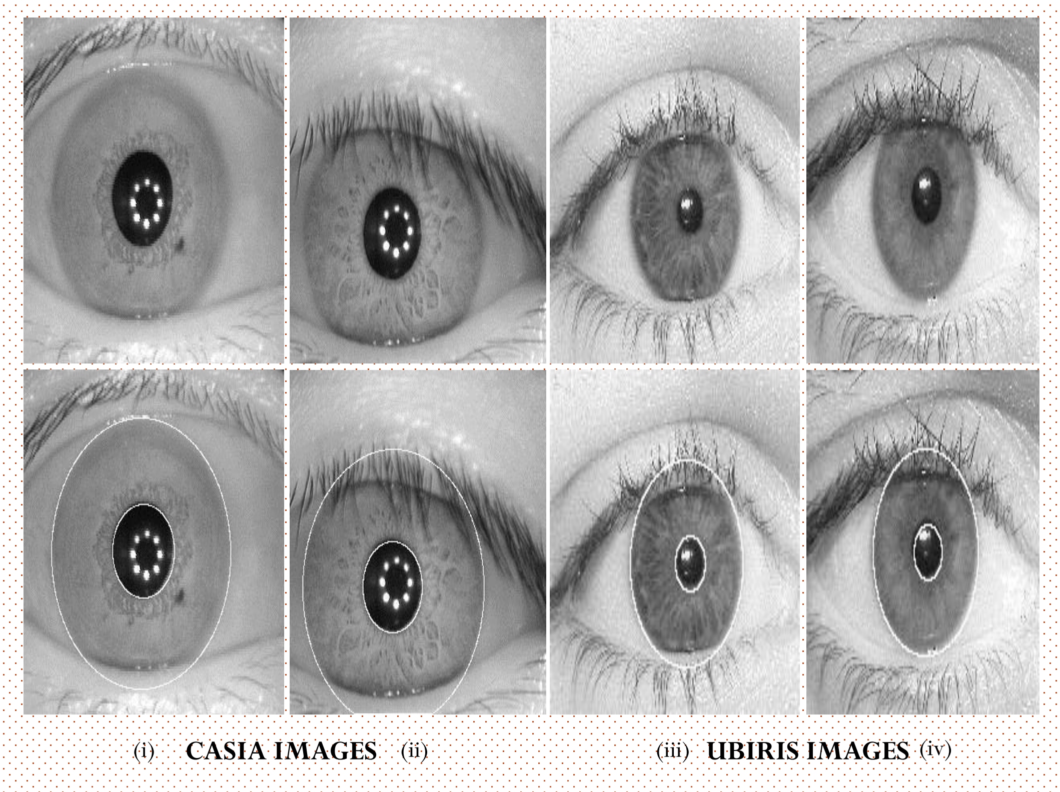

FIGURE A.5: Segmentation of CASIA and UBIRIS iris images

from the raw image using the CASIA and UBIRIS iris databases. This is the most important stage in the preprocessing stage of iris recognition system. In figure A.5, the column marked (i) and (ii) depicts images extracted from CASIA database while columns marked (iii) and (iv) depicts images taken from UBIRIS database. Column (i) shows an image which has not been badly occluded by eyelashes but some iris regions are occluded by the top and bottom eyelids. The second column marked (ii) have been badly occluded by top eyelashes and both top and bottom eyelids. From the UBIRIS images in column marked (iii), the image is badly occluded by top eyelashes and both top and bottom eyelids, whereas the column marked (iv) depicts the image occluded by top eyelashes and top eyelids but less occluded by bottom eyelid.

A.2.2 Eyelash and eyelids detection

To address the areas affected by noise either eyelids, eyelashes, or specular reflection the identified noised area should be masked to enhance the matching performance. Masking of eyelashes in this work, was done by employing an adaptive threshold analysis to detect areas occluded by eyelashes. However, not all the eyelashes can be identified, so only eyelashes which will have serious effect (those which are darker than the iris region) on the template generation will be masked. Noise regions within the iris were also detected and masked as shown in a masked image in column (ii) of figure A.6.

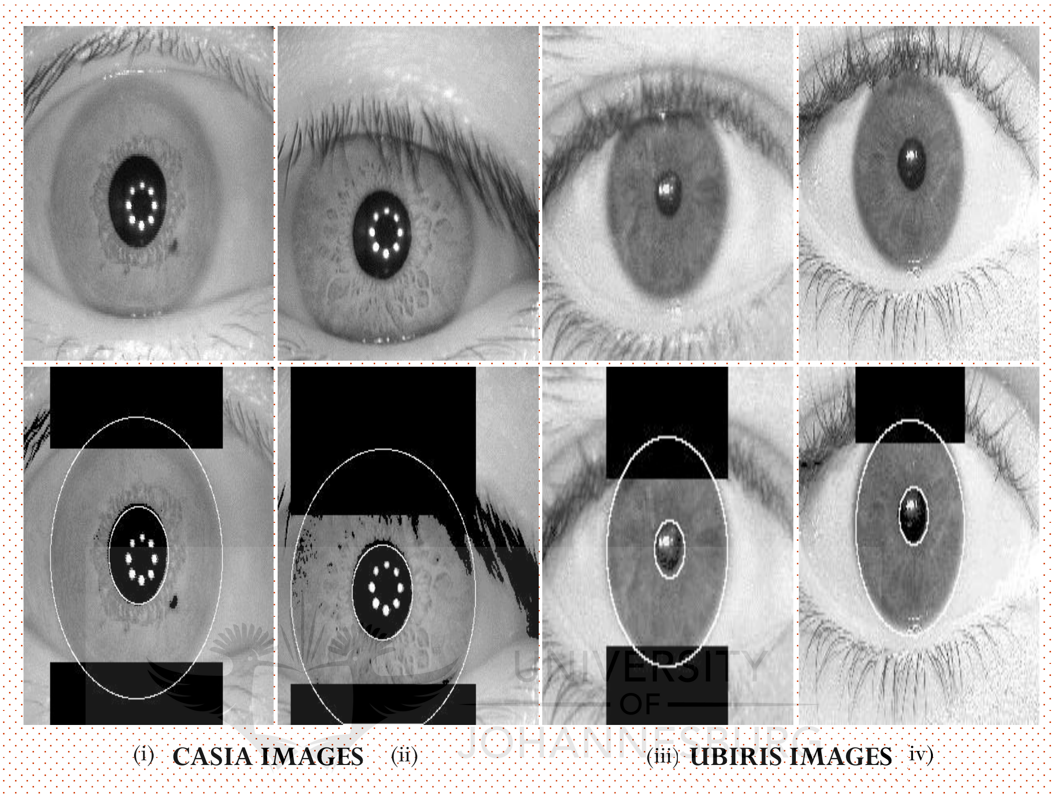

FIGURE A.6: Masking of CASIA and UBIRIS iris images

The images in figure A.6, depicts the masking process of both CASIA and UBIRIS images. As explained above, columns marked (i) and (ii) are images extracted from CASIA and (iii) and (iv) are images extracted from UBIRIS. Occlusion by noise such as eyelashes, eyelids is shown in all the columns (i)-(iv). However, column (ii) explicitly depicts an instance where an image is heavily affected by large amount of noise such as eyelashes, eyelids and some specular reflections. Some of the areas inside the iris region has also been affected with noise, as shown in column (ii) and these may cause serious effects when this image is matched with its other instances which won't be highly affected by the noise within the iris region.

A.2.3 Iris Normalization

Normalization is the process of transforming a segmented image into a fixed dimensions to avoid effects from changes in illumination, distance from camera and pupil dilation. The segmented iris image needs to be transformed into a fixed normalized dimension of polar coordinates in order to ease the feature extraction and templates matching process. As discussed in chapter 2, illumination causes the pupil to dilate leading to inconsistencies in segmented images. Normalization of these images produces an image of equal dimensions by mapping each point in an image into polar coordinates system. The procedure adopted in this work uses the famous Daugman rubber sheet model which has been explained in detail in chapter 2. The equation used to transform the iris region into a rectangular block of polar coordinates is shown in equation 2.4, in chapter 2. Results of the Daugman's normalization method is shown in figure A.7:

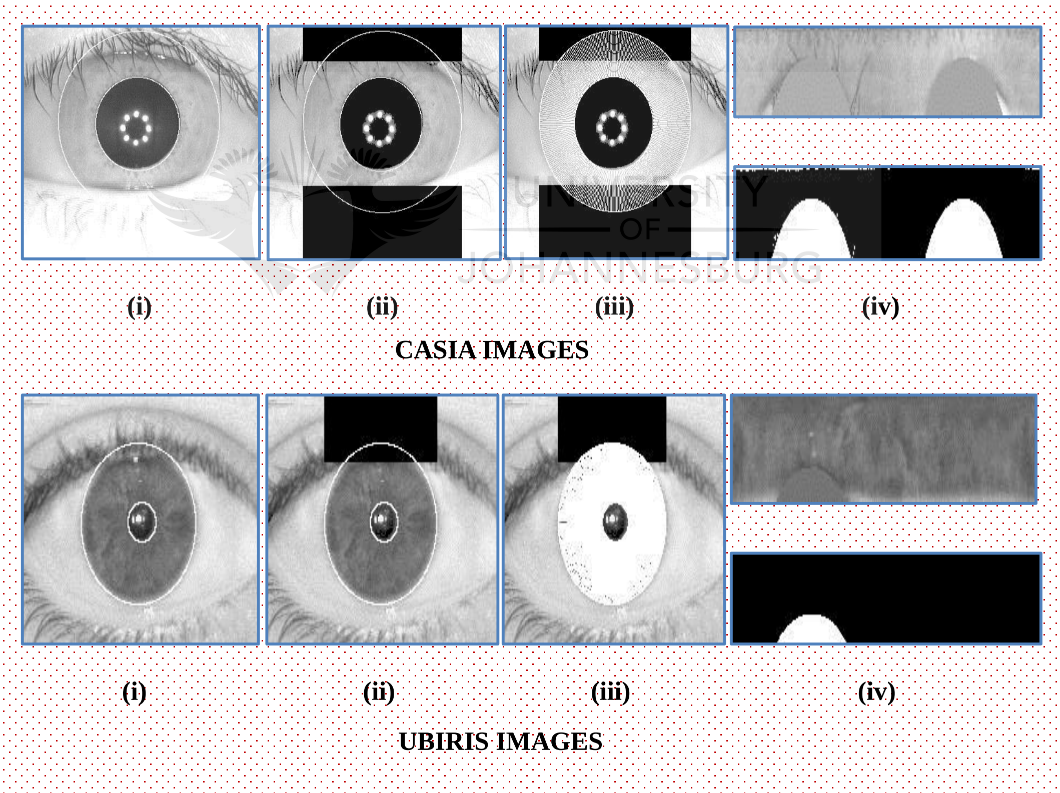

FIGURE A.7: Results of iris image normalization using both CASIA and UBIRIS images

Figure A.7 depicts the results of iris image normalization. Images numbers (iii) are showing the transformed rectangular co-ordinates into polar co-ordinates. To make the iris region more useful and manageable the normalized image is then converted into a rectangular block of fixed dimension, to ease the feature extraction and feature matching processes. After this transformation to rectangular block, features can be extracted using algorithm 1, and matched using the equation of the NHD shown in equation 2.8. The results of the NHD matching technique in terms of the ROC are depicted in the figure A.8 below. These results were tested using both CASIA and UBIRIS images.

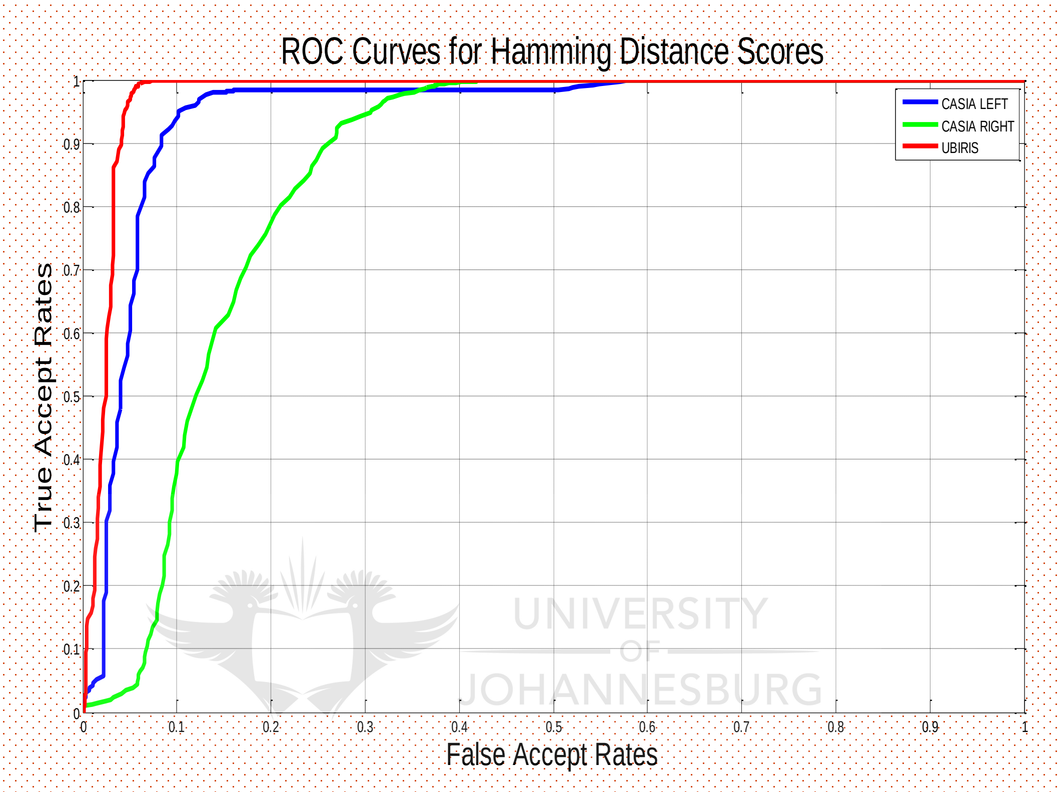

FIGURE A.8: ROC Curve for the NHD scores

Appendix B

Feature extraction using Multi-Lobe Differential filter

B.1 Feature Extraction

The procedure for extracting ordinal features involves determining the blobs or dark and light regions within the rectangular block of a normalized iris region. The basic idea of ordinal feature extraction as discussed by Sun *et al.,* [21] and Dong *et al.,* [24] evolved from [19]. This is accomplished by passing the MLDF feature extractor into a normalized iris region. To get the ordinal features from a normalized image, the image is divided into overlapping regions or blocks of fixed size of 16×64. The ordinal filter in equation 2.23 is convolved with each block and encode the iris template by capturing bits that results from the sign of the filter. Because templates were compared from regions with varying intensity levels, each region was allocated a fixed size of 5×5, with a scaling parameter $\sigma = 1.7$. The output of the feature extractor is the code determined by the output value of the equation 2.23 as discussed in chapter 2. Figure B.1 depicts the pictorial comparison of Gaussian lobes or regions used in this feature extraction process:

B.2 Weight Map for Matching

The matching algorithm used in this feature extractor is an advanced NHD called the WHD because it incorporates weights into the matching function. To generate the weights for each template, the following procedure was followed; based on the explanation found in [24]. If the test database has k training images then their iris templates can be denoted by a vector of templates as $\left(Templates = template_1, template_2, template_3, ..., template_k\right)$. From these templates $k \times k$ of intraclass matchings can be used to estimate the average

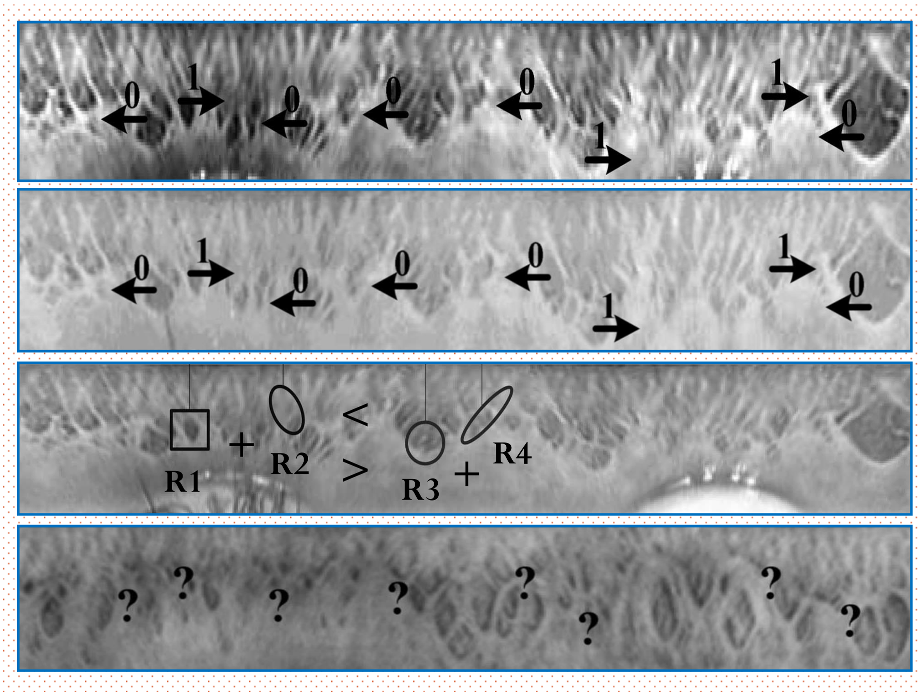

FIGURE B.1: The feature extraction using MLDF strategy [21]

matching results using equation B.1.

$$P = \frac{1}{k \times k} \sum_{a=1}^{k} \sum_{b=1}^{k} template_a \odot template_b \tag{B.1}$$

where P is a vector of bits denoted by $P = p_1, p_2, p_3, ..., p_n$, and which represents the probability of a match resulting to 1. The value of p_i also represents the stability of bits in the templates, and the bigger the value of p_i the more the stability of bit i. If for every given k iris templates given, the value of ($p_i = 1$) for a possible number of outcomes say q_1 times and ($p_i = 0$) for about q_0 times, implying that the sum of these possible outcomes results to the number of training iris templates (i.e $q_1 + q_0 = k$), then the average bit i can be computed using the equation B.2.

$$p_i = \frac{q_1^2 + q_0^2}{(q_1 + q_0)^2} \tag{B.2}$$

From this equation, the weight map can be computed using equation B.3.

$$w_i = 2\frac{q_1^2 + q_0^2}{(q_1 + q_0)^2} - 1 \tag{B.3}$$

This procedure needs to be updated every time when a new template in being matched. To update the weight map, equation B.4 is used because every template is different and contains different bits.

$$W_{n+1} = \frac{n^2 \times W_n + 2\sum_{m=1}^{n}(template_{n+1} \odot template_m - 1)}{(n+1)^2} \tag{B.4}$$

The results from this technique is illustrated in figure B.2 below using CASIA and UBIRIS images.

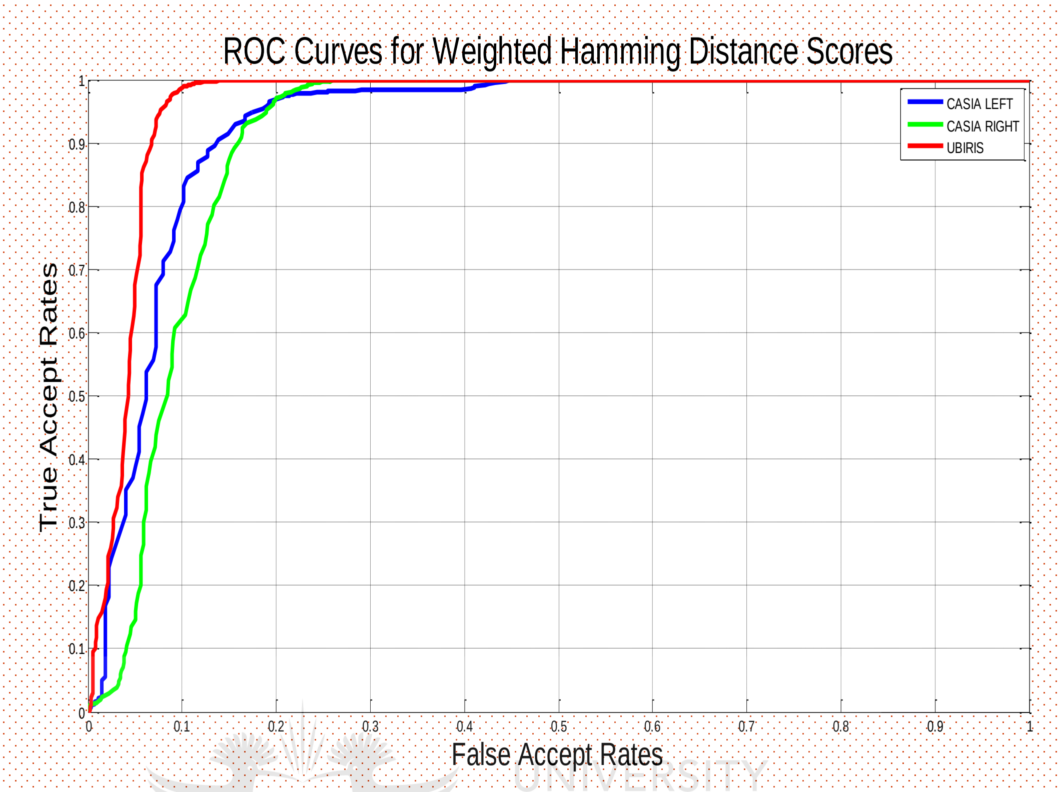

FIGURE B.2: ROC Curve for the WHD scores

Appendix C

Iris recognition based on Multi-Channel Gabor filtering

The pre-processig and segmentation stage has been explained in appendix A. This section will give details of feature extraction implemented in this work using Multi-Channel Gabor filtering as detailed by Tan [9]. The same approach was adopted by Zhu *et al.*, in [93] and Ma *et al.*, in [94]. The procedure followed in this work was adopted in [9].

C.1 Extracting Iris Features using Multi-Channel Gabor filtering

From the normalized iris image explained in appendix A, we let the even and odd symmetric Gabor filtering as discussed in chapter 2, equation 2.14 and 2.15 be $G_E(x, y)$ and $G_O(x, y)$ respectively. In [9], it was explained that four elemental simple cells can explain cortical channels which are tuned to a specific band of spatial frequencies and orientation. If we let $I(x, y)$ to be the input image and $J(x, y)$ be the output image, then the four cells from the output image can be expressed in terms of $J_i(x, y)$ where $i = 1, 2, 3, 4$. Then, for each output image we can have the following equations:

$$J_1(x, y) = \frac{1}{2}\left(|G_E(x, y) \otimes I(x, y)| + G_E(x, y) \otimes I(x, y)\right) \tag{C.1}$$

$$J_2(x, y) = \frac{1}{2}\left(|G_O(x, y) \otimes I(x, y)| + G_O(x, y) \otimes I(x, y)\right) \tag{C.2}$$

$$J_3(x, y) = \frac{1}{2}\left(| - G_E(x, y) \otimes I(x, y)| - G_E(x, y) \otimes I(x, y)\right) \tag{C.3}$$

$$J_4(x, y) = \frac{1}{2}\left(| - G_O(x, y) \otimes I(x, y)| - G_O(x, y) \otimes I(x, y)\right) \tag{C.4}$$

where the symbol $\otimes$ denotes the convolution of a 2D Gaussian filter in all the equations. Noting that the four elemental simple cortical cells represent only one visual cortical channel, the output image with four channels can now be written in terms of the following equation:

$$J(x,y) = \sqrt{\sum_{i=1}^{2} \Big(J_i(x,y) + J_{i+2}(x,y) \Big)^2} \tag{C.5}$$

Combining the above equations we produce the new output images which defines a computational model for visual cortical channels as explained in [9]. The equations for the new output images follows below:

$$J_E(x,y) = G_E(x,y) \otimes I(x,y) \tag{C.6}$$

$$J_O(x,y) = G_O(x,y) \otimes I(x,y) \tag{C.7}$$

From the two equations above, the features can be produced by using equation C.8, with parameters as explained in chapter 2.

$$J(x,y) = \sqrt{J_E^2(x,y) + J_O^2(x,y)} \tag{C.8}$$

The features extracted using equation C.8 are expressed in terms of mean (μ) and standard deviation (δ). Twenty four features are extracted as mean and twenty four features are extracted as standard deviations for each image. The total features becomes 48 and represented in a two column matrix with the first column as mean and the second column as standard deviation. The extracted features were matched using WED shown in equation 2.20 in chapter 2.

The results for this implementation based on the ROC curve is shown in figure C.1 below:

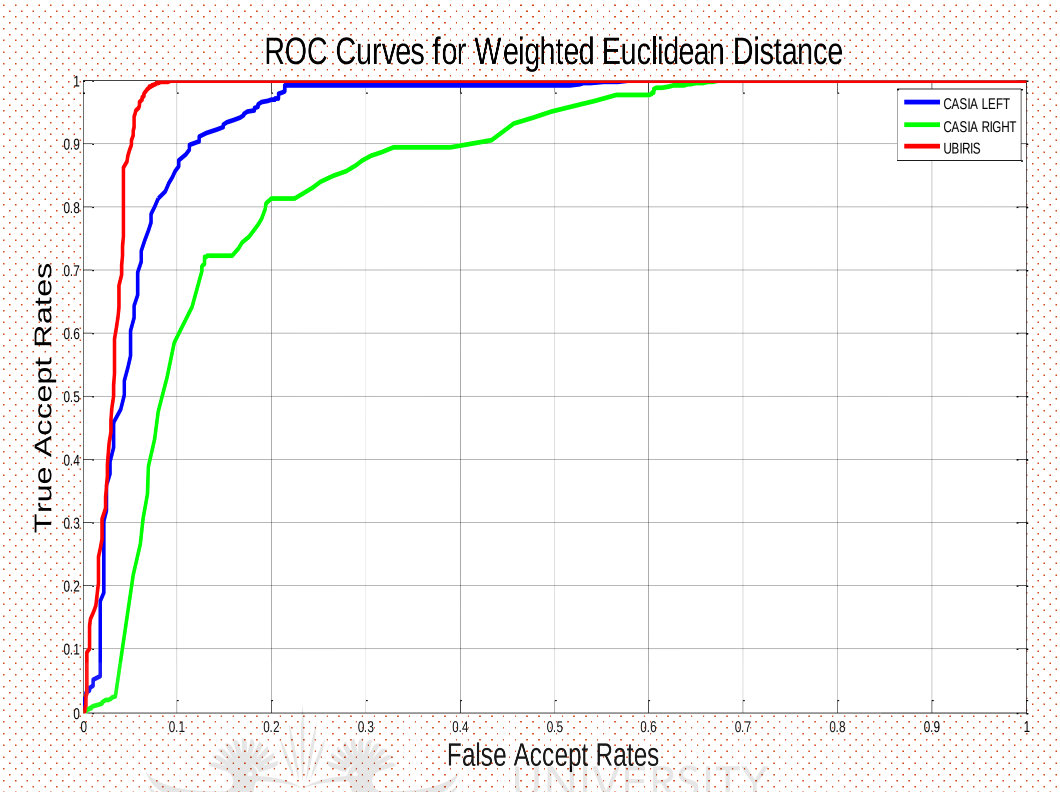

Figure C.1: ROC Curve for the WED scores

Appendix D

Iris recognition using Hierarchical Phase-Based Matching

The block based iris image matching is explained by the flow chart below:

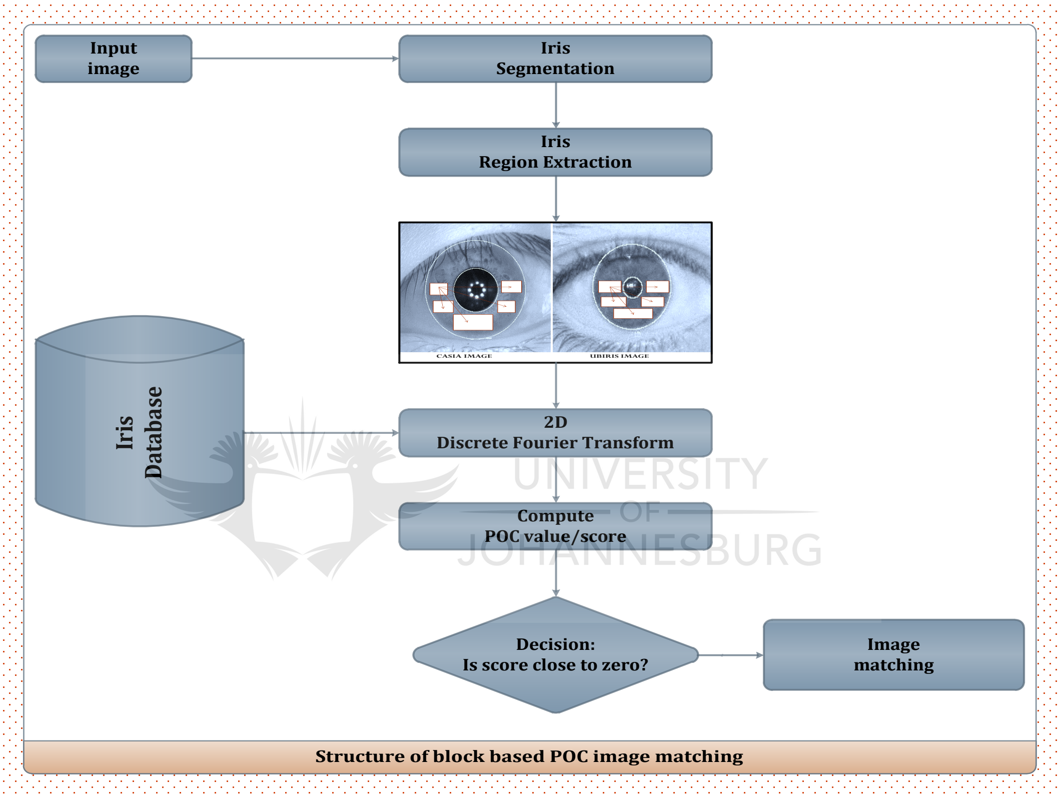

Figure D.1: HPB Flowchart [24]

The process of extracting the blocks is shown in algorithm 17. This method is difficult to automate when different databases are used. For this reason a MATLAB built-in function called $BLKPROC$ or *blockproc* was used to extract the blocks, because in this work the bottom block above the bottom eyelid was aimed to extract more features than the rest of the block. To achieve that, one function process four blocks and one function process the last big block separately. It is also easy and convenient to implement various function within the $BLKPROC$, main function.

Algorithm 4: Block Partition an Image into 5 Blocks of size, $S = 45 \times 25$

Input: A segmented image $I(x, y)$

Output: 5 Blocks of sub-images of equal dimensions 45×25, where 45 is the height and 25 is the width of the block

We need $I(x, y) \neq \emptyset$

Take the center of the image to be $C = (x_c, y_c)$

$[45\ 25] \leftarrow Size(S)$ which is the size of each block

for $\forall$ *sub-images* $S_i \in I(x, y)$ **do**

  $S_1 \leftarrow ((x_1 = x_c - 65), (y_1 = y_c - 10))$

  $S_2 \leftarrow ((x_2 = x_c + 70), (y_2 = y_c - 10))$

  $S_3 \leftarrow ((x_3 = x_c - 55), (y_3 = y_c + 20))$

  $S_4 \leftarrow ((x_4 = x_c + 55), (y_4 = y_c + 120))$

  $S_5 \leftarrow ((x_5 = x_c + 20), (y_5 = y_c + 30))$

return *Sub-images of* $I(x, y)$

—–*Compute the Phase Components*—–

-Compute phase components for each sub-region

-Compute match score for each block using equations 2.28 and 2.29

if *POC for* $f(n_i, n_j) \leftarrow S_i$ **then**

  Get matched images

return *Matched Images*

The results generated from this approach are presented below. The figures that follows compares images from the intra-class images and inter-class images for both CASIA and UBIRIS databases. Figure D.2 depicts the correlation using the between class variations. The results shown in figure D.2 are for CASIA left images only. Take note that the higher the correlation value the stronger the relationship, and vice versa.

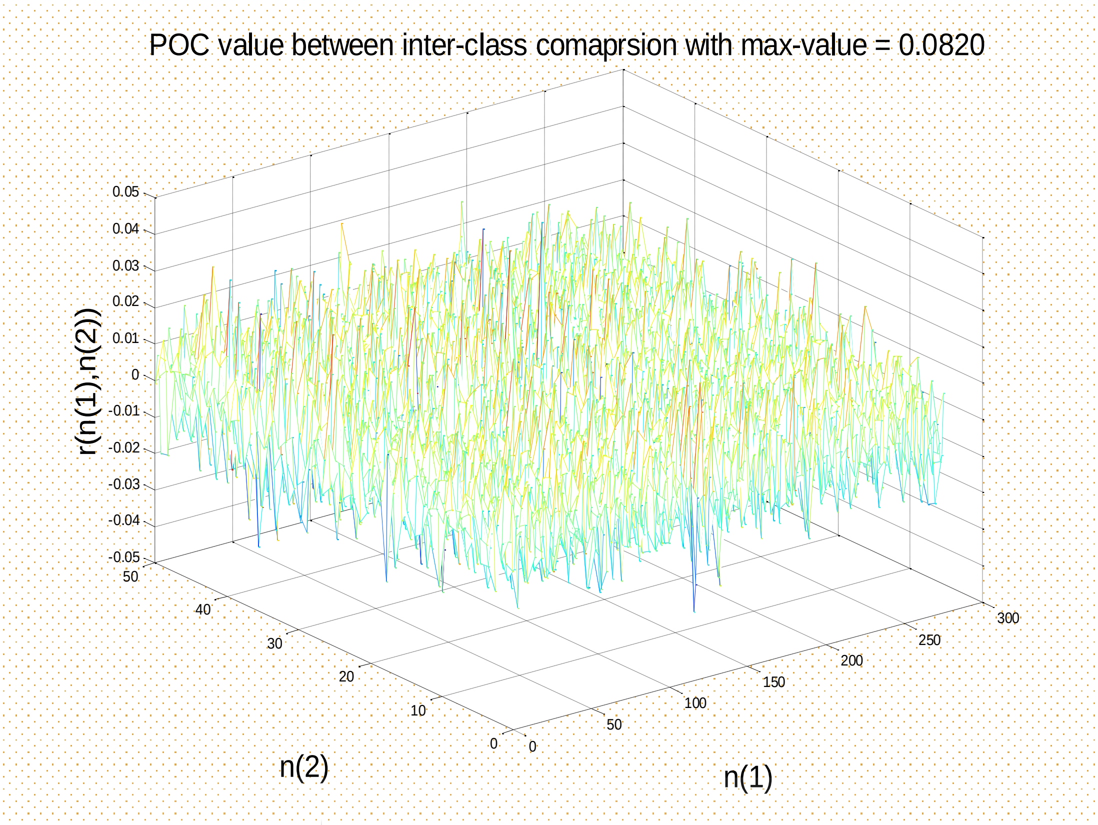

FIGURE D.2: POC for inter-class images using CASIA left eyes images

The POC for CASIA right eyes images are presented in figure D.3 below:

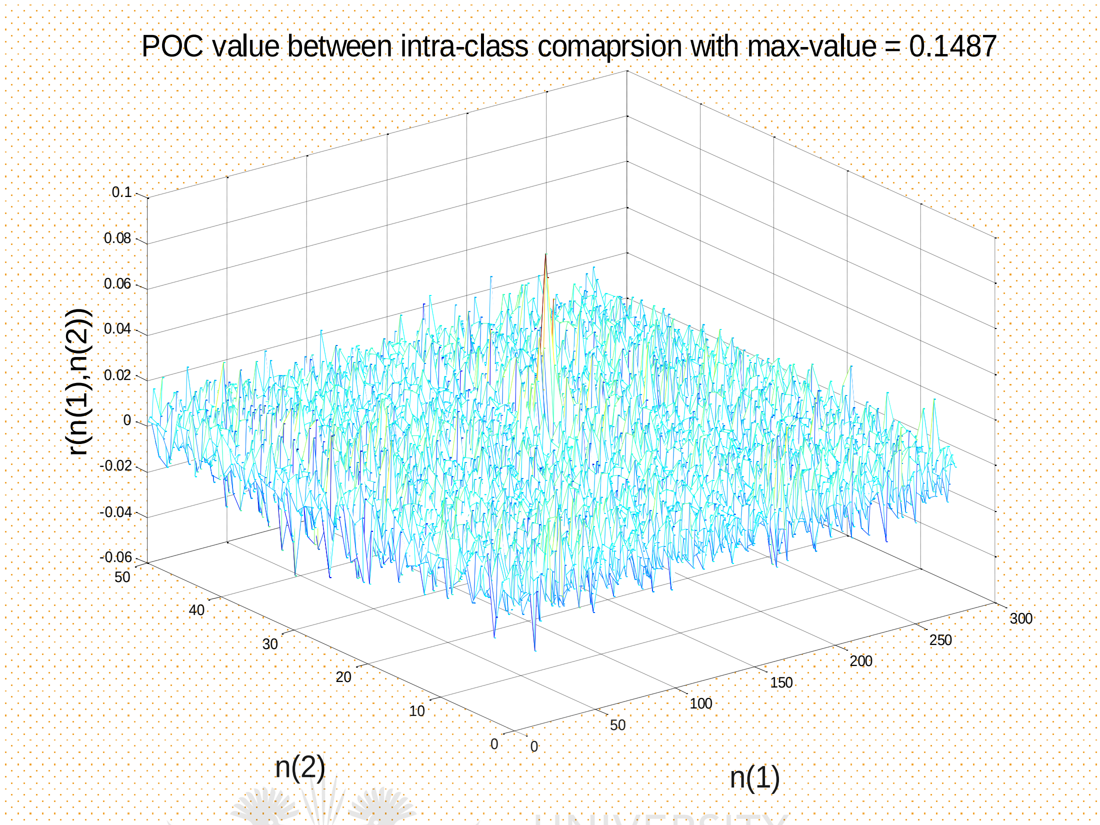

FIGURE D.3: POC for within class variations using CASIA right eyes images

The POC for images from UBIRIS images are presented in figure D.4 below:

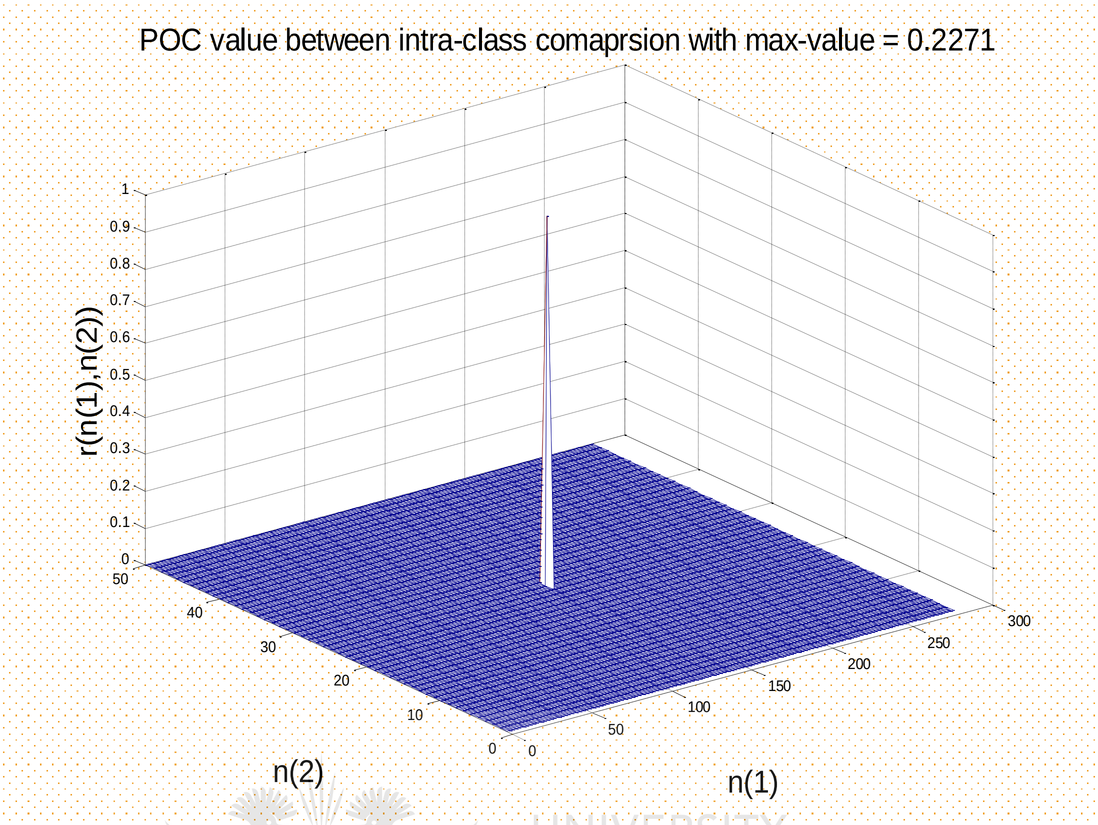

FIGURE D.4: POC for the same image using UBIRIS images

The POC within class variation using UBIRIS images are presented in figure D.5 below:

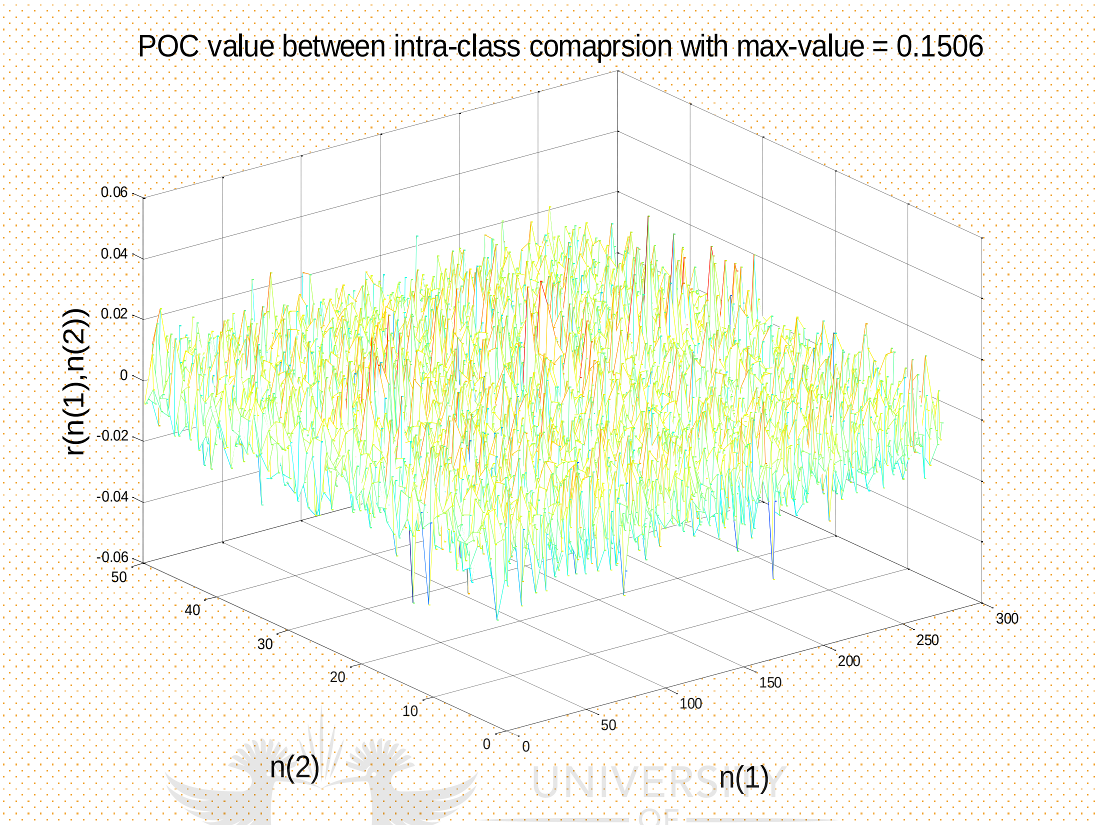

FIGURE D.5: POC for within class variation using UBIRIS images

The POC between class variation for images extracted from UBIRIS database are presented in figure D.6 below:

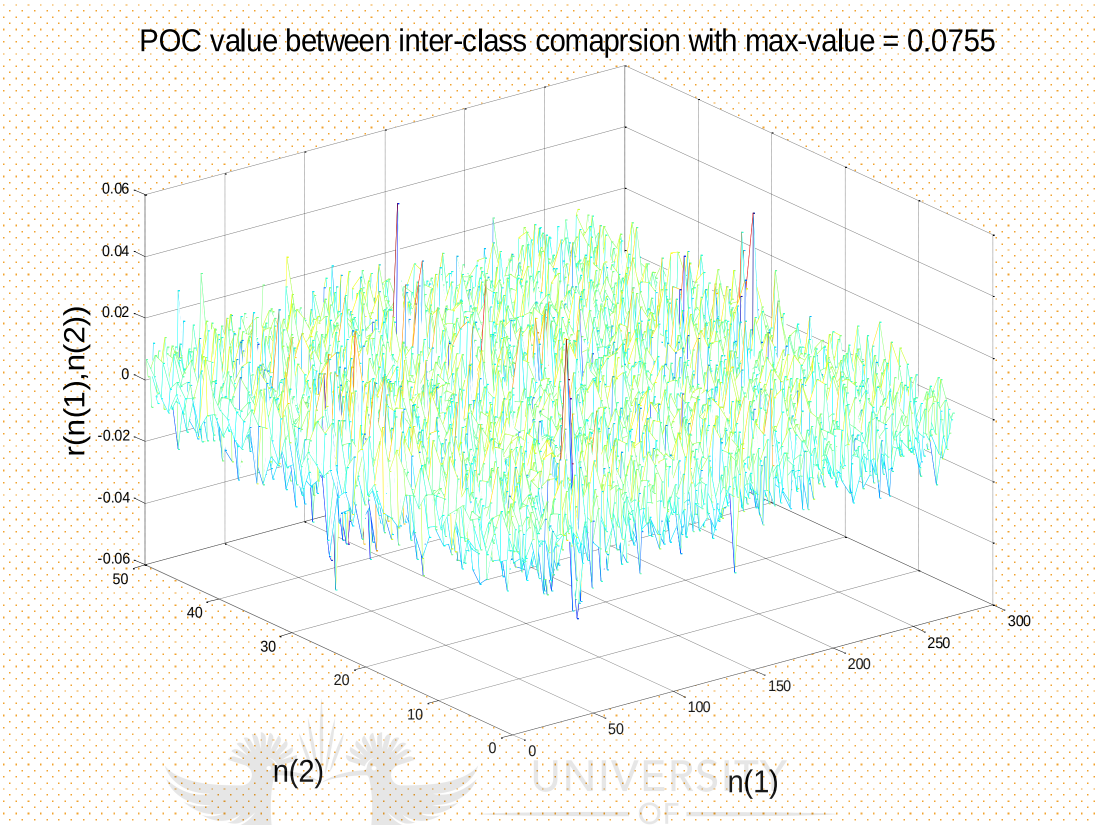

FIGURE D.6: POC for between class variation using UBIRIS with images

The ROC curve for the analysis of this iris recognition system was also implemented. The results from this technique is illustrated in figure D.7 below using CASIA and UBIRIS images.

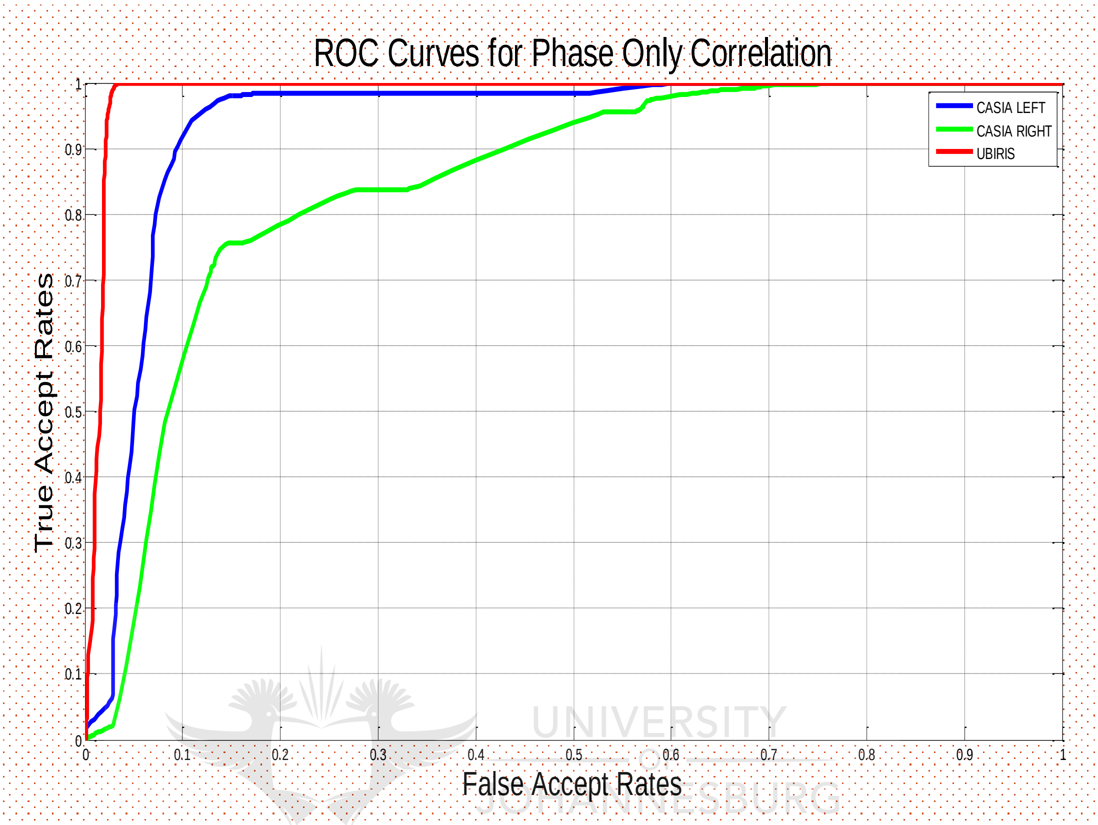

FIGURE D.7: ROC Curve for the POC scores